Geochemistry and Petrology of the Matokulma, Palojärvi, and Hongonniittu Gabbro intrusions, Central Finland Granitoid Complex

Master's Thesis
Seppo Karvinen
7.11.2019
Department of Geosciences
and Geography
Faculty of Science
University of Helsinki

Tiedekunta/Osasto — Fakultet/Sektion — Faculty	Laitos — Institution — Department
Faculty of Science	Department of Geosciences and Geography

Tekijä — Författare — Author

Seppo Karvinen

Työn nimi — Arbetets titel — Title

Geochemistry and Petrology of the Matokulma, Palojärvi, and Hongonniittu Gabbro intrusions, Central Finland Granitoid Complex

Oppiaine —Läroämne — Subject

Geology

Työn laji — Arbetets art — Level	Aika — Datum — Month and year	Sivumäärä — Sidoantal — Number of pages
Master's Thesis	11/2019	111 +3 Appendices

Tiivistelmä — Referat — Abstract

The Central Finland Granitoid Complex (CFGC) is a large (44,000 km^2) plutonic core of a Svecofennian (Paleoproterozoic, 1.91–1.82 Ga) arc complex, formed from collisions of several volcanic arcs and their accretion over the Karelian craton. The CFGC consists mostly of granitic to granodioritic rock types. Mafic-ultramafic plutonic rock types are not common, and they consist of mostly small gabbro-diorite intrusions, which may have ultramafic parts. There are two distinct belts around the CFGC, where Ni-Cu potential mafic-ultramafic intrusions are situated – Vammala and Kotalahti. The intrusions within these belts were formed during the height of magmatism within the CFGC (1.89–1.87 Ga). They host Ni-Cu mineralizations, some of which have been economically exploited. The mineralizations are hosted by olivine-rich ultramafic cumulates. The intrusions formed from hydrous tholeiitic basalts (10–12 wt-% MgO) with arc-type trace element chemistry. The difference between Vammala and Kotalahti type intrusions (clinopyroxene and orthopyroxene-dominated, respectively) are attributed to the rock type of the assimilated country rock.

In this thesis, three previously unknown or poorly studied mafic-ultramafic intrusions (Matokulma, Palojärvi, and Hongonniittu) within the CFGC are studied in detail. The petrology, similarity to Vammala-Kotalahti type intrusions, parental magma compositions, ore potential, and petrogenesis of the intrusions are described. Rock samples and field observations were gathered during the summer of 2017. Whole-rock geochemistry, mineral geochemistry, isotope geochemistry, and geophysics are used to describe the petrology of the intrusions. Matokulma and Palojärvi intrusions are studied in detail, compared to Hongonniittu intrusion, which was not studied as intricately.

The Matokulma intrusion is the least evolved (whole-rock median Mg#=72) of the studied intrusions and consists of tholeiitic melagabbros where clinopyroxene±orthopyroxene and plagioclase are the main cumulus phases within interstitial, magmatic amphibole (magnesio-hastingsite to pargasite in composition). Orthopyroxene and plagioclase are intercumulus phases in some samples. There are also mafic dikes that intrude the tonalitic country rock that surrounds the gabbro. The dikes are similar to the gabbros in geochemistry although they are generally more evolved. Trace element geochemistry suggests that the gabbros and dikes are genetically connected, and the dikes possibly represent the residual magmas of the gabbros.

The Palojärvi intrusion is noticeably more evolved than the Matokulma intrusion (median Mg#=49), which is apparent in the iron and titanium-rich mineral and whole-rock geochemistry. The strongly tholeiitic melagabbros are composed of both orthopyroxene and clinopyroxene as cumulus phases with plagioclase and common Fe-Ti oxide, often within interstitial magmatic amphibole (magnesio-hastingsite to magnesio-ferri-hornblende in composition). The Fe-Ti oxides are mostly ilmenomagnetite but both magnetite and ilmenite grains are present in same samples. Based on a few mineral analyzes, the ilmenomagnetite contains up to 1.4 wt-% V_2O_3. U-Pb age determination samples from a leucogabbro dike within the intrusion and granite that crosscuts the intrusion yielded weighted average $^{206}Pb/^{207}Pb$ ages of 1883.4±4.8 Ma and 1893.8±7.1 Ma, respectively. The age results are in contrast to the intrusive relationship observed in the field. However, considering the margin of error of the results, the granite can be younger than the gabbro, 1887 Ma and 1888 Ma, respectively. The age of ca. 1.89 Ga is at the early stage of the most voluminous mafic-ultramafic magmatism in the Svecofennian terrane.

The parental magmas of the Matokulma and Palojärvi intrusions were evolved and contained approximately 5 wt-% and 2 wt-% MgO, respectively. The presence of magmatic amphiboles in most samples indicate that the parental magmas were hydrous. Samples from all intrusions plot similarly in primitive mantle normalized Rare Earth Element (REE) and Normal-Mid-Ocean Ridge Basalt (NMORB) normalized spider diagrams. Similar patterns indicate a similar source for the parental magmas. The trace element geochemistry has signatures of subduction related fluid metasomatism. The rocks are enriched in large ion lithophile elements (LILE) and depleted in High Field Strength Elements (HFSE). These geochemical characteristics indicate that the studied intrusions crystallized from a hydrous, NMORB-like evolved basaltic magma, which has experienced fluid metasomatism.

The studied intrusions differ from olivine-rich ultramafic cumulates of Vammala and Kotalahti type intrusions based on their more evolved, gabbroic composition and because of this, they are not Ni-Cu ore potential. Palojärvi may host a Fe-Ti-V mineralization, if there are magnetite-rich layers within the intrusion.

Avainsanat — Nyckelord — Keywords

Central Finland Granitoid Complex, CFGC, Svecofennian, gabbro, geochemistry, petrology, petrogenesis, ore potential, magmatic amphibole

Ohjaaja tai ohjaajat – Handledare – Supervisor or supervisors

Tapani Rämö, Hannu Makkonen

Säilytyspaikka — Förvaringsställe — Where deposited

HELDA - Digital Repository of the University of Helsinki

Muita tietoja — Övriga uppgifter — Further information

Tiedekunta/Osasto — Fakultet/Sektion — Faculty	Laitos — Institution — Department
Matemaattis-luonnontieteellinen tiedekunta	Geotieteiden ja maantieteen osasto

Tekijä — Författare — Author

Seppo Karvinen

Työn nimi — Arbetets titel — Title

Matokulma, Palojärvi ja Hongonniittu gabrointruusioiden geokemia ja petrologia, Keski-Suomen granitoidikompleksi

Oppiaine —Läroämne — Subject

Geologia

Työn laji — Arbetets art — Level	Aika — Datum — Month and year	Sivumäärä — Sidoantal — Number of pages
Pro Gradu	11/2019	111 +3 liitettä

Tiivistelmä — Referat — Abstract

Keski-Suomen granitoidikompleksi (myöh. granitoidikompleksi) on laaja (44000 km^2), svekofennisen (paleoproterotsooinen, 1.91–1.82 Ga) kaarikompleksin plutoninen ydin, joka muodostui usean saarikaaren törmäyksistä ja akreetioista Karjalan kratonin päälle. Granitoidikompleksi koostuu suurimmaksi osaksi graniiteista ja granodioriiteista. Mafiset-ultramafiset kivet eivät ole yleisiä ja ne ovat useimmiten pienikokoisia gabro-dioriitti-intruusioita, joissa voi olla ultramafisia osueita. Granitoidikompleksin ympärillä on kaksi malmipotentiaalista vyöhykettä, Vammala ja Kotalahti, joissa mafisten-ultramafisten intruusioiden yhteydessä on Ni-Cu-mineralisaatioita. Näitä Ni-Cu-mineralisaatioita on hyödynnetty taloudellisesti. Vammala- ja Kotalahti-tyypin intruusiot muodostuivat granitoidikompleksin magmatismin päävaiheessa (1.89–1.87 Ga). Mineralisaatioiden isäntäkivinä ovat yleensä runsaasti oliviinia sisältävät ultramafiset kumulaatit. Nämä intruusiot muodostuivat vesipitoisesta tholeitiitisesta basaltista, joka sisälsi 10–12 p-% MgO ja oli hivenainekoostumukseltaan saarikaari-tyyppiä. Vammala-tyypin intruusioissa klinopyrokseeni on yleisempi, kun taas Kotalahti-tyypin intruusioissa ortopyrokseeni on hallitseva. Tämä koostumusero johtuu magman kontaminaatiosta, johon vaikuttaa assimiloidun isäntäkiven koostumus.

Tässä pro gradu -työssä tutkitaan kolmea, aikaisemmin huonosti tunnettua tai tuntematonta Keski-Suomen granitoidikompleksin sisällä sijaitsevaa intruusiota, jotka ovat Matokulma, Palojärvi ja Hongonniittu. Työssä kuvataan intruusioiden petrologia, samankaltaisuus Vammala-Kotalahti-tyypin intruusioihin, kantamagman koostumus, intruusioiden malmipotentiaali sekä petrogenesis. Kivinäytteet sekä kenttähavainnot kerättiin kesällä 2017. Intruusioiden petrologia esitellään kokokivi-geokemian, mineraalikemian, isotooppigeokemian ja geofysiikan keinoin. Matokulma- ja Palojärvi-intruusiot tutkittiin yksityiskohtaisesti, mutta Hongonniittu-intruusiota ei tutkittu resurssipulan takia yhtä tarkasti.

Matokulma on tutkituista intruusioista vähiten kehittynyt (kokokivikemian mediaani Mg#=72) ja koostuu tholeiittisista melagabroista, joiden pääamineraaleina on klinopyrokseeni±ortopyrokseeni ja plagioklaasi kumulusfaaseina magmaattisen interkumulusamfibolin sisällä. Ortopyrokseeni ja plagioklaasi ovat interkumulusfaaseina joissain näytteissä. Gabroa ympäröivää tonaliittista isäntäkiveä leikkaavat myös mafiset juonet. Nämä juonet ovat geokemialtaan gabrojen kanssa samankaltaisia, vaikkakin kehittyneempiä. Hivenainekoostumuksen perusteella gabrot ja juonikivet liittyvät toisiinsa ja juonet edustavat mahdollisesti gabrojen jäännemagmaa.

Palojärven intruusio on Matokulmaa huomattavasti kehittyneempi (kokokivikemian mediaani Mg#=49), joka näkyy kokokivi- ja mineraalikemiassa korkeina rauta- ja titaanipitoisuuksina. Palojärven melagabrot ovat voimakkaasti tholeiittisia ja ne koostuvat sekä orto- että klinopyrokseeneista kumulusfaaseina yhdessä plagioklaasin ja Fe-Ti-oksidin kanssa magmaattisen interkumulusamfibolin sisällä. Fe-Ti-oksidi on pääasiallisesti ilmenomagnetiittia, mutta sekä magnetiittia ja ilmeniittiä esiintyy erillisinä rakeina samoissa näytteissä. Ilmenomagnetiitti voi muutamien analyysien mukaan sisältää jopa 1.4 p-% V_2O_3. U-Pb-iänmääritysnäytteiden intruusion sisältä leukogabrojuonesta ja melagabroa leikkavasta leukograniitista ovat painotetun keskiarvon mukaan vastaavasti 1883.4±4.8 Ma ja 1893.8±7.1 Ma. Nämä tulokset ovat ristiriidassa kenttähavaintojen kanssa, joiden perusteella graniitti leikkaa gabrointruusiota. Tulosten virhemarginaalien perusteella graniitti voi kuitenkin olla gabroa nuorempi – vastaavasti 1887 Ma ja 1888 Ma). Iänmääritysten mukaan intruusion ikä on noin 1.89 Ga, mikä ajoittuu svekofennisen magmatismin päävaiheen alkuun.

Matokulman ja Palojärven kantamagmat olivat kehittyneitä ja sisälsivät vastaavasti 5 p-% ja 2 p-% MgO. Magmaattisen amfibolin yleisyys kertoo siitä, että kantamagma oli vesipitoinen. Kaikkien intruusioiden näytteet ovat samankaltaisia alkukantaisen vaipan (engl. Primitive Mantle) tai normaalin keskiselännebasaltin (engl. Normal Mid-Ocean Ridge Basalt, NMORB) mukaan normalisoiduilla hivenalkuaine spider-diagrammeilla. Samankaltaiset trendit viittaavaat yhteiseen lähteeseen. Hivenalkuaine-geokemiassa on viitteitä subduktioon liittyvästä fluidimetasomatismista, jossa sopeutumattomien alkuaineiden ns. LILE (engl. Large Ion Lthophile Elements) konsentraatiot kivessä ovat kohonneita ja HFSE (High Field Strength Elements) ovat köyhtyneitä. Edellä mainitut geokemialliset piirteet viittaavat siihen, että tutkitut intruusiot kiteytyivät vesipitoisista, NMORB-tyyppisistä kehittyneistä basalttisista sulista, joiden koostumukseen vaikutti subduktioon liittyvä metasomatismi.

Tutkitut intruusiot eroavat Vamma-Kotalahti-tyyppisistä, runsaasti oliviinia sisältävistä ultramafisista intruusioista kehittyneemmän, gabroidisen koostumuksensa perusteella, jonka takia ne eivät ole Ni-Cu-malmipotentiaalisia. Palojärven intruusio voi sisältää Fe-Ti-V-mineralisaation, jos intruusiosta löytyy magnetiitti-rikkaita kerroksia.

Avainsanat — Nyckelord — Keywords

Keski-Suomen granitoidikompleksi, Svekofennia, gabro, geokemia, petrologia, petrogenesis, malmipotentiaali, magmaattinen amfiboli

Ohjaaja tai ohjaajat – Handledare – Supervisor or supervisors

Tapani Rämö, Hannu Makkonen

Säilytyspaikka — Förvaringsställe — Where deposited

HELDA – Helsingin yliopiston digitaalinen arkisto

Muita tietoja — Övriga uppgifter — Further information

Table of contents

1. INTRODUCTION

Historically, most of the exploited Ni-(Cu) sulfide mineralizations in Finland are hosted by Svecofennian (~1.88 Ga) mafic-ultramafic intrusions located in central and southern Finland, surrounding the Central Finland Granitoid Complex (CFGC) (Papunen and Gorbunov 1985, Peltonen 2005, Maier 2015, Makkonen 2015). They are situated in two major metallogenic belts around the CFGC, one that is roughly EW and the other NW-SE aligned – Vammala and Kotalahti Nickel Belts, respectively. Svecofennian mafic-ultramafic intrusions have been extensively researched since the late 1960s due to their economic significance (e.g. FINNICKEL database (Makkonen et al. 2009), Häkli 1971, Lamberg 2005, Makkonen 2015 and the references therein, Makkonen et al. 2017 and the references therein, Mäkinen 1987, Papunen and Gorbunov 1985). Some research has been done with the mafic-ultramafic intrusions within the CFGC (e.g. Rämö 1986, Peltonen and Elo 1999, Peltonen 2005, Kärkkäinen and Bornhorst 2003).

In this thesis, three previously unknown or poorly researched gabbro intrusions (Matokulma, Palojärvi, and Hongonniittu) located in the south-central part of the Central Finland Granitoid Complex (CFGC) are studied (Figure 1). The intrusions were mapped and sampling was done during the summer of 2017. The samples and observations obtained during this period are used to describe the petrology, petrography, and geochemistry of the intrusions. Whole-rock and mineral geochemistry are used to calculate the parental melts of the intrusions, as well as to assess the ore potentiality of the intrusions. The geochemical intrusions are then compared to the Ni-Cu ore potential, Vammala and Kotalahti type intrusions. Finally, the petrogenetic models for the intrusions are introduced.

Whole-rock and mineral geochemistry, together with U-Pb age determination and whole-rock Sm-Nd data from Palojärvi intrusion provide new information about the timing and petrology of mafic-ultramafic intrusions within the CFGC and their ore potential. This study is done as a part of the Geological Survey of Finland's (GTK) Au Mineral Potential Evaluation project of Länkinpohja-Jämsä area.

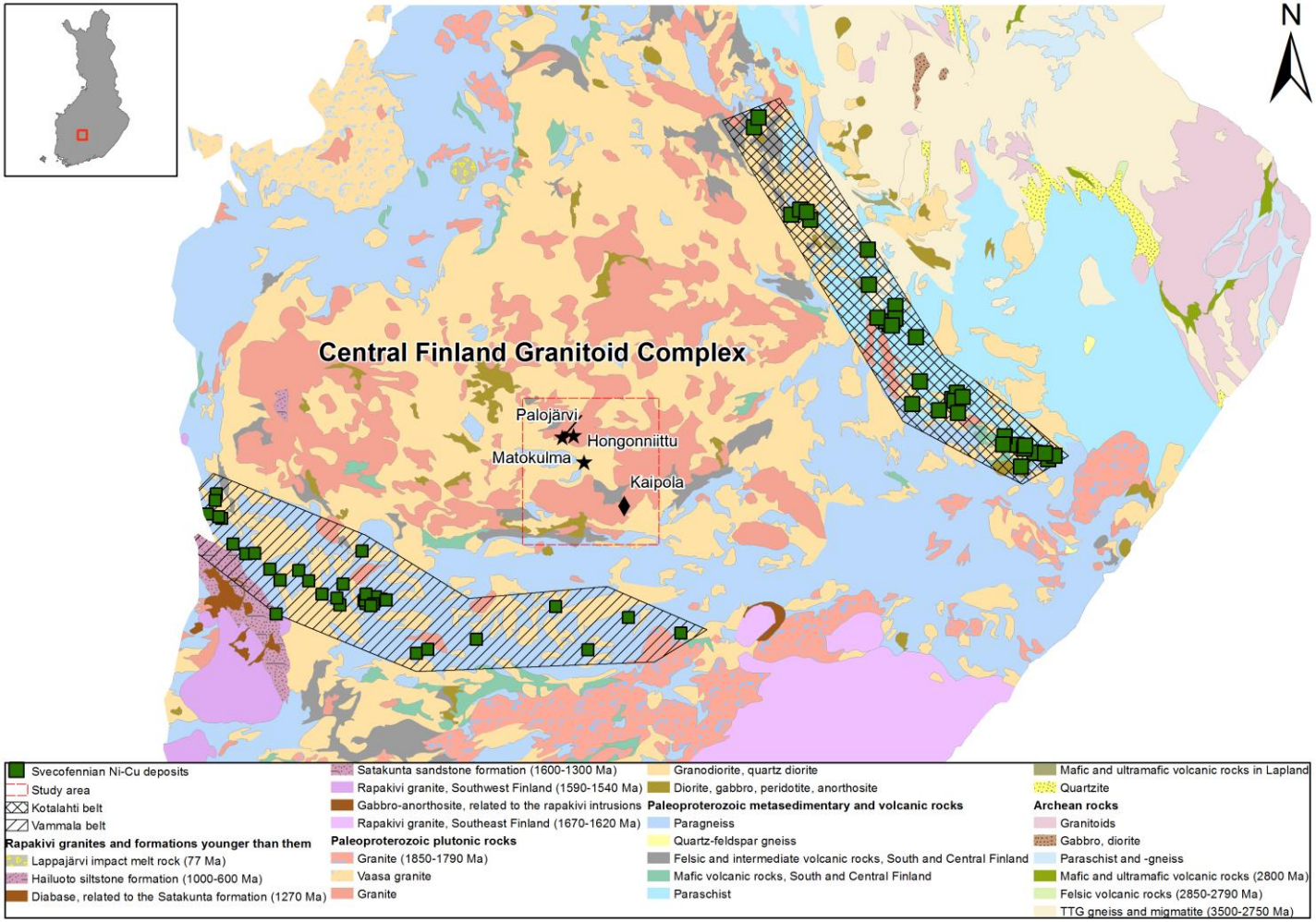

Figure 1. Study area and regional geology. The studied intrusions are marked with stars, nearby Kaipola layered intrusion is marked with a diamond symbol. The study area is marked with a red box, Vammala and Kotalahti belts are marked with solid line and cross-hatched polygons, respectively. Ni-Cu deposits within these belts are marked with green squares. The red box shows the area within the Central Finland Granitoid Complex that is discussed in this thesis, containing the studied intrusions and Kaipola layered intrusion. The location of the Svecofennian Ni-Cu deposits and the bedrock map are from the Geological Survey Of Finland. The geological map is the 1:5 000 000 Bedrock map of Finland.

2. GEOLOGICAL SETTING

2.1 Regional geology

2.1.1 The study area

The intrusions studied in this thesis are Palojärvi, Hongonniittu, and Matokulma (Figure 2). Palojärvi and Hongonniittu are located in the municipality of Keuruu, 5- and 10-kilometers northeast of the city of Mänttä-Vilppula, respectively. The two intrusions are clearly visible on an aeromagnetic anomaly map as strong positive anomalies. They are separated by roughly a kilometer of background magnetic values. The Matokulma intrusion is located 15 kilometers southwest of Palojärvi, in the municipality of Jämsä, and it shows up only as a slight positive anomaly. Palojärvi is the only intrusion of the three that has been studied previously (Akiander 1972, Sjöblom 1990) and drawn on the bedrock map (Sjöblom 1990, Nironen 2003). According to Sjöblom (1990.), the gabbros

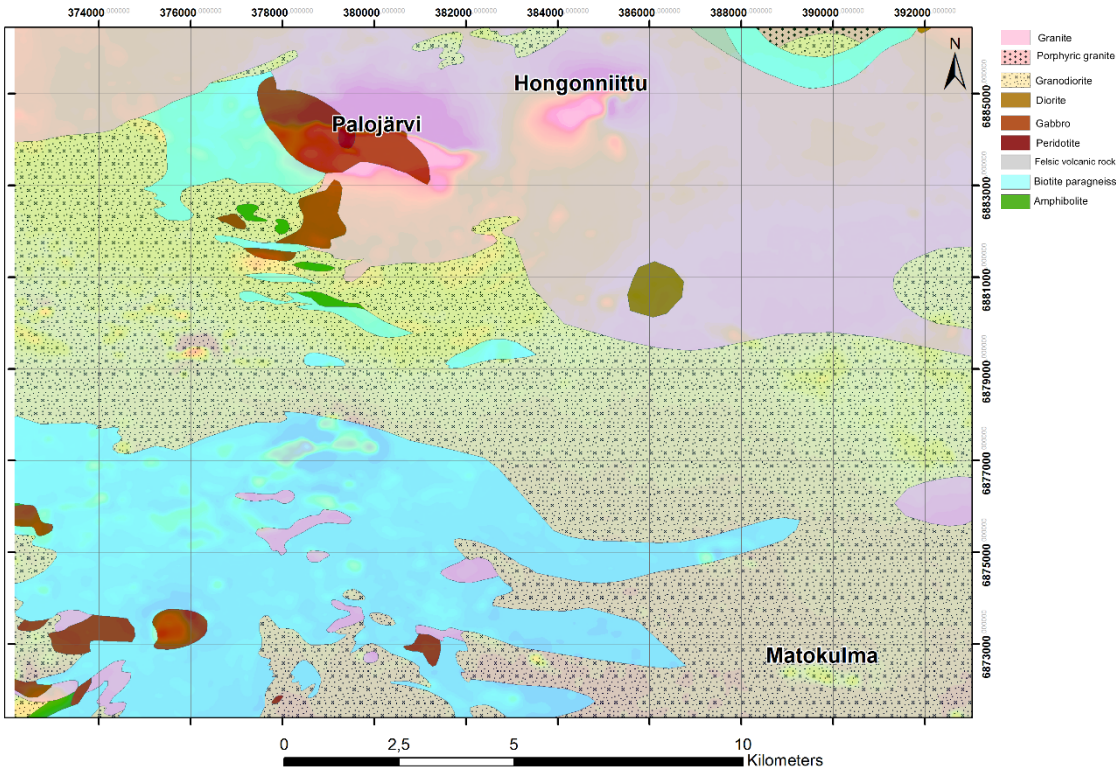

Figure 2. Study area with geological map overlain on aeromagnetic anomaly map. The studied intrusions are marked on the map. Palojärvi and Hongonniittu have strong positive (red colors) anomalies, with negative anomalies to the north of them (blue colors). Matokulma is also distinguishable as a weak positive anomaly. Palojärvi is marked on the bedrock map as a gabbro with a circular peridotitic center. Hongonniittu area is marked as granite and Matokulma as granodiorite. Seamless bedrock map (Bedrock of Finland (DigiKP)) and magnetic anomaly map from Geological Survey of Finland.

in the Mänttä area can be divided into pyroxene, hornblende, cummingtonite, and biotite gabbros.

On the bedrock map, the Palojärvi intrusion is an E-W to NW-SE elongated, ellipsoidal intrusion, which extends from Lake Palojärvi in the middle of the intrusion towards east, over road 58, and to west-northwest to islets in Lake Keuruuselkä. The intrusion is about 4200 m long and 1200 m, at maximum. On the bedrock map, most of the Palojärvi intrusion is composed of gabbro, but there is a circular peridotitic part in the middle of the intrusion.

Rautaruukki Oy conducted boulder tracing (Akiander 1972) in the Palojärvi area due to the strong magnetic anomaly clearly visible in airborne geophysics. Akiander (1972) found that the anomaly is caused by magnetite dissemination in a porphyric hornblende-pyroxene-gabbro. The few chemical assays showed that the magnetite is vanadium-rich, up to 1 wt-% in a magnetic separate. In the map sheet explanation for Mänttä area, Sjöblom (1990) describes the Palojärvi gabbros to be ophitic, magnetite-bearing hypersthene gabbros and that many of the gabbros in the area, including the one of Palojärvi, often contain cummingtonite, both as thin, fan-like acicular crystal groups and as larger plates, which can be poikilitic. According to Sjöblom (ibid.), there are also outcrops where there is porphyric biotite gabbro, with biotite appearing as narrow laths 1–5 cm in length.

Hongonniittu appears similarly to Palojärvi as a strong positive anomaly on the aeromagnetic anomaly map, but it has not been previously mapped and on current bedrock maps the area is classified as granite.

Matokulma was found during the regional re-mapping of Jämsä area on the summer of 2016. On the bedrock map, the Matokulma area is granodiorite.

2.1.2 The rock types of the Central Finland Granitoid Complex (CFGC)

The CFGC comprises an area of around 44,000 km^2 and consists of mostly of granodioritic to granitic plutonic rocks, as the name implies (Nironen et al. 2000). Mafic-ultramafic plutonic rocks are uncommon, as are volcanic rocks, which are primarily intermediate in composition, when present (Nironen 2003). Mafic plutonic rocks are mostly small gabbro-diorite intrusions, which occasionally contain ultramafic parts.

Mingling structures are often seen between mafic and granodioritic or tonalitic magmas (Nironen 2003). The CFGC is alkaline, which is seen in the relative prevalence of monzonitic intermediate rock types (Nironen 2003).

According to Nironen (2000), the plutonic rocks in CFGC can be divided into groups based on their mineralogy, degree of deformation, and cross-cutting relationships. The synkinematic rocks are foliated due to their emplacement during the strongest deformation in the area, whereas postkinematic rocks are only weakly foliated or non-foliated. The postkinematic rocks are typically massive to slightly foliated, quartz monzonitic or monzogranitic in composition, with an alkali affinity (Rämö et al. 2001) and often contain accessory fluorite (Nironen et al. 2000, Rämö et al. 2001).

Mafic rocks and some intermediate volcanic rocks show up as positive anomalies in aeromagnetic maps, as do magnetite-bearing granitoids (Nironen 2003). Postkinematic intrusions, however, display negative anomalies.

The crust and the lithosphere are anomalously thick in the CFGC area up to 65 km and 250, respectively (Lahtinen 2009 et al.) The Svecofennian domain has been overprinted by high temperature-low pressure (HT/LP) (T = 700–800ºC, P = 4–5 kbar) metamorphism (Korsman et al. 1999 and references therein), which was coeval with the synkinematic plutonic rocks. Amphibolite and, up to granulite facies metamorphism was reached in the supracrustal rocks around the CFGC. A more recent study shows similar metamorphic conditions for the supracrustal rocks within the CFGC high amphibolite to granulite facies occurring at 1.89–1.88 Ga (Hölttä and Heilimo 2017), but the plutonic rocks of the CFGC were not studied in the study.

2.1.3 The evolution of the CFGC

The Central Finland Granitoid Complex is the core of the Proterozoic Svecofennian arc complex, located in the Fennoscandian Shield (Korsman et al. 1999). The Svecofennian orogeny was a complex tectonic process, which lasted from 1.91 Ga to 1.82 Ga (Nironen 1997), with a major magmatic episode between 1.90–1.87 Ga (Lahtinen et al. 2005).

The CFGC is adjoined by the Bothnia belt to the west and Tampere Schist Belt to the south (Nironen 2003). The Tampere Schist Belt consists of arc-affinity volcanic rocks (1.90–1.88 Ga), of a variety of compositions, and mainly turbiditic metasedimentary

rocks (1.92 Ga) (Kähkönen 1987, Kähkönen et al. 1989, Kähkönen 2005). Savo arc (Pyhäsalmi primitive island arc (Korsman et al. 1999)), is 1.93–192 Ga in age and located on the east side of the CFGC, between the CFGC and Archean terrain.

Nironen (1997) attempted to explain the Proterozoic evolution of the whole Fennoscandian shield. The model starts with the opening of an ocean through rifting at 1.95 Ga, followed by the consecutive accretion of two volcanic arc complexes onto the Archean continent, between 1.90–1.87 Ga. The tectonic regimes changed throughout the orogeny and possibly involved a microplate.

Lahtinen et al. (2005), based on new isotopic and geophysical data, introduced a more complex model which involved more components and a non-continuous timeline. The components of this model include Karelian, Kola and Norbotten cratons, several island arcs, and microcontinents.

According Lahtinen et al. (2005), the Svecofennian orogeny, rather than being a continuous, single orogenic event, composed of five orogenic stages, which partly overlap, both in time and space. The orogenies took place between 1.92–1.79 Ga. The model has four stages; the accretion of microcontinents (1.92–1.87 Ga), the continental extension stage (1.86–1.84 Ga), collision between continents (1.84–1.79 Ga), and lastly, the orogenic collapse and stabilitization (1.79–1.77 Ga). This model has been refined in later publications (Lahtinen et al. 2009, Lahtinen et al. 2014). Lahtinen et al. (2014) explain the current circular shape of the CFGC as being an originally linear arc which was buckled into the current form through collisions.

Mikkola et al. (2017) contest the theory of Lahtinen et al. (2009, 2014) where the Keitele microcontinent was attached to the Savo arc prior to accretion to the Karelian craton. Mikkola et al. (2017) argue that the involvement of the Keitele microcontinent unnecessarily complicates the tectonic models and that the isotopic evidence supporting the presence of the microcontinent can be explained by the varying age of the rocks in the Savo arc itself.

2.2. Svecofennian mafic-ultramafic intrusions

Most of the Ni-Cu mineralized mafic-ultramafic intrusions in Svecofennian terrain emplaced during the height of the Svecofennian orogeny, between 1.885–1.875 Ga (Peltonen 2005). Major Ni-Cu mineralizations occur only in the 1.88 Ga intrusions (Peltonen 2005). These intrusions are located around the CFGC in two mineralized belts – Vammala and Kotalahti Nickel Belts (Figure 1) (Häkli 1971, Häkli et al. 1979, Mäkinen and Makkonen 2004, Peltonen 2005). This magmatic event relates to the the first assembly of Colombia supercontinent, the accretion and collision of arcs and microcontintents, and the resulting amalgamation of Fennoscandia and Laurentia (Eilu and Lahtinen 2013)

The intrusions have been classified and grouped with different criteria. The intrusions can be classified as type IV mafic-ultramafic intrusions (Naldrett 1989), based on their emplacement in an active orogenic belt. Peltonen (2005) divides the intrusions to three groups according to their geotectonic location. Group I, which includes the intrusions of the Western Finland arc complex, is further divided into Ia and Ib; intrusions close to the Archean craton margin and intrusions of the Tampere and Pirkanmaa belts, respectively. The Kotalahti and Vammala type intrusions belong to groups Ia and Ib, respectively, and they have a high potential for magmatic Ni-Cu sulfide mineralizations. Group II intrusions are the synvolcanic intrusions of the Southern Finland arc complex. These intrusions have low potential for sulfide or oxide mineralizations. Intrusions of group III are the Ti-Fe-P gabbros of the CFGC, which have low potential for sulfide mineralizations, but they might host Fe-Ti oxide and apatite mineralizations.

Mäkinen (1987) grouped the intrusions based on the dominating mineral into Kotalahti and Vammala-type inrusions, where orthopyroxene and clinopyroxene dominate, respectively, and to gabbros, which are more evolved and further fractionate into diorites and quartz diorites.

The Svecofennian mafic-ultramafic intrusions crystallized from tholeiitic basalts with approximately 10–12 wt-% MgO (Peltonen 1995a, Makkonen 1996, Peltonen 2005, Makkonen et al. 2017) and high volatile content, based on the commonness of magmatic amphibole (Peltonen 1995a, Peltonen 2005). The emplacement took place during the

height of the Svecofennian orogeny and metamorphism (Mäkinen and Makkonen 2004, Makkonen 2005, Peltonen 2005).

2.2.1 Kotalahti belt

The Kotalahti Ni Belt, as coined by Gaál (1972), is a NW-SE trending metallogenic shear zone (Papunen 2003) situated near the accretionary boundary between CFGC and Archean gneiss terrain (Mäkinen and Makkonen 2004), also called Raahe-Ladoga shear zone (e.g. Kahma 1973, 1978, Ekdahl 1993).

Mafic-ultramafic intrusions are found in Proterozoic mica gneisses and also in Archean gneisses (Makkonen 2005). In the Kotalahti area, intrusions occur in the contact zone of Archean rocks and Proterozoic craton margin sequence, which consists of black schists, limestones and calc-silicate rocks, quartzites, amphibolites, amphibole-feldspar, and cordierite-mica gneisses (Mäkinen and Makkonen 2004). Mica gneiss is a typical country rock and contaminant in the intrusions (Peltonen 1995, Makkonen 1996, Mäkinen and Makkonen 2004). The intrusions are varying in size, up to several kilometres long and a few hundred meters wide in the surface section (Mäkinen 1987, Makkonen 1996, 2015).

In the Kotalahti area, the host rocks of the mineralizations are olivine to olivine-orthopyroxene cumulates, orthopyroxenites, ophitic gabbronorites, poikilitic gabbros, and diorites (Papunen 2003). Disseminated sulfides are common in ultramafic rocks and poikilitic gabbros whereas the ophitic gabbros and diorites are almost barren. The primary mineral assemblage is often altered to serpentine, chlorite, and amphiboles. The magmatic contact to the country rock, when present, is compositionally amphibolitic and fine-grained or metapyroxenitic and of a variety of grain sizes (Mäkinen and Makkonen 2004).

The Kotalahti area has experienced four distinct deformation events (Mäkinen and Makkonen 2004). The strongest deformation event, D_2, led to the overthrusting of Proterozoic rocks onto the Archean cration (Mäkinen and Makkonen 2004). The emplacement of Kotalahti and nearby Rytky intrusions took place during D_2 when magma intruded into the contact zone between the Archean and Proterozoic lithologies. The layering of the intrusions was inverted during the sequent D_3 stage, in which the area was folded SW-NE compression. The D_2 event generated a variety of migmatite structures in the country rock, when metamorphism took place in upper amphibolite facies (Korsman

and Glebovitsky 1999). The migmatites feature fragments of mafic-ultramafic rocks. According to Makkonen (2005), the latent heat of crystallization promoted the formation of migmatite neosomes.

The age of Kotalahti intrusion is 1883± 6 Ma, based on a U-Pb zircon age obtained from a gabbro (Gaál 1980).

Mäkinen (1987) assigns the differences between Kotalahti and Vammala type intrusions to different crystallization depths, rather than compositional differences of parental melts, with Kotalahti magmas crystallizing in greater depths. Assimilation of Archean felsic material has also been suggested to be a trigger for the preferential crystallization of orthopyroxene over clinopyroxene and the trigger for sulfide saturation and exsolution (Makkonen 1996, Peltonen 2005, Mäkinen and Makkonen 2004, Makkonen and Huhma 2007, Makkonen et al. 2008).

The Kotalahti mine produced 12.36 Mt of Ni and Cu ore, with average grades of 0.6 % and 0.2, respectively (Makkonen 2015). The mineralized intrusions contain a sulfide assemblage of pyrrhotite, pentlandite, chalcopyrite as disseminations of varying grain-sizes and abundances, and breccias. Massive sulfide ores and metallic copper can also be found (Makkonen et al. 2008). A certain kind of massive ore type, offset ore, occurs in stratigraphic floors, within the wall rock (Makkonen 2015). Jussi orebody in Kotalahti deposit is a classic example of this (Papunen and Koskinen 1985, Makkonen 2015). Jussi orebody contains higher nickel grades than the bulk ore of Kotalahti (Papunen and Koskinen 1985). PGE values are low in general and show distinct Pt-depletion on chondrite-normalized diagrams (Papunen 1986, Makkonen and Halkoaho 2007).

The Kotalahti magmas are associated with high temperature shear zones through which the magmas ascended from midcrustal levels (Makkonen 2005). Due to the EMORB affinities (Makkonen 1996, Makkonen and Huhma 2007) and the relation of the intrusions and comagmatic volcanic rocks, together with metasedimentary material, a back-arc setting has also been suggested for the geotectonic setting for Kotalahti type intrusions.

Peltonen (2005) suggests that the intrusions of Kotalahti belt are formed through the ascension of subduction related primitive mafic magmas through shear zones caused by the closure of the basin between Archean craton and the arc complex.

2.2.2 Vammala belt

Vammala Nickel Belt is a sublinear, discontinuous feature with mafic-ultramafic intrusions located to the south of the Tampere Schist Belt (Häkli 1971, Papunen and Gorbunov 1985, Peltonen 1995a). The intrusions are found within medium to high-grade migmatites, mostly of arenaceous to argillaceous protoliths, with minor metavolcanics and chemical sediments (Peltonen 1995). The intrusions occur as plugs or pipes (Papunen et al. 1979) or lenses and boudins 'floating' within the migmatitic paragneisses (Peltonen 1995a). Schollen migmatites are the most common migmatite type (Häkli 1979, Makkonen 2015). The mafic-ultramafic rocks can be categorized into ultramafic-only, mafic, and gabbro-hornblendite units formed by differentiation in large granitoid batholiths (Peltonen 1995a).

The ultramafic cumulate bodies are small, 100–1000 m in length, and host all of the economic and most of the sub-economic Ni-Cu ores in the Vammala belt. The ultramafic intrusions are peridotites, pyroxenites or amphibolites in composition. The mafic intrusions are either small, pyroxene gabbros or norites in composition or up to several kilometers long, with a mafic-ultramafic sequence. These intrusions can host sub-economic Ni-Cu ores. The ultramafic rocks units can be subdivided into intrusive bodies with well-preserved mineralogy and textures and amphibolites with metamorphic mineralogy and textures (Peltonen 1995 a).

The Vammala complex ultramafic rocks are composed of olivine ± chromite and olivine-clinopyroxene ± chromite cumulates (Peltonen 1995a). The cumulates are poikilitic ortho or mesocumulates, with the latter texture being more pervasive in the core of the bodies. Intercumulus space is usually filled by poikilitic clinopyroxene as large, several centimeter oikocrysts. Magmatic amphibole and phlogopite, and less commonly orthopyroxene, are also present as intercumulus phases in the ultramafic intrusions of Vammala belt (Peltonen 1995a). Chromium and magnesium-bearing hercynite is present in the upper part of the hornblenditic layer in the Vammala intrusion (Häkli et al. 1979).

The Vammala intrusion hosts the largest Ni-Cu deposit within the Vammala belt, with 6.4 Mt ore of average ore grades of 0.71 wt-% Ni and 0.44 wt-% Cu (Peltonen 1995b). Orebodies occur as 5–70 m thick slabs of disseminated to massive ore. Most of the sulfides in the Vammala type ultramafic intrusions occur as interstitial disseminations and net-textured ores or as sulfide cumulates close to the country rock contact (Häkli et al.

1979, Peltonen 1995b). The major sulfide assemblage in mineralized intrusions is pyrrhotite, pentlandite, chalcopyrite ± cubanite ± mackinawite (Peltonen 1995b). In unmineralized intrusions of the Vammala belt, the ratios of pentlandite/pyrrhotite and chalcopyrite/pyrrhotite are much lower and chalcopyrite can be totally absent, as is the case in Posionlahti intrusion. Some of the sulfides are oxidized into magnetite, pyrrhotite being the most heavily affected (Häkli et al. 1979). Pyrrhotite is also locally altered into pyrite and marcasite. PGE values are low and chondrite-normalized spider diagrams display Pt depletion (Papunen 1986, Makkonen and Halkoaho 2007).

The parental magma of Vammala-type intrusions had arc-type trace element compositions (Peltonen 1995a,b). According to Peltonen (1995a, 2005), the ultramafic, weakly differentiated cumulates in the Vammala belt represent midcrustal arc cumulates that were formed from feeder dikes between lower and upper crustal magma complex, where the upper crustal part has eroded away.

The chromites from the Vammala deposit are anomalously zinc-rich, which Peltonen (1995b) attributes to the Zn-enrichment of the parent magma which was caused by the assimilation of turbiditites, including black schist, and transport by C-O-H-S fluids during the ascension of the parental magma. Introduction of external sulfur through assimilation of black schist caused sulfur saturation and exsolution of a sulfide phase from which the Ni ores formed (Peltonen 1995a,b). The sulfides are PGE depleted on chondrite-normalized diagrams (Papunen 1986). According to Peltonen (1995b), this depletion is due to the segregation of minute amounts of sulfides before emplacement to the level where the cumulates formed.

The Vammala complex is approximately 1890 Ma in age, based on zircon and monazite U-Pb ages from two mafic pegmatoids (Häkli et al. 1979).

3. METHODS

3.1 Fieldwork

The field work and mapping of the study area took place during May-July of 2017. Notes and geological observations were saved as geospatial data to a field computer using GTK's Kapalo application, which is an ArcMap extension. Outcrop photographs were taken with Kapalo mobile phone application. Magnetic susceptibility was measured from bedrock observation points with a handheld analyzer. A digital GMS-2, or in some cases, an analogue JH-8 analyzer was used. A total of 85 hammer and portable rock drill samples were taken from which polished thin sections, whole-rock geochemical, age determination, and petrophysical analyses were made. The author was accompanied by GTK's field assistant Antti Mäkelä during the rock drilling. Matokulma and Palojärvi were the main research targets whereas Hongonniittu was left for less consideration, due to time constraints.

3.2 Whole-rock geochemistry

X-Ray Fluoresence (XRF) method was used to analyze whole-rock geochemistry. Inductively Coupled Plasma-Optical Emission Spectrometry (ICP-OES) was used for the analysis of Platinum Group Elements (PGE) in selected samples. Some samples were also analyzed for trace elements with Inductively Coupled Plasma–Mass Spectrometry (ICP-MS) and ICP-OES, respectively. Samples for XRF and PGE analyses were prepared and analyzed in Labtium Sodankylä (work order 45695) with in-house methods 175X and 176X for XRF, and 705P for PGEs. XRF analyses were done from pressed powder pellets. Trace element and REE analyses were made in Labtium Kuopio (work order 45721), with methods 308M and 308P, respectively. Carbon content of the samples was also analyzed in Kuopio (method 811L).

3.3 Isotope geochemistry

3.3.1 U-Pb zircon

Large, several kilogram hammer samples were taken from observation points SIKA-2017-17 and SIKA-2017-101. The samples were prepared and analyzed in GTK Espoo's facilities.

The samples were first broken with a jaw crusher and pulverized in a swing mill, lighter minerals are then separated from dense minerals with the use of a shaking table. The concentrate is treated with heavy liquids; methylene-iodide (D=3.35) and Clerici solution (D=4.25). After this, magnetic minerals were removed, first with a handheld Nd-magnet and then with a Franz magnetic separator. By using a stereo microscope, the most euhedral and prismatic zircon grains were hand-picked and mounted into epoxy resin, which was halved and polished. Back-scattered electron (BSE) images were taken with a scanning electron microscope (SEM) for targeting spot analysis sites.

The U-Pb dating analyses were performed with a Photon Machine Excite laser ablation (LA) system connected to a Nu Plasma AttoM single collector inductively coupled plasma mass spectrometer (ICP-MS). Samples were ablated within a HelEx ablation cell (Müller et al. 2009) in He gas flow of 0.4 and 0.1 l/min. Before insertion to the plasma, the mixture was mixed with Ar gas flow of 0.8 l/min. To achieve maximum sensitivity, the gas mixture is optimized daily. Ablation conditions were, for beam diameter, pulse frequency, and beam energy density; 25 μm, 5 Hz, and 2 J/cm^2, respectively. Measurements included a pre-ablation, a 10 s on-mass background measurement, and a 30 s ablation with a stationary beam. Calibration standard GJ-1 (609 ± 1 Ma; Belousova et al. 2006) was used throughout the measurements. The standard sample was run before, periodically between, and after analytical analyses.

The presence of common ^{204}Pb was monitored by observing mass 204. The ^{204}Hg originates from the He supply, and the observed counting rate has been stable. The contribution of ^{204}Hg was eliminated with the on-mass background measurements. Glitter program (Van Achterbergh et al, 2001) was used for raw data corrections. Further data reduction was performed using an Excel spreadsheet written by Dr. Yann Lahaye and Dr. Hugh O'Brien of GTK.

The plotting of the results and age calculations were made with Isoplot/Ex 3 program (Ludwig 2003) by Dr. Hannu Huhma and additionally by Dr. Tapani Rämö.

3.3.2 Sm-Nd

Sm-Nd analyses were made in GTK Espoo. The samples were prepared from the same hand samples and prepared and pulzerized the same way as the U-Pb zircon analyses. 120–200 mg of the powdered whole-rock sample was spiked with a ^{149}Sm-^{150}Nd tracer after which the mixture was dissolved in a Teflon bomb with HF-$HFNO_3$ solution. The bombs were then heated for 48 hours, the granite sample in an oven at 180º C and the gabbro in a Savillex screw-cap beaker on a hot plate. The samples were carefully evaporated of fluorides with HNO_3 and then dissolved in 6.2 N HCl. The light rare elements (LREE) were separated from Sm and Nd by conventional cation exchange chromatography, using a modified Teflon-HDEHP (hydrogen di-ethylhexyl phosphate) method of Richard et al. (1976). The total procedural blanks were <0.6 ng (nanograms) and <1.2 ng, for Nd and Sm, respectively. The samples were then diluted to 100 ppb Nd and Sm and placed into disposable 2 ml beakers with 1.5 ml 2 % HNO_3.

The samples were analyzed with using a standard liquid sample introduction system involving a 50 μm meinhart nebulizer, a DSN and a Nu Instruments multi-collector inductively coupled plasma mass spectrometer (MC-ICP-MS) at low mass resolution ($\Delta m/m = 400$). The isotopic measurements were performed in static mode using 5 Faraday detector and 10 blocks of integrations, lasting some 5 seconds.

LaJolla standard reference material was diluted down to 200 ppb Nd and used to monitor the precision and accuracy of the measurements at the beginning and the end of each analysis session. Nd ratios were normalized to $^{146}Nd/^{144}Nd = 0.7219$. The error estimation for $^{147}Sm/^{144}Nd$ analyses is better than 0.4 %. The average analyzed $^{143}Nd/^{144}Nd$ ratio for the LaJolla standard was 0.511822±0.000004 (2 SD, n=4). The accepted value for LaJolla standard, on the basis of 944 values from worldwide laboratories (http://georem.mpch-mainz.gwdg.de/), is 0.511844. The value for analyses has been adjusted accordingly, resulting in a correction of +0.43 on all εNd values.

The samples were analyzed by Yann Lahaye and Leena Järvinen of GTK.

3.4 Mineral chemistry

Mineral compositions were analyzed with EPMA from polished thin sections. The main goal of the analysis was to determine the main components and Ni content of orthopyroxene and olivine. The samples were chosen on the basis that they contain one or both of these minerals. Clinopyroxene, amphibole, micas, oxides, feldspar, and apatite analyses were also made from certain samples.

EPMA study was carried out in GTK Espoo's microprobe laboratory by Mr. Lassi Pakkanen. The author was present only during the setting of some analysis points. Qualitative Electron-Dispersive X-ray Spectroscopy (EDS) analyses were sometimes made to identify phases and textures, such as small, dense minerals or exsolutions. The instrument used in the study was a Cameca SX100. In silicate and apatite analyses acceleration voltage of 15 kV, beam current and diameter of 20 nA and 5 µm were used. For oxide analysis, the conditions were 15 kV, 40 nA, and 1 µm.

The standards used for silicate analyses were diopside (Si, Mg, Ca), almandine (Al), hematite (Fe), rhodonite (Mn), vanadium (V), rutile (Ti), cobaltite (Co), chromite (Cr), sphalerite (Zn), pentlandite (Ni, S), tugtupite (Na, Cl), and barite (Ba).

Diopside, almandine, hematite, rhodonite, vanadium, rutile, chromite, sphalerite, and pentlandite were also used in the oxide analyses.

Celestine (La), apatite (P, Ca) were used together with diopside, almandine, rhodonite, and chromite as standards for the apatite analyses.

3.5 Geophysics

3.5.1 Petrophysics

The petrophysical properties of all samples were measured at GTK Kuopio. Ordinary physical properties mass, volume, and density and magnetic properties; magnetic susceptibility, mass susceptibility, intensity of remanent magnetization were measured

and Q-ratio calculated for all samples. The measurement procedures are described in Airo and Säävuori (2013).

3.5.2 Gravity measurements

GTK conducted gravity measurements as profiles over the studied intrusions (Figure 3). One profile was made over Palojärvi, one over Hongonniittu, and another two over Matokulma. The petrophysical properties (densities) of the hand samples were used in the modelling of the results. Matti Niskanen (GTK) produced Bouguer anomaly models based on results, which are presented and discussed in chapter 4.5.2. The Bouguer anomaly measurements were adjusted to regional levels provided by the Finnish Geodetical Institute (FGI) by linear fitting.

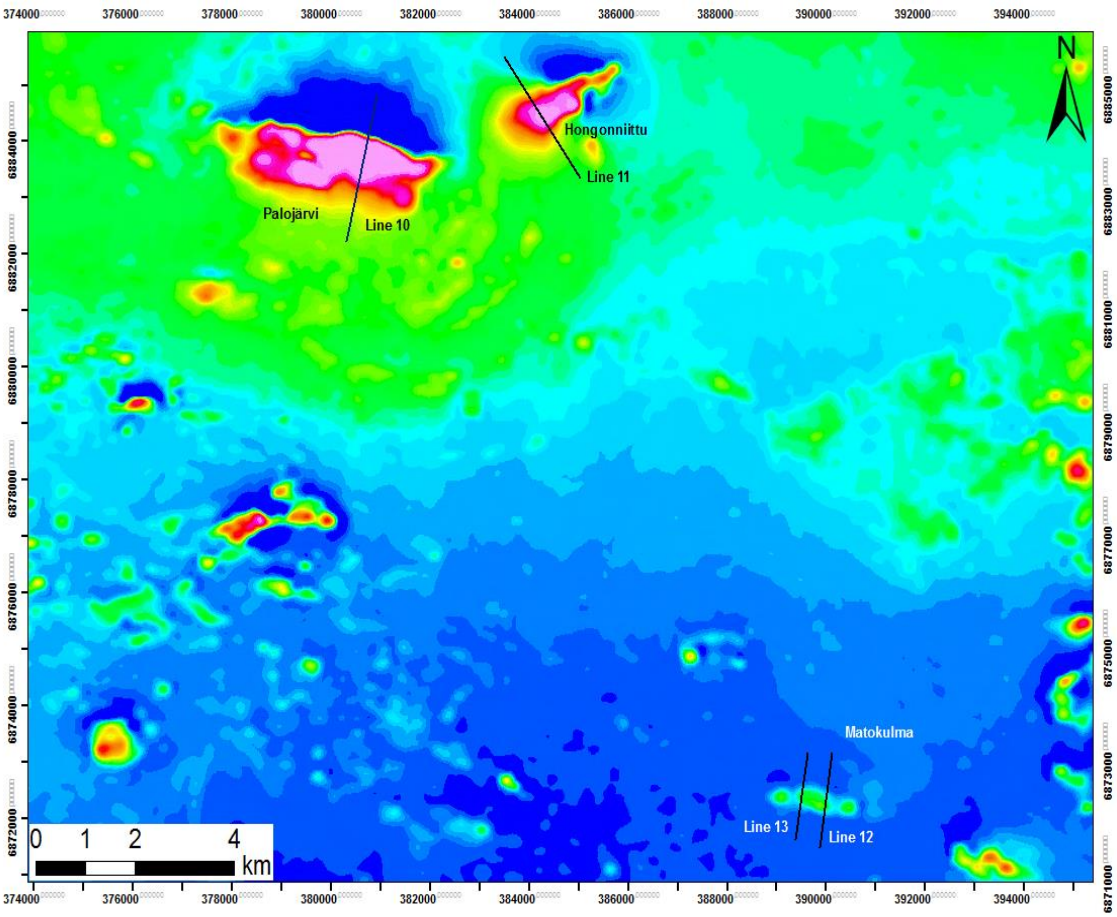

Figure 3. Map of the Bouguer anomaly profiles over the studied intrusions on a magnetic anomaly map (Red = maximum, blue = minimum). Line 10 goes over the gabbroic (positive magnetic anomaly) area over Palojärvi, line 11 over Hongonniittu, lines 12 and 13 (lower right corner) over Matokulma.

3.6 Data analysis and visualization

GCDKit 5.0 (Janousek et al. 2006), a program written and run in R-language, and Microsoft Excel 365 were used for statistical analysis of the geochemical data and for plotting figures.

4. RESULTS

4.1 Field observations

4.1.1 Matokulma

The field observations from Matokulma are shown in Figure 4. Matokulma is at the surface plan section an elliptical intrusion about 1700 m in length and about 330 m in width. The easternmost part of the intrusion is well exposed and accessible due to clearcutting and steeper topography.

The mafic rocks in Matokulma are usually melagabbros, dark green in appearance with white to pink anhedral crystals of plagioclase, when present. Black to dark green, round, porphyric amphiboles give the rocks their color and texture. In most outcrops the amount of plagioclase varies within few dozen centimeters so that the appearance of rocks changes from fully dark green ultramafic to dark green with white or pink plagioclase, gabbroic. There are some outcrops on the southern side in the middle of the intrusion with black-and-white gabbros, with black amphibole, and abundant white plagioclase.

Compositional layering is visible on one outcrop (SIKA-2017-6, Figure 5), located on the eastern end of the intrusion. The observed layers are up to 20 centimeters in width with compositions varying from fine-grained dark green ultramafic to medium-grained gabbroic, with white plagioclase. The layers have a dip direction/dip of 250/70.

In the eastern part of the intrusion there are outcrops where sheared mafic dikes intrude the gabbro or the tonalitic country rock (e.g. outcrop SIKA-2017-28.1, Figure 6A). The

dikes are 0.2–1.5 m in width, dark gray in color, and dip steeply (70–80º) towards north (350-010) (Figure 6B). The dikes are present both on the northern and southern edge of the intrusion, and between. They are composed of deformed, round, black amphiboles in a fine-grained gray groundmass. Some of the dikes have less weathered leucocratic veins and coarser black amphibole. On observation point SIKA-2017-169, the mafic dike cuts garnet-tonalite country rock (Figure 7A). The tonalite has mafic enclaves and the dike also has xenoliths of tonalite within (Figure 7B).

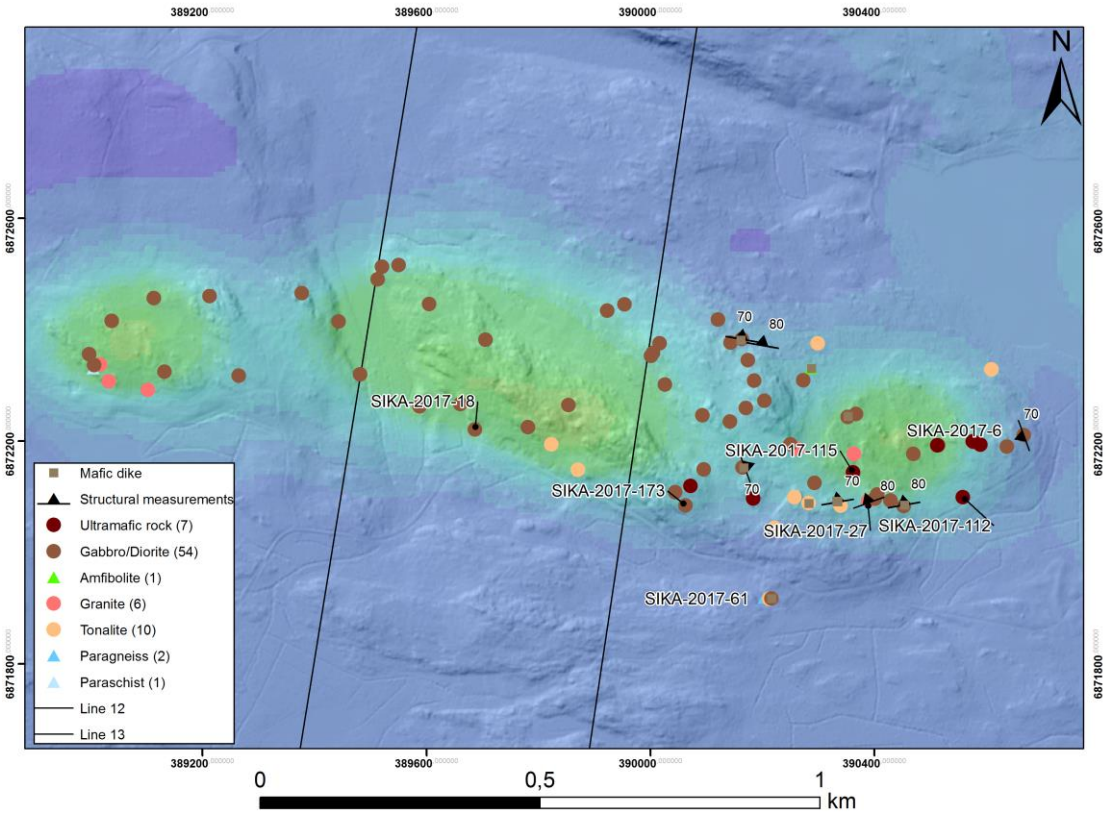

Figure 4. Observations from Matokulma. Number of observations in parentheses after rock type. Observation points mentioned in writing are marked. The background layer is a digital elevation map (DEM), overlain with an aeromagnetic anomaly map (Yellow– maximum, blue – minimum). DEM from National land survey of Finland.

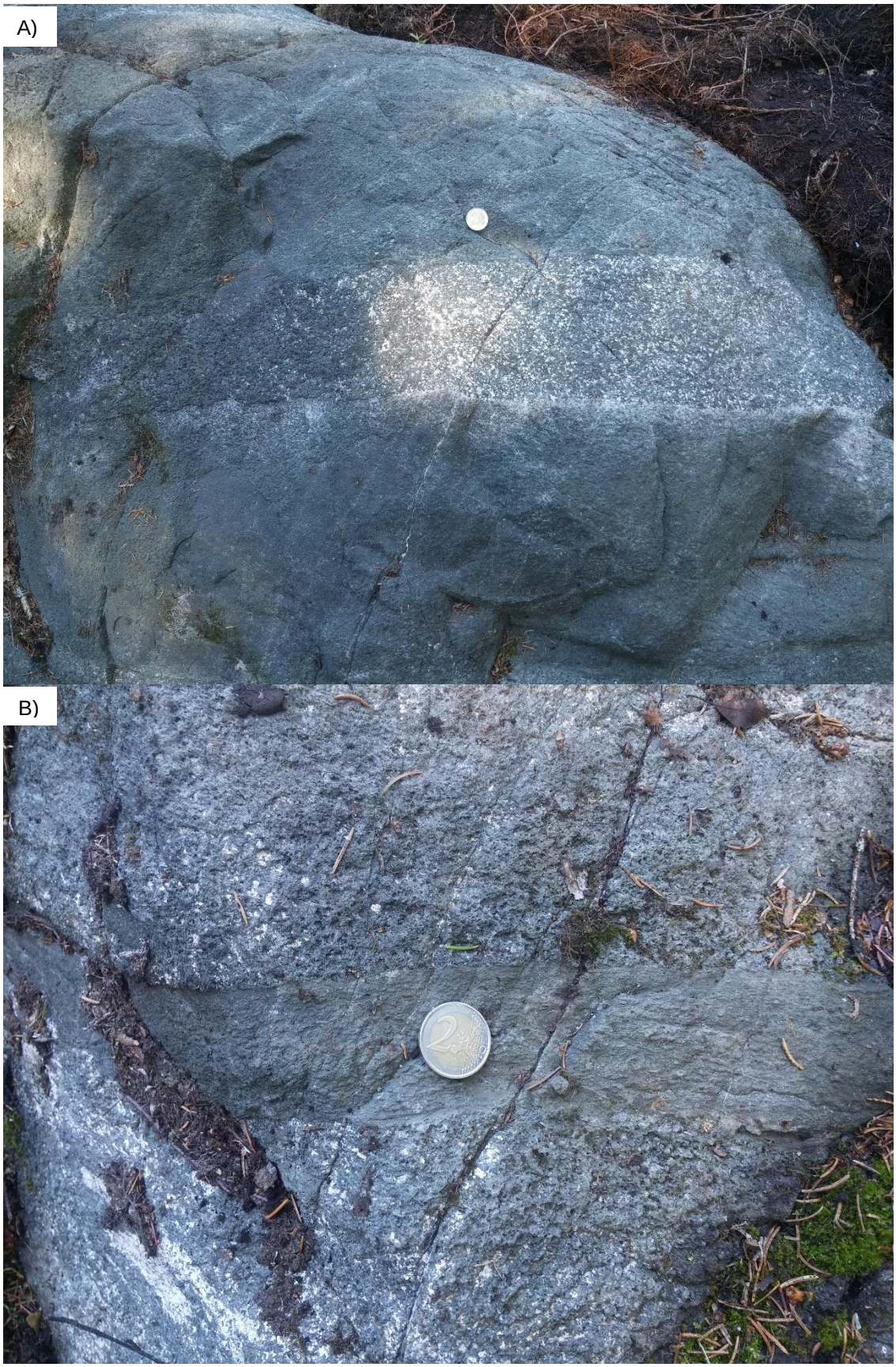

Figure 5. Magmatic layering on outcrop SIKA-2017-6. A) A coarse-grained layer is seen in the middle, with a leucocratic, anorthositic narrow section beneath it before gradation to more melanocratic and fine-grained mafic layer. B) Ultramafic, fine-grained layer between coarser, gabbroic layers (sample SIKA-2017-6.4). The coin is approximately 2.6 cm in diameter.

Figure 6. Mafic dikes in Matokulma. A) Mafic dike crosscuts tonalitic country rock and dips towards NNW (outcrop SIKA-2017-28). B) Laminar, NE-dipping structure formed by thin sheets of coarser mafic minerals (SIKA-2017-58).

Figure 7. A) Mafic dike cutting the garnet-tonalite country rock. B) A close up of the country rock and the mafic enclaves within it. Observation point SIKA-2017-169

In observation point SIKA-2017-121, the dike is schistose and has lenses of light-colored plagioclase and quartz.

The contact area between the mafic rocks and country rock is visible on the southern side. The rocks surrounding the intrusion are garnet-biotite-tonalite, granite, and biotite-mica schist. There is a contact zone on outcrop SIKA-2017-27, consisting of garnet-paragneiss with euhedral 1 to 3 cm garnet crystals in a fine-grained biotite rich mass (Figure 8).

Figure 8. Large, euhedral garnets in paragneiss, adjacent to the Matokulma intrusion. Observation point SIKA-2017-27.

The paragneiss also has an inclusion of coarser arenaceous material. A few meters from the paragneiss is a mixed rock, composed of coarse green amphibole, white plagioclase, quartz, and epidote.

The mixed rock is situated between the gabbro and the paragneiss. Similar mixed rock can also be found further to the west on outcrop SIKA-2017-18.

Granite is found in the center of the intrusion on a few outcrops. The granite is light to pink in color and medium grained. The relationship between the gabbro and the granite is unclear, except on outcrop SIKA-2017-115, where the gabbro and the granite are in contact and display a mingling texture (Figure 9). The granite in contact with the gabbro

is more leucocratic and finer-grained, than farther away from the contact. Granite is also present as the country rock on the southern edge of the western part of the intrusion.

Quartz-feldspar-filled fractures and veins and also aplite dikes are observed in some of the outcrops.

Some of the weathered boulders from the gabbroic rocks are rusty in appearance. Most of the mafic rocks in Matokulma have very low magnetic susceptibilities when measured with a handheld analyzer. In many cases, the value is below detection limit and at most, $2000 \cdot 10^{-5}$ SI. The median value is $50 \cdot 10^{-5}$ SI.

Figure 9. A) Mingling texture between leucogranite and melagabbro from observation point SIKA-2017-115, from Matokulma. The granite nearest to the contact with the gabbro is fine-grained and white. B) Close up of mingling texture between granite and gabbro.

4.1.2 Palojärvi

Palojärvi intrusion is in surface plan section up to 3400 m long and 900 m wide in E-W and N-S, respectively. Most of the observations are from the well exposed area (Figure 10). The bedrock is poorly exposed on the eastern side of the intrusion and fewer observations were made.

The mafic rocks in Palojärvi are usually dark gray to greenish gray, middle to coarse-grained, often porphyric, melagabbros. Porphyric dark green or black amphibole 10–20 mm, up to 40 mm in size is present in virtually all mafic rocks which are, in ultramafic cases, macroscopically exclusively composed of coarse-grained amphibole. The amphibole is usually present as round grains. The gabbros are usually composed of amphibole, light plagioclase, and dark brown biotite. Porphyric gabbros often have bumpy weathering surfaces (Figure 11A).

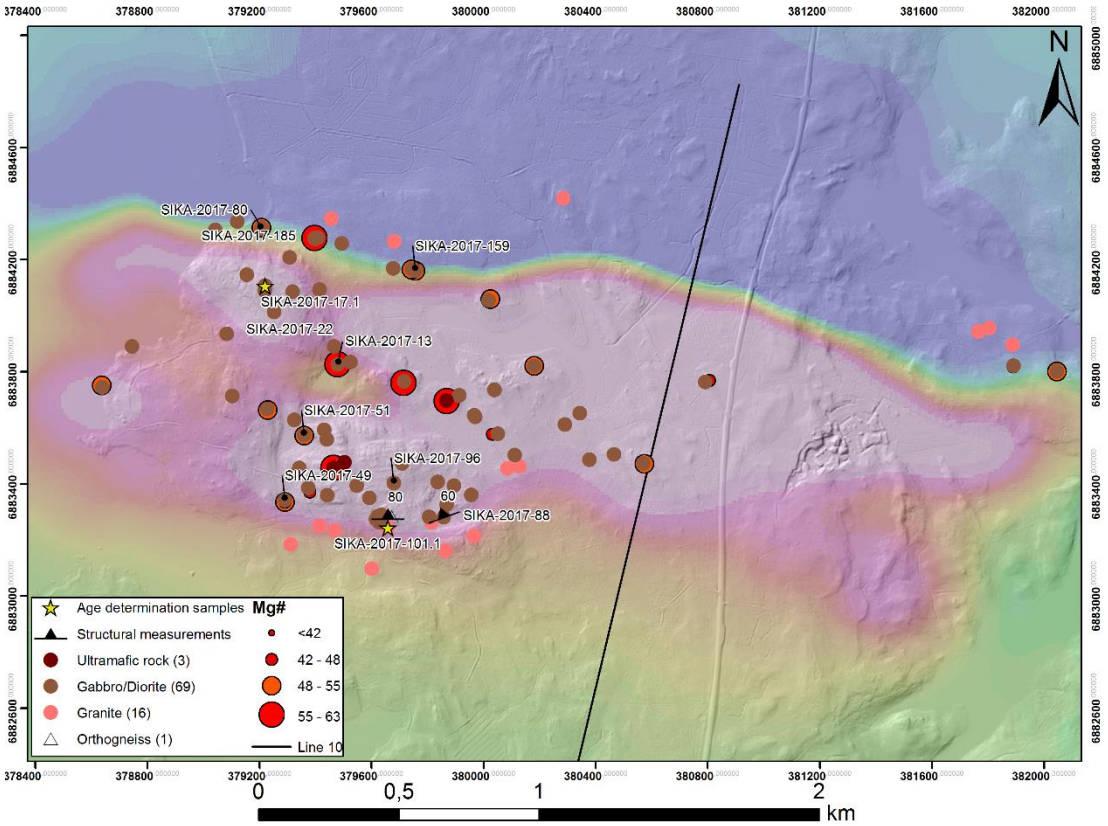

Figure 10. Observations from Palojärvi. Number of observations in parentheses after the rock type. Age determination samples are marked with a star. Observation points mentioned in the text are marked. Background map is DEM, overlain with a magnetic anomaly map (Blue – minimum, pink – maximum). .DEM from National land survey of Finland.

Black-and-white gabbros/diorites are also present (SIKA-2017-13,-96,-159, and -185). They are composed of porphyric, light plagioclase, black to dark green amphibole, dark brown biotite, and often contain some quartz (Figure 11B). These outcrops are located on the northern and southern edges of the intrusion, except for SIKA-2017-13.1, which is located in the middle.

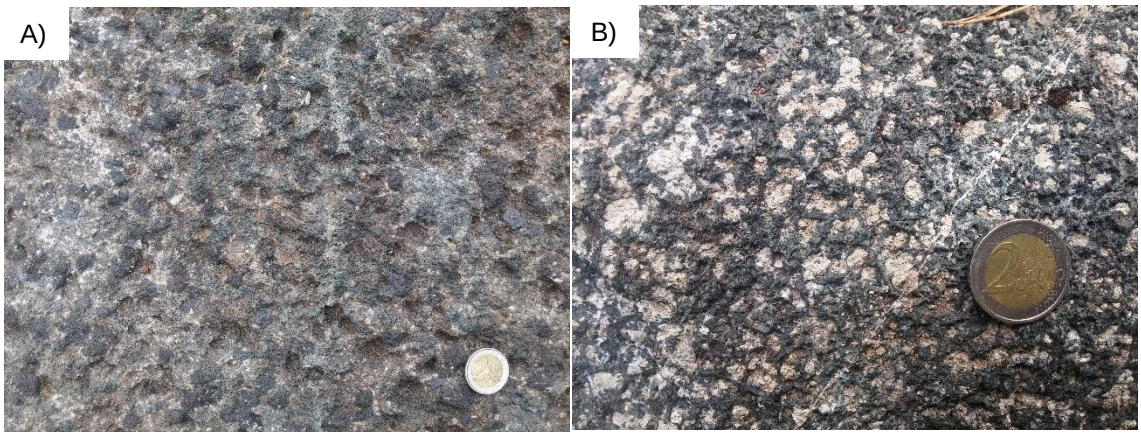

Figure 11. A) Porphyric gabbro with a bumpy weathering surface. Observation point SIKA-2017-80. B) Porphyric plagioclase (light), which is more weathered than the surrounding dark green amphibole. Observation point SIKA-2017-159.

Granite is found both on the northern and southern side of the intrusion. Haukkavuori, located near the SE contact of the intrusion, is composed of foliated, light-colored granite. Similar granite is present also to the east of Haukkavuori. The granites are strongly foliated and often quartz-rich. They are medium-grained, leucocratic, light to pink, and with a small amount of mafic minerals, amphibole and biotite. Felsic veins and dikes are common throughout the intrusion and they often contain mafic inclusions. Some dikes are pegmatitic and up to 10 cm in width. A garnet-bearing dike with mafic inclusions cuts the gabbro at observation point SIKA-2017-22.1.

The marginal zone of the gabbro is seen on the southern side of the intrusion. The contact area between the gabbro and granite is gneissose, with granite being on the south and the gabbro on the north side, respectively (Figure 12A). The strike of the gneissose contact varies from 120 to 70–80, with steep dips towards North.

Compositional layering is seen near the contact zone, at observation point SIKA-2017-88 (Figure 12B). There the layers have a steep dip towards NW (340/70). Samples SIKA-2017-88.1 to 88.3 are taken from overlapping layers. The layered mafic rock is intruded by felsic dikes and veins with mafic inclusions. The layers are compositionally gabbroic, with gradation towards plagioclase-rich, anorthositic, with varying grain sizes and proportions of light plagioclase and amphibole. The layers are cut by leucocratic

plagioclase-rich dikes. Similar, but not as clear, layering is seen in observation point SIKA-2017-51.

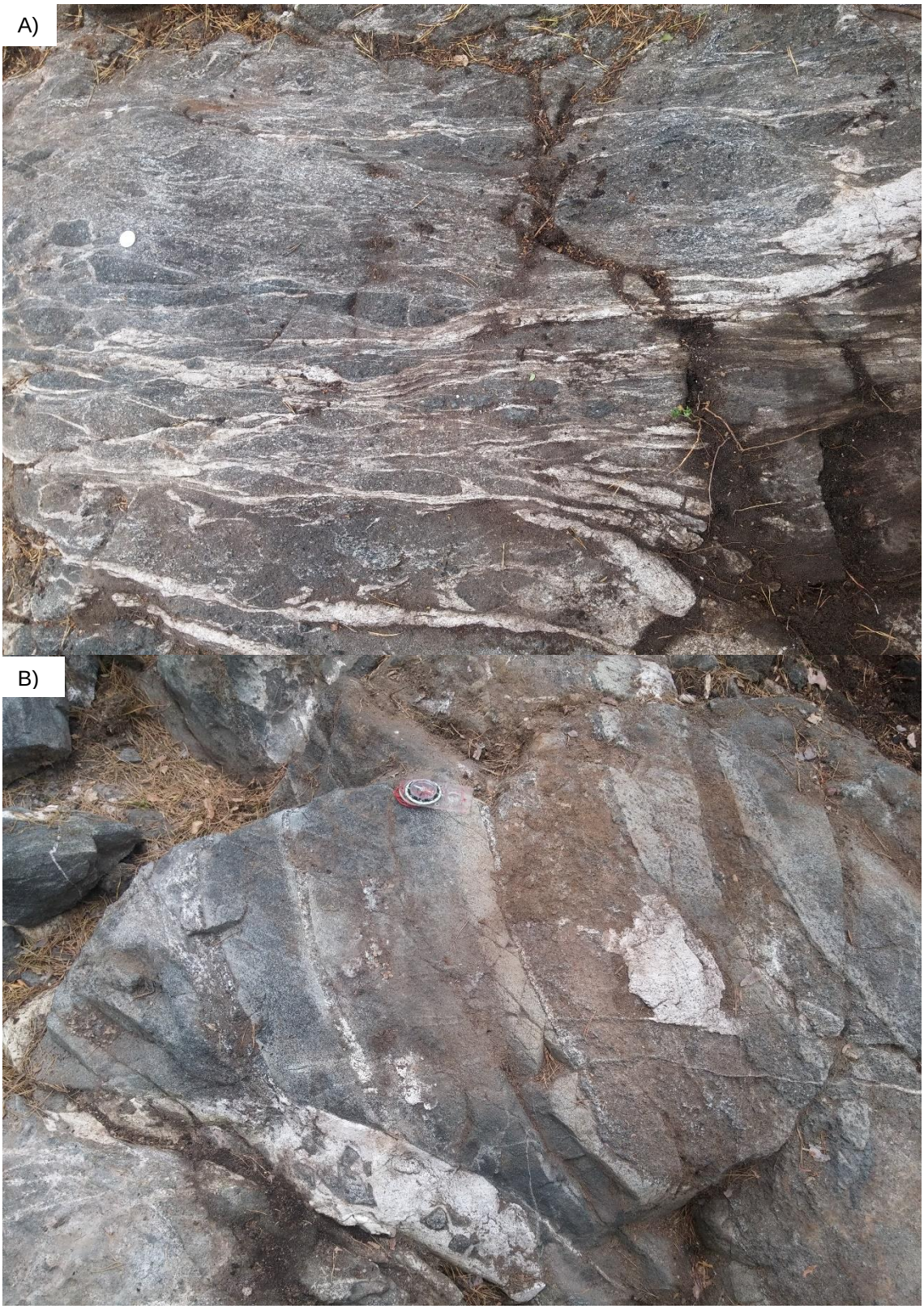

Figure 12. A) Gneissose contact area on the southside of Palojärvi intrusion. Observation point SIKA-2017-164. B) Layered gabbro with layers dipping towards NNW (340/70). Felsic dike cuts the layering and contains mafic inclusions. The compass is on a layer that gradually changes from melagabbro towards more plagioclase-rich. Observation point SIKA-2017-88.

Contact relationship textures are seen at the edges the intrusion on some observation points. Granite and granodiorite outcrops occasionally have rounded mafic inclusions (Figure 13 A-B). A chaotic mafic rock is seen at observation point SIKA-2017-49, on the southwestern edge of the intrusion (Figure 13 C-E). The mafic rock is cut by felsic veins. The chaotic rock contains many inclusions or enclaves, the most conspicuous are the pear-shaped inclusions with mafic, melanocratic centers and leucocratic edges, surrounded by smaller leucocratic, ellipsoid inclusions. Similar structures are also seen at the northern edge (SIKA-2017-159, Figure 14 A-C).

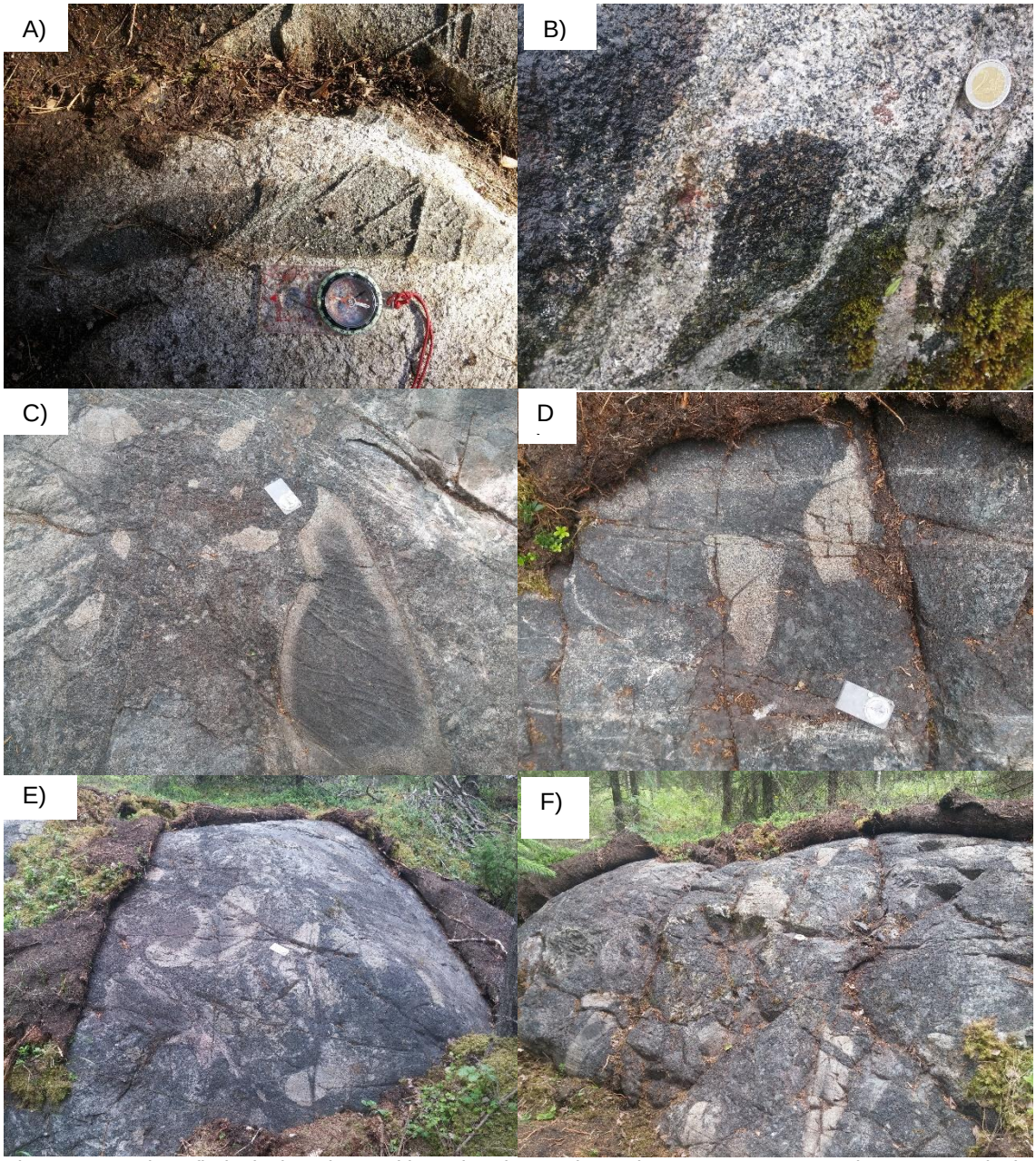

Figure 13. A-B) Mafic inclusions in granitic rock. Observation points SIKA-2017-11 and -22, respectively. In B), garnet-bearing leucocratic dike has stoped surrounding gabbro. C-F, Chaotic mingled rock at observation point SIKA-2017-49 near the SW edge of Palojärvi intrusion. C) shows a mafic, ellipsoidal blob with leucocratic edges. Leucocratic blobs next to coarse amphibole grains (above the compass).

Figure 14. Mingling between mafic and felsic magmas. Round enclaves of fine-grained gabbroic material within more leucocratic and coarser-grained dark-green amphibole. Observation point SIKA-2017-159, northern edge of Palojärvi intrusion.

Mafic rocks have high but variable magnetic susceptibilities. The values on the same outcrop may change from thousands to tens of thousands of units in a matter of a few centimeters. Mean value for the mafic rocks is $6000 \cdot 10^{-5}$ SI, with values up to $20{,}000 \cdot 10^{-5}$ SI.

4.1.3 Hongonniittu

Hongonniittu intrusion is at the surface plan section an irregular ellipsoid in shape and about 1400 m long and 500 m, respectively (Figure 15). The intrusion is oriented NE-SE. Most of the rock types in Hongonniittu are medium-grained, dark gray to greenish black gabbros which are occasionally highly weathered and crumble when struck with a hammer. The gabbros are composed of black amphibole, light plagioclase, and brown biotite. The amphibole is occasionally present both as porphyric grains 10–30 mm in size and also even-grained with plagioclase. Pegmatitic granite and gneiss is also found in the area.

Magnetic susceptibilities range from 0 to $15{,}000 \cdot 10^{-5}$, with a mean of $5600 \cdot 10^{-5}$. The values are, as in Palojärvi, highly variable within just centimeters.

The rock types in Hongonniittu seem similar to the ones in Palojärvi but due to time constraints were not thoroughly mapped.

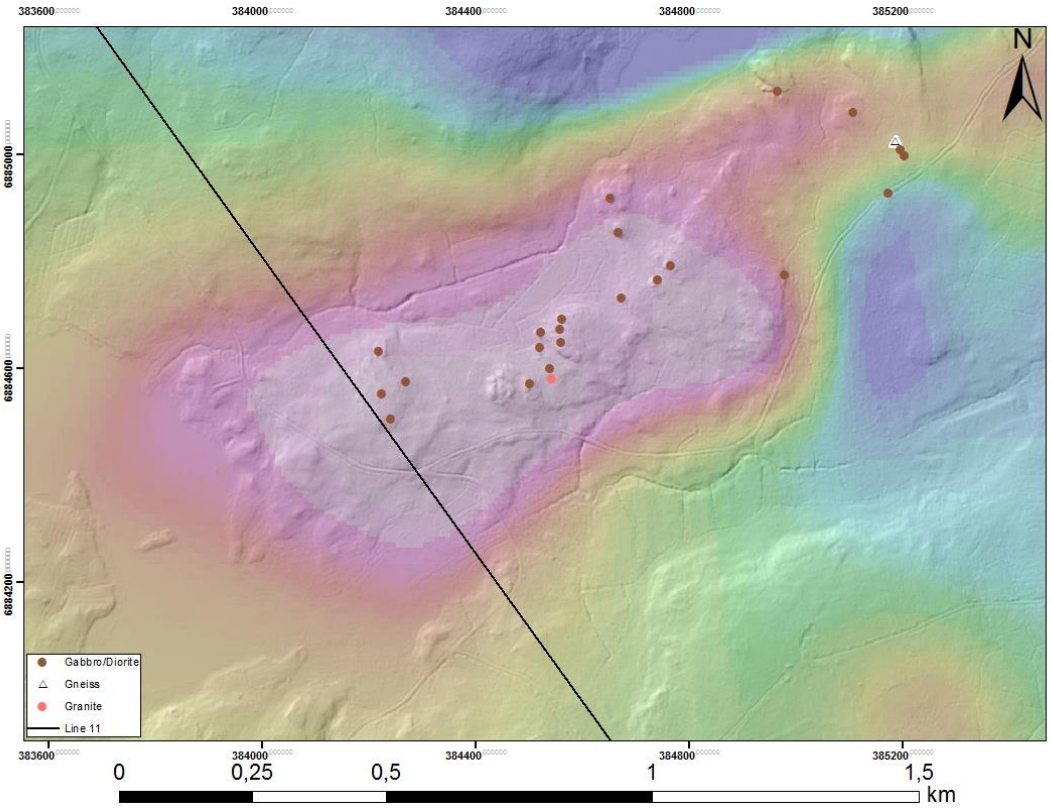

Figure 15. Observations from Hongonniittu. Background map is DEM, overlain with an aeromagnetic anomaly map (Blue – minimum, red – maximum). DEM from National land survey of Finland.

4.2 Petrography

4.2.1 Matokulma

Gabbro

All of the mafic rocks from Matokulma are altered to some degree, many of them intensively. The better-preserved samples have distinguishable pyroxene and primary amphibole phases. In the more altered samples, the mineral phases present are mostly actinolite-tremolite and chlorite or serpentine, seriticized plagioclase, and sometimes carbonate or talc, most often as fracture filling.

Most samples appear to be cumulates, where euhedral to subhedral plagioclase is the main cumulate phase, usually with subhedral clinopyroxene, but sometimes also with orthopyroxene. The clinopyroxene grains are often partly resorbed and have bubbly interiors and altered grain boundaries. Poikilitic intercumulus amphibole encloses the cumulate phases. In some samples orthopyroxene and, also plagioclase, are in the intercumulus phase. Opaque phases, mainly pyrite and chromite but also chalcopyrite, are present in trace amounts. No olivine was found from any of the samples.

The most mafic samples are composed of amphibole and clinopyroxene with or without orthopyroxene (Figure 16). Plagioclase may be present as a minor cumulus or intercumulus phase or both. Present are also secondary amphibole, chlorite ± serpentine, with possible minor opaque minerals and carbonate.

Amphibole is by volume usually the most abundant mineral followed by either clinopyroxene or plagioclase. Based on the modal mineralogy and the predominant poikilitic texture of amphiboles, the samples can be classified as poikilitic amphibole

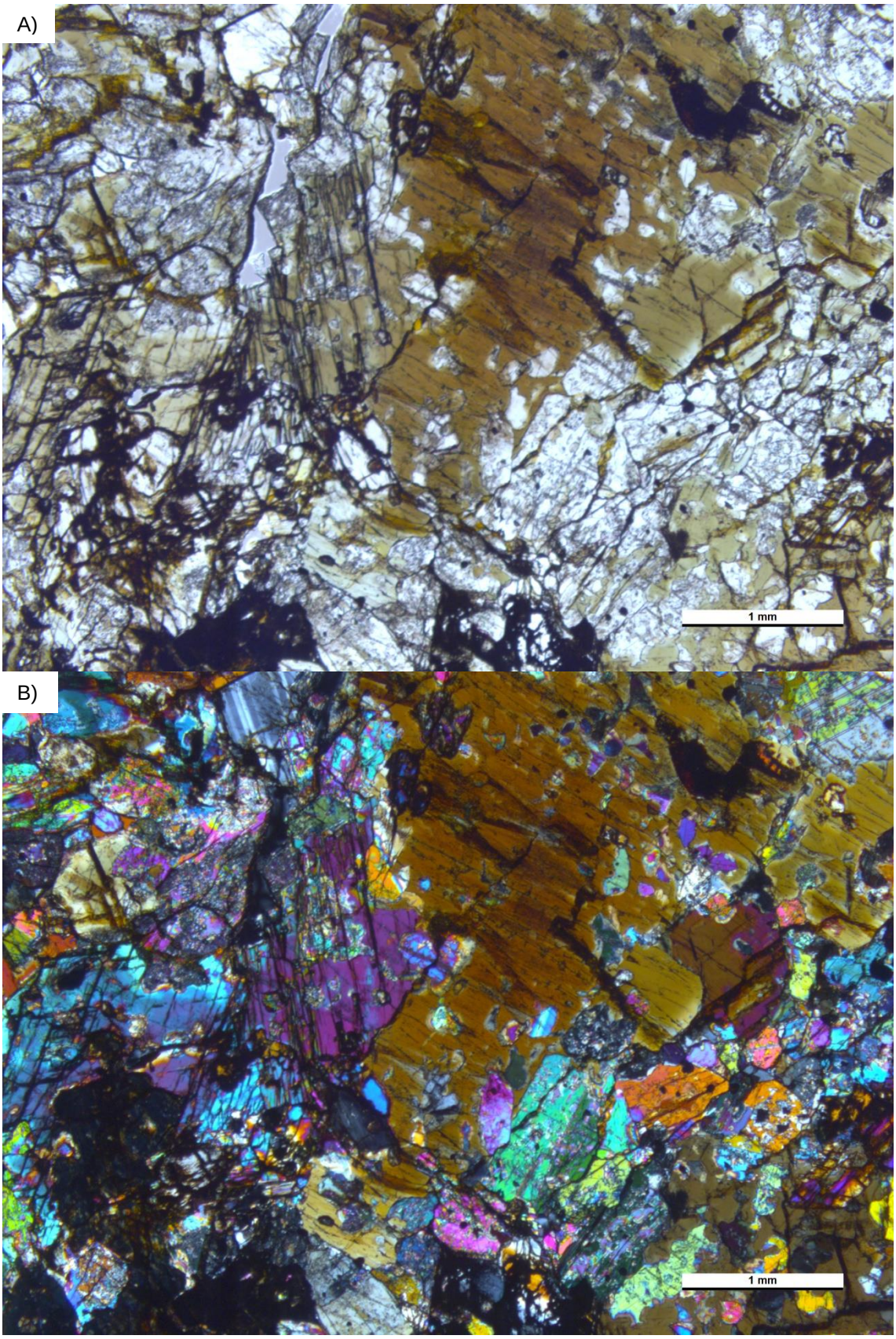

FIGURE 16. Poikilitic gabbro-norite from Matokulma. Amphibole shows cleavage, pleochroism in brown, and blue to purple IF colors. Orthopyroxene is present as dark brown, stained, cumulus crystals in PPL. Clinopyroxene is light in PPL and displays a bubbly texture and brighter, 3º IF colors. Plagioclase is present as an intercumulus phase. Photomicrographs of sample SIKA-2017-115.2. A) PPL, B) XPL.

gabbros, poikilitic amphibole gabbro-norites, and the heavily altered samples as amphibolites.

Based on the preserved cumulus textures, the clinopyroxene crystallized first, followed by orthopyroxene and plagioclase and finally poikilitic amphibole.

Amphibole

Poikilitic amphibole is present in most samples. It is present in large anhedral, poikilitic crystals which are pleochroic, light-light brown-dark brown in plane-polarized light (PPL). In some samples the amphiboles display pleochroism in more green to light blue colors. In the more primitive samples, the amphiboles are stained by opaque black or rusty pigment, which is often oriented parallel to the cleavage directions. Many clinopyroxene crystals have a rim of pleochroic amphibole, which has different optical properties than the surrounding intercumulus amphibole. There is sometimes weakly pleochroic actinolite within the poikilitic amphibole, formed by amphibolitization of cumulus clinopyroxenes. This process is evident in less altered samples were cumulus clinopyroxene crystals are rimmed by actinolite. Some highly altered samples are composed mostly of actinolite. Amphibole is also replaced by biotite in some samples and, in some samples, further altered to chlorite.

Clinopyroxene

Together with plagioclase, clinopyroxene is the most abundant cumulus phase. Clinopyroxene is usually subhedral and partially altered or resorbed, either from the rim in contact with the poikilitic amphibole or from the middle of the grain where their texture appears bubbly (Figure 17). Clinopyroxene appears light brown in PPL.

Orthopyroxene

Orthopyroxene is light or stained reddish-brown in plane-polarized light and often displays pleochroism from light to light red. Orthopyroxene is usually subhedral, 1–2 mm in diameter, and in cumulus phase together with clinopyroxene ± plagioclase, but in sample SIKA-2017-173.1, it is also present in as a poikilitic intercumulus phase.

Plagioclase

Plagioclase is present in most samples and is usually at least partly seriticized and saussuriticized or otherwise pigmented, and in many samples completely altered.

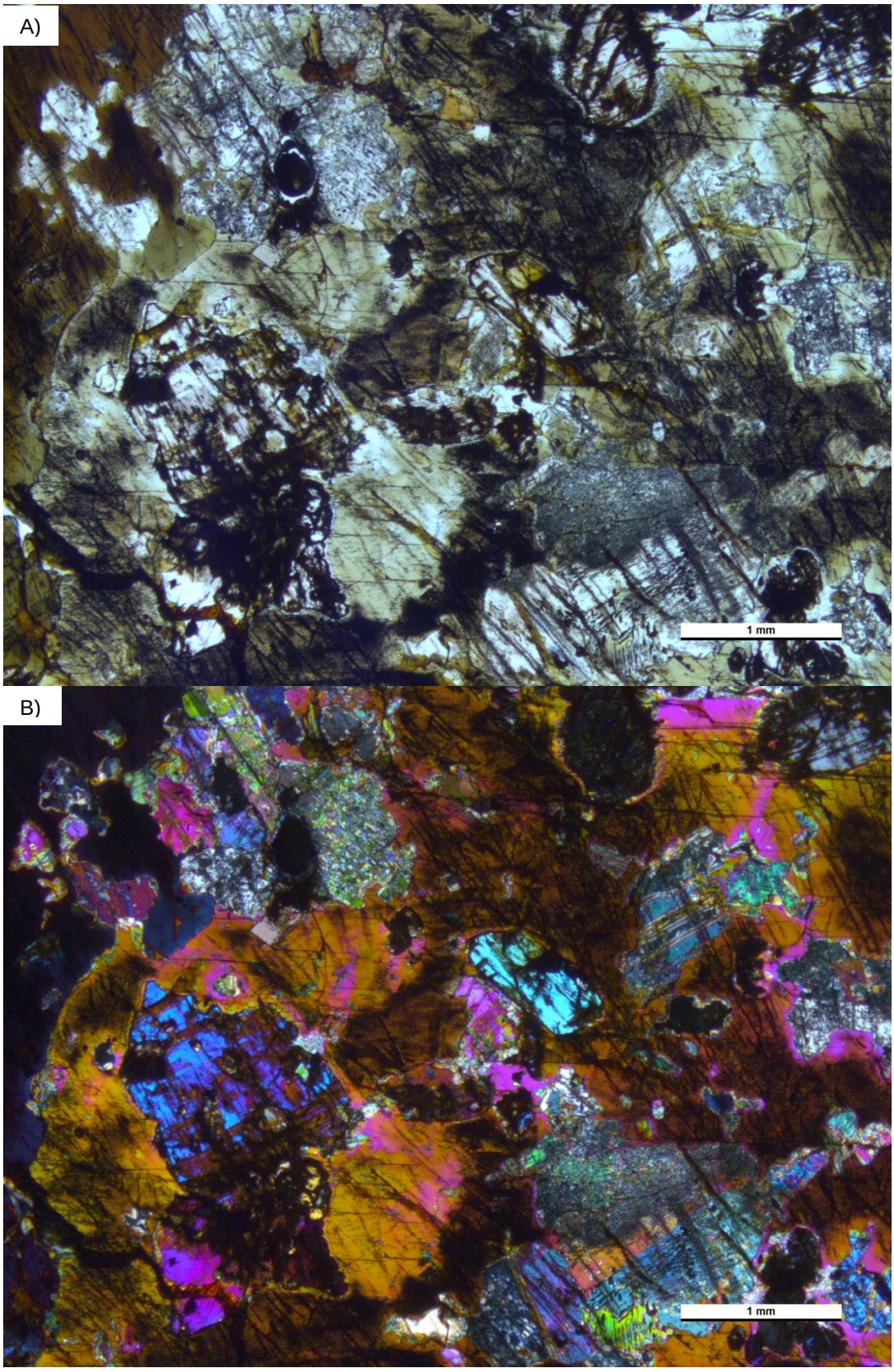

Figure 17. Cumulus orthopyroxene and clinopyroxene within poikilitic amphibole. Orthopyroxene is present as euhedral cumulus crystals, which are stained brown. Clinopyroxene occurs as mostly anhedral crystals, with bubbly, resorbed textures. Some clinopyroxene crystals display twinning. Photomicrographs of sample SIKA-2017-115.2. A) PPL top, B) XPL.

Plagioclase occurs most often in cumulus phase as euhedral to subhedral crystals. In the most primitive samples, plagioclase is present as a late, interstitial phase.

Phlogopite and biotite

Pleochroic, colorless to pale orange mica is present in the more primitive samples as a minor mineral. Phlogopite displays plastic deformation textures and is often altered from the interior, where there is a colorless mineral with high interference colors, or throughout to chlorite. Some crystals have an opaque mineral stripe, which is oriented parallel to the length axis of the crystal. Dark brown, pleochroic biotite is common in more altered samples.

Chlorite

Chlorite is present in the more altered samples, within the poikilitic amphibole, most likely replacing clinopyroxene or as further alteration product of phlogopite/biotite. It displays pleochroism from colorless to light green with anomalous blue-gray or ink blue IF colors.

Serpentine

Serpentine is, together with chlorite, present in the more altered samples. Serpentine is most likely the alteration product of orthopyroxene.

Opaque

Opaque phases are not common in most samples. When present, chromite and pyrite are the most common phases. Some pyrite grains have chalcopyrite inclusions. Pyrrhotite is uncommon.

Other phases

Titanite is present in some samples located at the edge of the intrusion. Apatite is a common accessory mineral in many samples. K-feldspar is present in sample SIKA-2017-115.2.

Dike rocks

The dike rocks are strongly altered, and primary minerals are present only in sample SIKA-2017-58.1, which is later described in detail, together with sample SIKA-2017-119.1. Other samples are composed of sericitized plagioclase, pleochroic light green or dark green to green amphibole, brown biotite, which is often altered into chlorite with anomalous ink-blue interference colors, and varying amounts of quartz and opaque minerals. The strongly altered samples are often fine-grained, foliated, and sheared. Amphibole is often present as groups of coarser, platy grains. Quartz, if present, occurs as groups of deformed grains or as elongated grain aggregates, oriented parallel to the foliation.

Sample SIKA-2017-58.1

The sample is nonfoliated and composed of phenocrysts of subhedral to anhedral clinopyroxene and orthopyroxene in a ground matrix of euhedral, often sectored plagioclase, with accessory biotite and dark green amphibole (Figure 18). Orthopyroxene displays light green–light red pleochroism and up to 2º IF colors. Some of the grains are partly or completely surrounded by dark green pleochroic amphibole (uralitized). Clinopyroxene is light brown in color, has a bubbly texture, displays 2º IF colors, and has a reaction rim in contact with plagioclase. Pyroxenes occur often as glomeroporphyritic groups. Most of the plagioclase crystals are euhedral, randomly oriented, and largely unaltered. Some plagioclase crystals are equal in size to the largest anhedral pyroxene crystals. Opaque, often occurring as exsolutions of biotite, and euhedral apatite crystals are present as minor phases. Opaque phases are chromite and magnetite. The sample is classified as gabbro-norite, based on the prevalence of plagioclase and presence of both pyroxenes in roughly equal ratios.

Sample SIKA-2017-119.1

The sample is highly altered, sheared, and foliated. It is fine grained and actinolite-rich in composition. Besides light-light green pleochroic actinolite, the other phases are highly altered plagioclase, dark brown biotite, and opaque minerals. The opaque minerals are in conjunction with biotite and amphibole and are often composed of intergrowths of several phases.

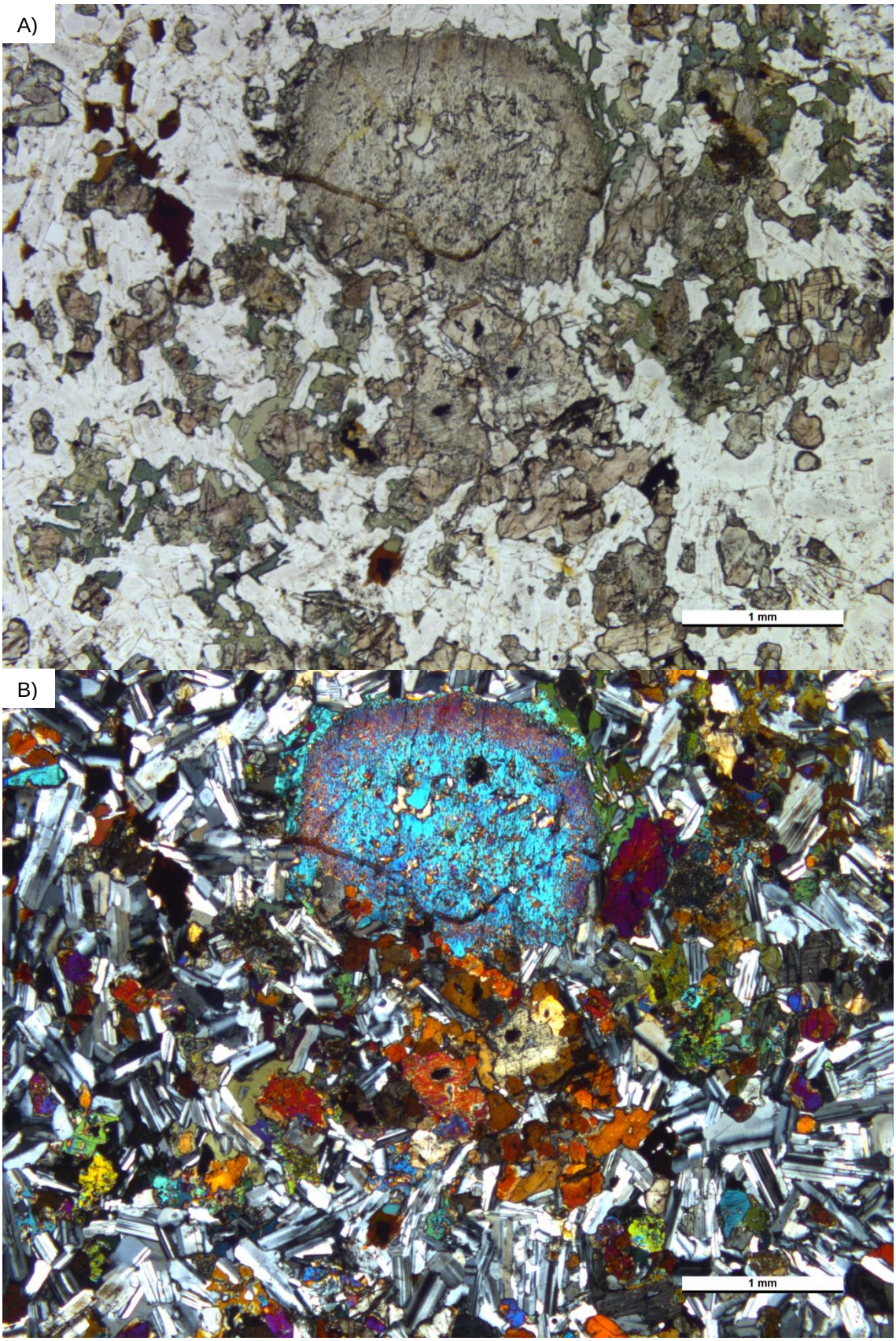

Figure 18. Dike rock from Matokulma with porphyric pyroxenes in a groundmass of euhedral plagioclase crystals. The large, circular crystal in the top middle is clinopyroxene. Dark green to blue green crystals are amphibole, orthopyroxene displays dark gray to orange and clinopyroxene blue to yellow, 2º interference colors. The porphyric clinopyroxene and many plagioclase crystals are zoned. Pyroxene-plagioclase contacts often have amphibole. Photomicrographs of sample SIKA-2017-58.1. A) PPL B) XPL.

4.2.2 Palojärvi

Gabbros

The samples from Palojärvi are composed mostly of poikilitic, pleochroic primary amphibole, seriticized cumulus plagioclase ± orthopyroxene ± clinopyroxene, and Fe-Ti oxides. Actinolite is a common alteration phase.

Other minerals present are biotite, which is sometimes chloritized, metasomatic actinolite-tremolite and/or cummingtonite. Opaque minerals, mostly Fe-Ti oxides and occasionally pyrite or chalcopyrite, are very common in certain samples, both as discrete grains and grain aggregates. Accessory apatite is common, and some samples also have anhedral quartz and zircon. Symplectitic textures are seen in many samples (e.g. SIKA-2017-51.1) surrounding plagioclase grains and completely altered cumulus crystals, likely pyroxenes, within poikilitic amphibole. The reaction coronas are perhaps amphibole-spinel symplectite, which is optically isotropic at times, probably due to varying ratios of amphibole and spinel.

The samples are classified as gabbro-norites, olivine-norites, gabbros, which all contain amphibole. Orthopyroxene is more abundant than clinopyroxene.

Amphibole

Poikilitic amphibole is present in most samples and is usually the most abundant phase after plagioclase. It encloses cumulus phases, which are a combination of plagioclase, clinopyroxene, orthopyroxene, and opaque. Poikilitic amphibole is anhedral, pleochroic in colorless-green-brown colors. In many samples, the amphiboles are pigmented by opaque exsolutions. Amphibole makes up 2/3 of certain samples.

Actinolite is present as weakly light green-clear pleochroic thin, prismatic or acicular crystals. Actinolite often surrounds pyroxenes or the outer rim of poikilitic amphiboles. Many samples also have poikilitic, pleochroic amphiboles with clear, slightly brown, non-pleochroic areas, composed of prismatic to acicular or fibrous crystals. The mineral is most likely cummingtonite, based on the clear to light brownish color, oblique extinction, common twinning, and 2° IF. As many samples are deformed, the extinction of crystals cannot always be used to distinguish between ortho and clinoamphiboles.

Cummingtonite seems to represent alteration products of both the primary poikilitic amphiboles and orthopyroxenes as they are often situated at the center of poikilitic amphiboles or at the edges or cracks of orthopyroxene grains, often in contact between orthopyroxene and plagioclase.

Orthopyroxene

Orthopyroxene is present both as cumulus and intercumulus phases. Orthopyroxene crystals are subhedral in cumulus and anhedral in intercumulus phase. Orthopyroxene is pale to light brown in PPL and pleochroic from light-light green to light red, with 1° IF colors. In some samples, orthopyroxene is altered into acicular to fibrous amphibole (Figure 19). When orthopyroxene encloses cumulus olivine, the grain boundaries between orthopyroxene and surrounding plagioclase are symplectitic.

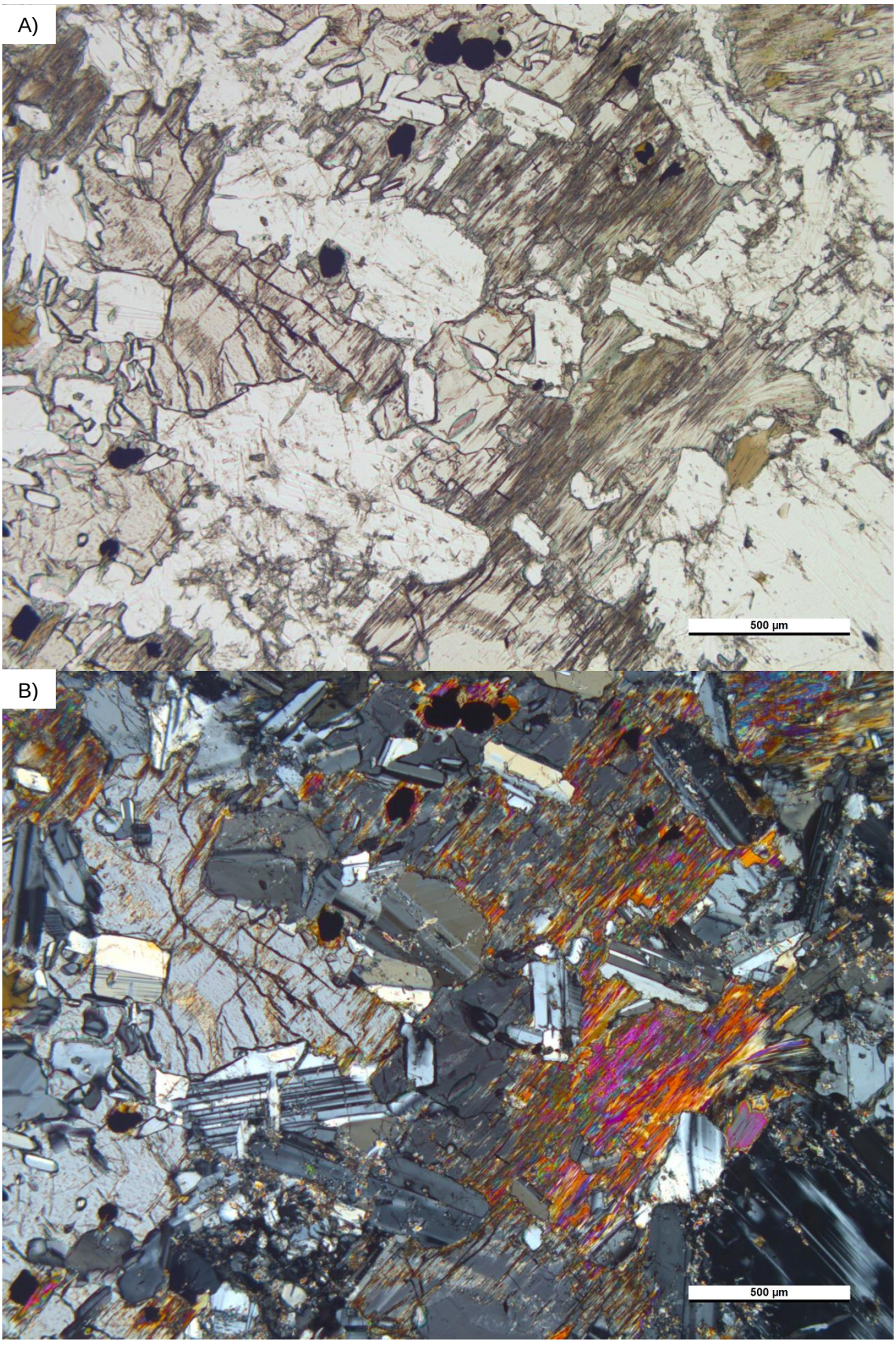

Figure 19. Orthopyroxene (light grey-brown) is partially altered to fibrous amphibole (orange to purple colors), most likely cummingtonite. Orthopyroxene partially encloses plagioclase and opaque minerals (magnetite). Photomicrographs of sample SIKA-2017-80.1. A) PPL B) XPL.

Clinopyroxene

Clinopyroxene is present in a few samples. In sample SIKA-2017-156.1, clinopyroxene is present as large, porphyric, light brown, round to elongated grains, which are mantled by dark green, pleochroic amphibole (Figure 20). Some of the clinopyroxene are completely altered to amphibole. The clinopyroxene displays 2° to 3° IF colors and, in some grains, sectored extinction. In sample SIKA-2017-88.1, clinopyroxene is present in both fine and coarse-grained part of the thin section (Figure 24). These crystals enclose euhedral plagioclase and apatite and they are surrounded by a ring of metasomatic dark green pleochroic amphibole.

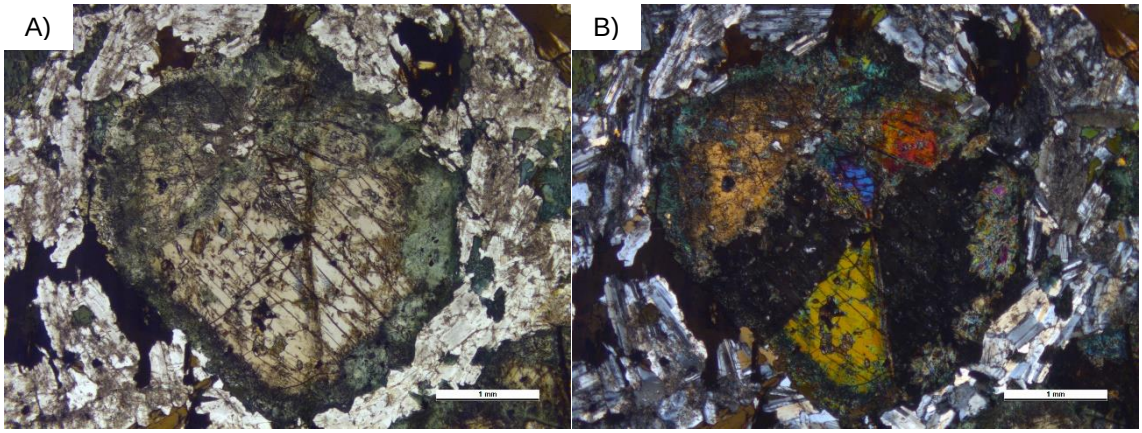

Figure 20. A large clinopyroxene phenocryst displaying cryptic zonation (or a glomerocryst) with a uralitic rim. Notice the plagioclase surrounding the clinopyroxene displays an almost trachytic texture. Photomicrographs of sample SIKA-2017-156.1 A) PPL B) XPL.

Plagioclase

Plagioclase is the most abundant phase after amphiboles. Plagioclase crystals are usually euhedral, zoned, and often with overgrown grain boundaries. The crystals are often heavily seriticized or saussuritized, and display undulatory extinction. Euhedral phenocrysts are up to 3 mm in length.

Mica

Biotite is present in most samples as reddish-brown to dark brown or clear to brown pleochroic crystals, which are often chloritized. Biotite is sometimes poikilitic and encloses plagioclase. Chlorite is pleochroic in green or anomalous, ink-blue colors. Opaque is often exsolved from biotite. In sample SIKA-2017-80.1, poikilitic phlogopite encloses cumulus olivine and plagioclase and acicular opaque minerals.

Opaque minerals

Opaque minerals are present in virtually all samples, as discrete grains, grain aggregates, and as amoeba-like, symplectitic exsolutions from mafic minerals (Figure 21 E-F). Often the grains are broken and tattered. Many opaque minerals have a dark gray interior and a black exterior when examined in PPL. Reflective light examination reveals that the opaque mineral is often magnetite, with ilmenite exsolutions (Figure 22 A-B). There are also ilmenite grains with magnetite exsolution lamellae. Dark green isotropic grains and grain aggregates are present in some Mg and Fe-rich rich samples (Figure 21, A-C). The larger grains are euhedral, isometric crystals, likely spinel.Sulfide phases are less common. Pyrite and chalcopyrite are present in minute concentrations in some samples (Figure 21 F, Figure 21 C-D).

Olivine

Olivine is present only in SIKA-2017-80.1. Olivine occurs as a cumulus phase together with plagioclase as 1 mm sized subhedral, rounded grains within poikilitic amphibole, orthopyroxene, and phlogopite (Figure 23). Olivine crystals within poikilitic amphibole are at least partially altered to dark red-brown mass (iddingsite) and magnetite. Olivine outside the poiklitic amphibole, in contact with plagioclase is completely altered and surrounded by green pleochroic amphibole. The crystals have usually a brownish pigment and display upper 2° IF colors.

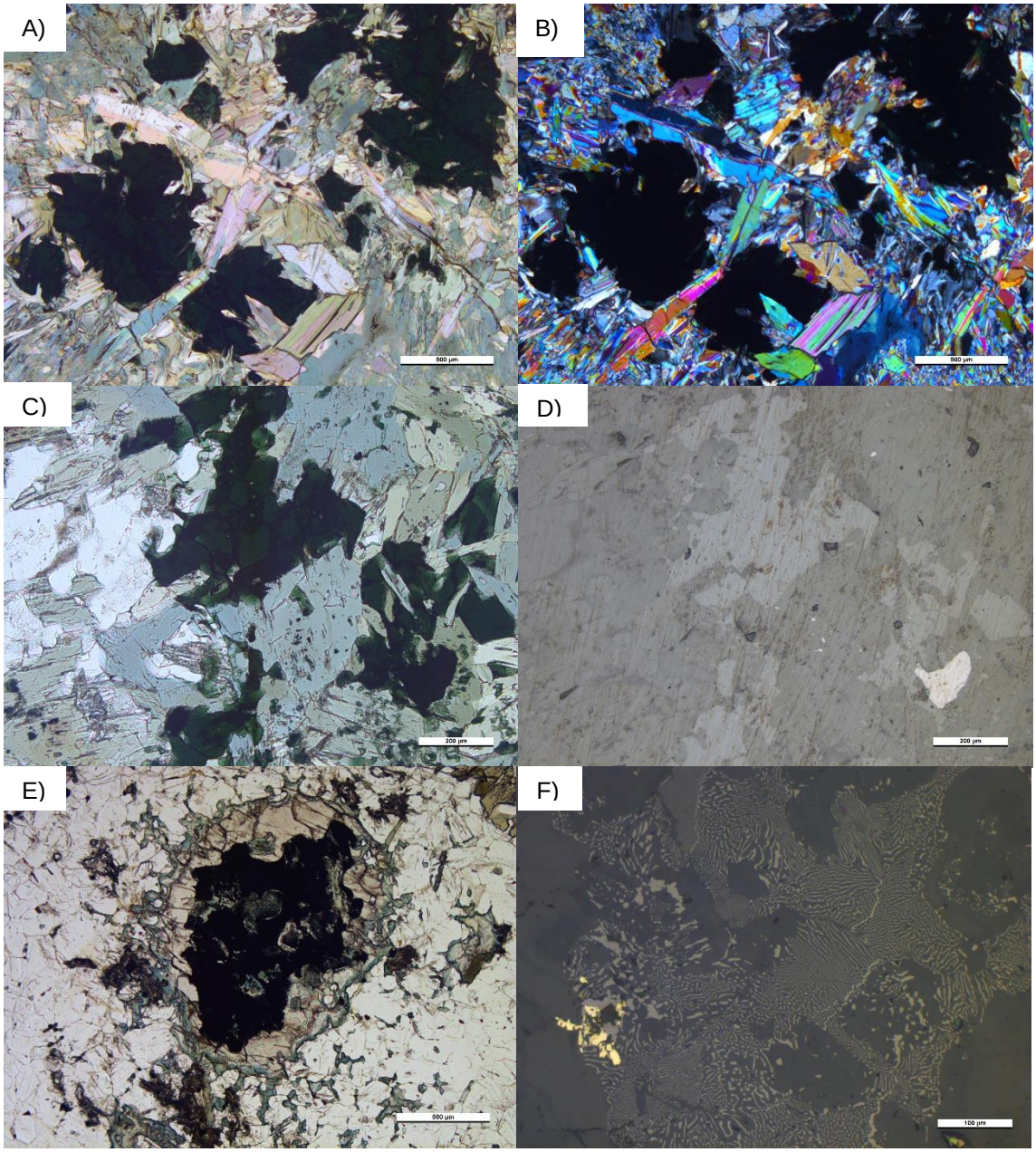

Figure 21. Photomicrographs of oxides and sulfides. A-D) Isotropic, dark green mineral, which is present in MgO and Fe_2O_3t rich, altered samples. The mineral has higher reflectivity (metallic gray) than silicate phases (duller gray) in D). E) is a picture of an orthopyroxene, with a symplectitic, opaque interior. Notice also the narrow amphibole rim on the edge of the orthopyroxene grain. F) is a magnification of the opaque area, showing the symplectite, composed of magnetite and a silicate phase. A glomerocryst of chalcopyrite (golden) and pyrite (yellow-white) is also seen. Pictures A), C) and E) are taken in plane-polarized view with a polarizing microscope, B) is with cross-polarized view, D) and F) are in reflected light.

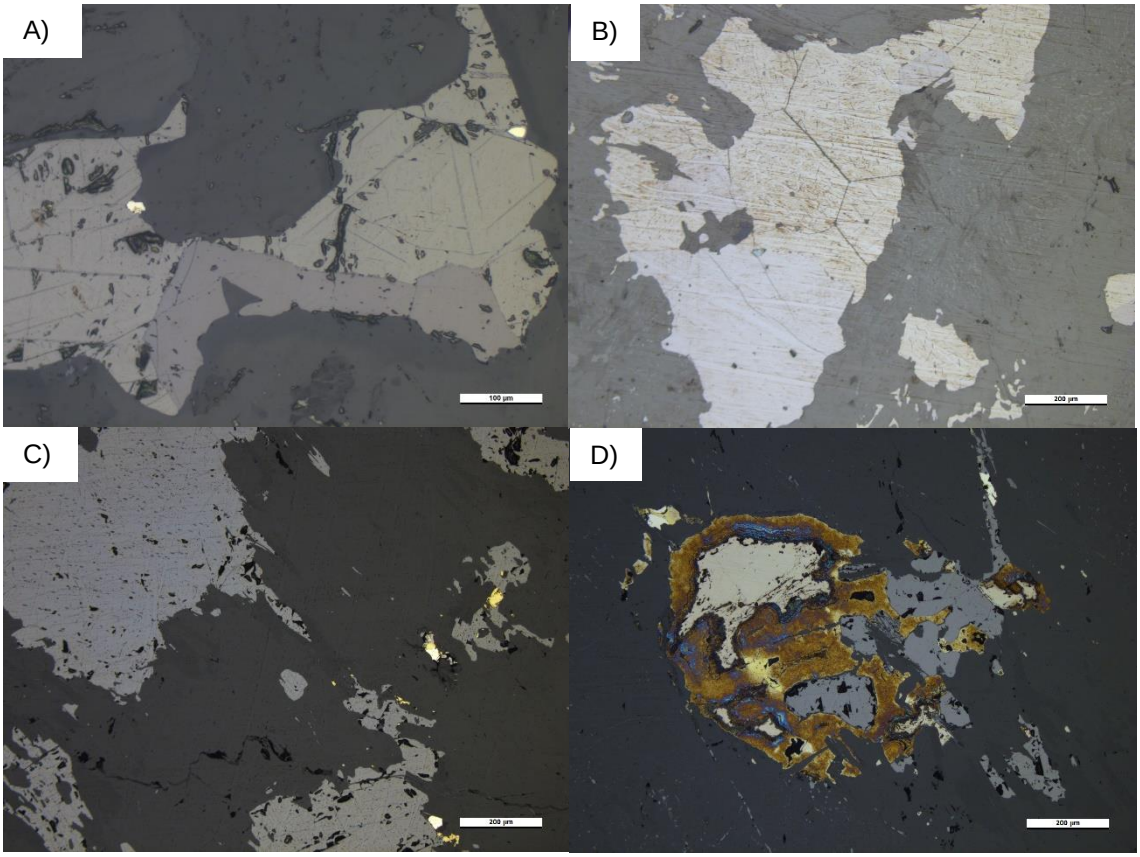

Figure 22. Photomicrographs of oxide and sulfide phases in reflected light. A) Magnetite (creamy white) with triangular gray exsolutions of ilmenite and an anhedral grain of ilmenite (brown-gray) on the bottom. Small grains of pyrite (yellow-white) are also seen at the edges of magnetite. The pyrite on the left contains an inclusion of chalcopyrite (yellow). Sample SIKA-2017-1.1. B) Magnetite (white) with exsolutions of ilmenite (dark gray) showing evidence of annealing, 120º degree angles between crystals, which have been broken and tattered. The brown pigment is most likely the result of a poor polish. Sample SIKA-2017-51.1. C) Magnetite (bluish-gray) with ilmenite exsolutions (dark gray) and small grains of chalcopyrite (bright yellow) and pyrite (yellow-white). D) Oxidized grain aggregate containing magnetite (light gray), pyrite (dull yellow-white) and chalcopyrite (bright yellow). C-D) Sample SIKA-2017-14.1.

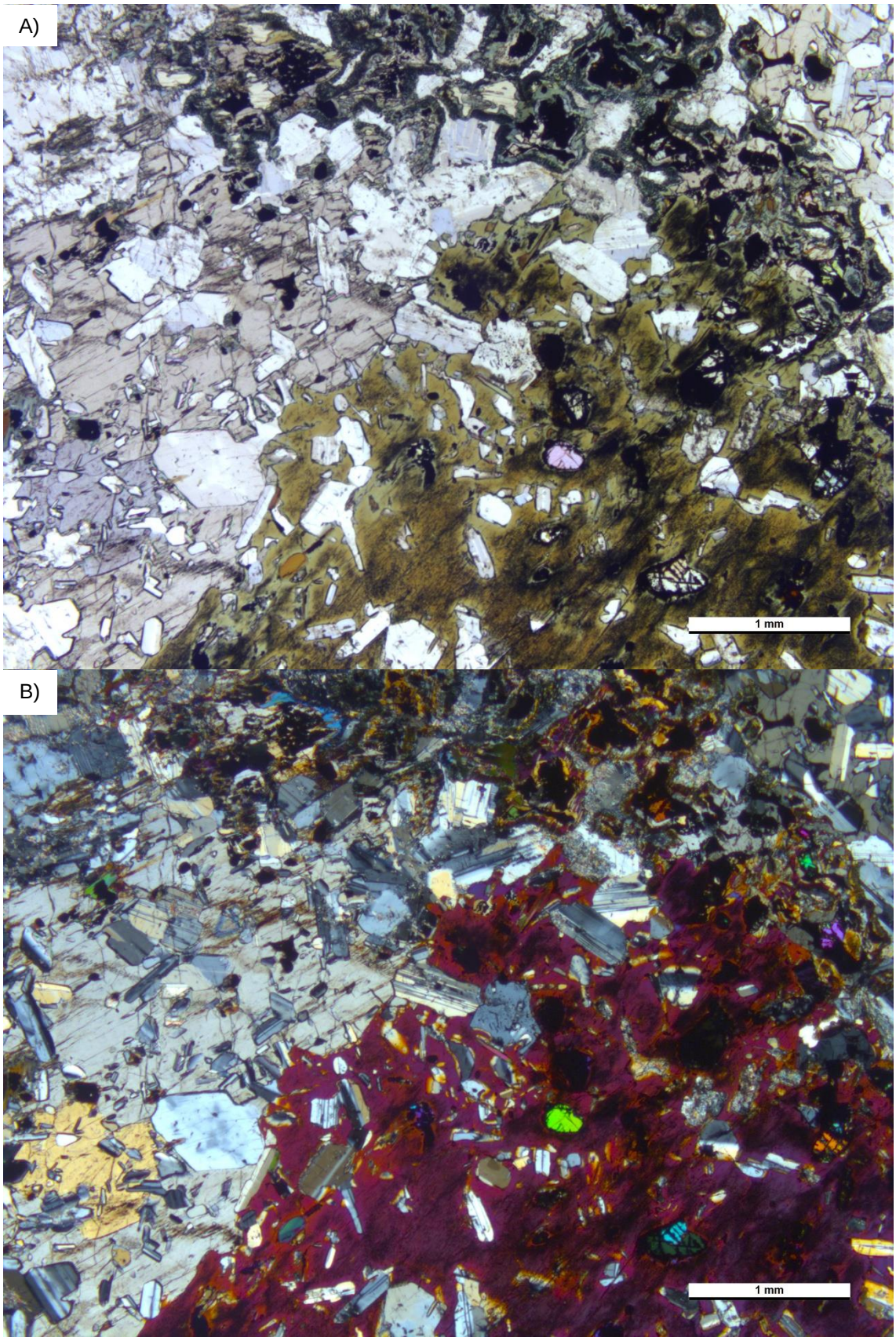

Figure 23. Olivine-norite, where cumulus olivine (bright colors) and plagioclase (white) is enclosed in poikilitic amphibole (greenish-brown and red-to-purple colors) and orthopyroxene (light brown and gray colors). Orthopyroxene-plagioclase grain boundary is symplectitic. Olivine outside the poikilitic amphibole, in contact with plagioclase is completely altered. Top image is plane-polarized, below is cross-polarized. Photomicrographs of sample SIKA-2017-80.1. A) PPL B) XPL.

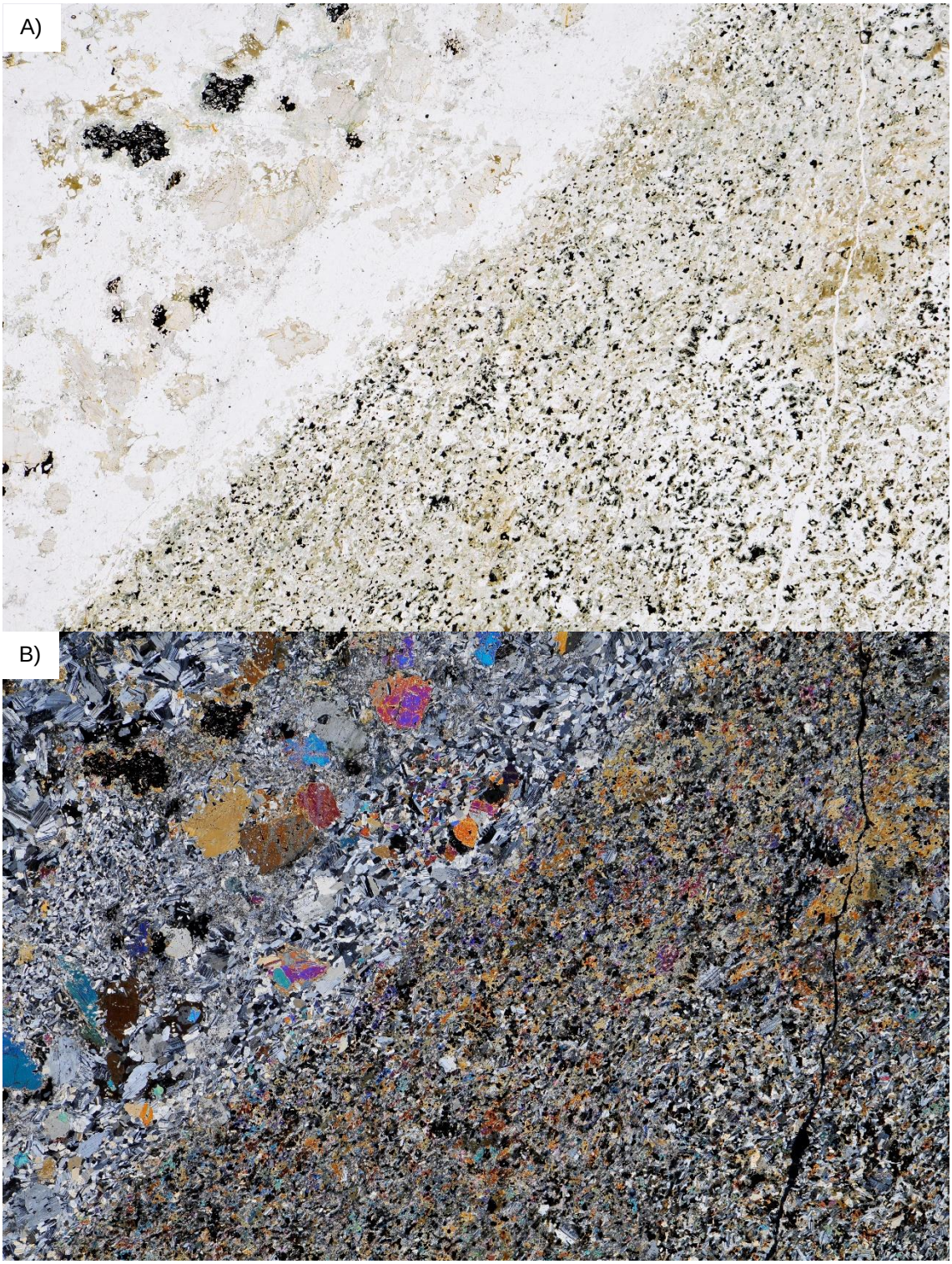

Figure 24. Photomicrographs of a thin section showing two adjacent layers of varying grain sizes (sample SIKA-2017-88.1). Clinopyroxene, orthopyroxene, plagioclase, and amphibole are the major phases in both domains. Opaque minerals, mostly magnetite and ilmenite, are also present in both sections. Top picture is in plane-polarized light, below in cross-polarized. A) PPL, B) XPL.

4.2.3 Hongonniittu

There are four samples from the Hongonniittu area. The mineralogy and textures of the samples are similar to those of Palojärvi. The samples are composed of poikilitic amphibole, which commonly displays blueish-green to brown pleochroism, enclosing plagioclase and opaque minerals. Plagioclase is present both as cumulus and intercumulus phases. Plagioclase is often strongly seriticized and displays undulatory extinction. Reddish-brown biotite, actinolite, chlorite or carbonate are also present in most samples.

4.3 Whole-rock geochemistry

Major element geochemistry is presented as volatile free where the original values of major element oxides have been recalculated to 100 %. Some samples have original totals as low as 92.11 wt-%. Median total values are 95.48 wt-%. The median values for main and trace chemical components for all intrusions are presented in Table 1. All original analyses are presented in Appendix 1. Magnesium number (Mg#) is calculated from the molar ratios of MgO against $MgO+FeO_{tot}$ (equation 1). The differences in the valence of iron are approximated by assuming 15 % of the total iron to be Fe^{3+}.

$$\mathrm{Mg\#} = 100 * \left(\frac{\left(\frac{\mathrm{MgO}}{40.3044}\right)}{\left(\frac{\mathrm{MgO}}{40.3044}\right) + 0.85 * \left(\frac{0.8998 * \mathrm{Fe_2O_{3_t}}}{71.844}\right)} \right) \quad (\mathrm{eq.}\,1)$$

CIPW norms were calculated with GCDkit, which uses the CIPW calculation method of Hutchinson (1974, 1975). Median compositions of the studied intrusions are given in table 1 X. Full CIPW norm results for all whole-rock analyses are given in Appendix 2.

The median chemical compositions and ranges of samples from the gabbros in the studied areas and also mafic dikes from Matokulma are presented in Table 1. The whole-rock geochemical patterns are shown in MgO versus other oxides (Figure 26) and in AFM and CMA diagrams (Figure 27A-B).

There were some discrepancies in Hf and Zr results of ICP-OES analyses.

Samples SIKA-2017-3.1 and SIKA-2017-119.1 were analyzed twice. The concentration of Hf (detection limit 0.5 ppm) in the second analysis was half of the concentration in the first one with both samples. The average of the repeat analyses was used.

The concentrations of Zr and V were analyzed both with ICP-OES and XRF (Figure 25) The detection limits of Zr and V are 10 ppm with XRF and 5 ppm with ICP-OES, respectively. All of the samples analyzed with ICP-OES have lower concentrations of Zr than the samples analyzed with XRF, median of ICP/XRF concentration ratios are 0.66. The concentrations of V analyzed with ICP-OES are however always higher or equal, compared to XRF analyses and the ICP/XRF concentration ratios are, on median, 1.15. This is most likely due to the sample preparation where pulverized rock is digested with HF and $HClO_4$ and fused into a lithium metaborate-sodium perborate bead for analysis.

Zircon as a refractory mineral might not have dissolved entirely which would explain the large discrepancy between the concentrations analyzed with XRF and ICP.

Only one sample (SIKA-2017-154.2, Hongonniittu) had noble metal concentrations exceeding the detection limit (5 ppb); at 6 ppb Au.

The original ICP-OES and ICP-MS analyzes are given in Appendix 3.

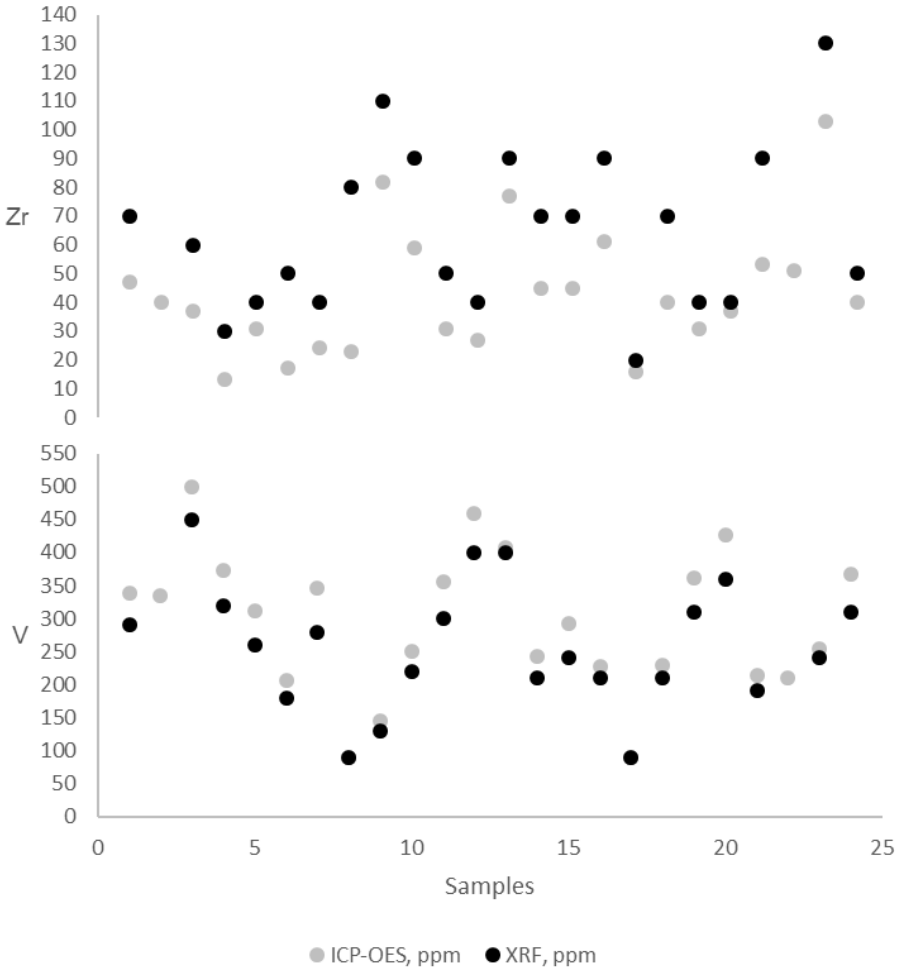

Figure 25. Comparison of ICP-OES (gray symbols) and XRF (black symbols) analyses for Zr (top) and V (bottom). Concentrations in ppm.

4.3.1 Matokulma

Gabbroic samples

The gabbroic samples from Matokulma (n=19) are basic according to the median SiO_2 concentration of 50.16 wt-%. The range of silica is 48.97–51.54 wt-%. TiO_2 has a median concentration of 0.55 wt-% and a range of 0.37–0.72 wt-%. TiO_2 increases slightly with increasing MgO. Al_2O_3 shows a strong negative correlation with MgO. Al_2O_3 has a median concentration of 11.16 wt-% and a wide range of 6.23–18.03 wt-%. The range of MgO is 8.32–15.29 wt-% with a median value of 12.65 wt-% and it positively correlates with Fe_2O_{3t}, which has a median value of 11.46 wt-% and a range of 7.91–13.44 wt-%. MnO concentrations also positively correlate with Fe_2O_{3t}. MnO has a median value 0.19 wt-% and a rather restricted range of 0.14–0.23 wt-%. CaO has a median value of 12.59 wt-%, a range of 9.74–14.10 wt-%. Alkalis are quite low, Na_2O and K_2O have median values of 1.18 wt-% and 0.59 wt-% and ranges of 0.75–1.64 wt-%, 0.36–1.43 wt-%, respectively. Median value and range for P_2O_5 are 0.07 wt-% and 0.01–0.11 wt-%. Median Mg# is 72 and it has a rather restricted range of 69–75. All samples are metaluminous based on A/CNK-A/NK diagram (molar ratio diagram of Al/Ca+Na+K and Al/Na+K, not shown). In the AFM diagram (Irvine and Baragar 1971) the samples plot into a cluster in the tholeiitic field, between the calc-alcaline series line and the F-M edge

CIPW norms

The samples from Matokulma are hypersthene (Hy) and olivine (Ol) normative. Normative plagioclase as albite + anorthite (Ab+An), diopside (Di), and Hy are the most abundant phases with median concentrations and ranges of 34% (19–54%), 29 %, (14–47 %) and 21 %, (7–32 %), respectively. Ol ranges from 0.3 to 13 and is 7 % on median. The mean An, Fo, and En percentages are 70, 65, and 67, respectively. All samples contain normative magnetite (Mt) and ilmenite (Il) and varying amounts of alkali feldspar (Or), with median values of 2 %, 1 %, and 3 %, respectively.

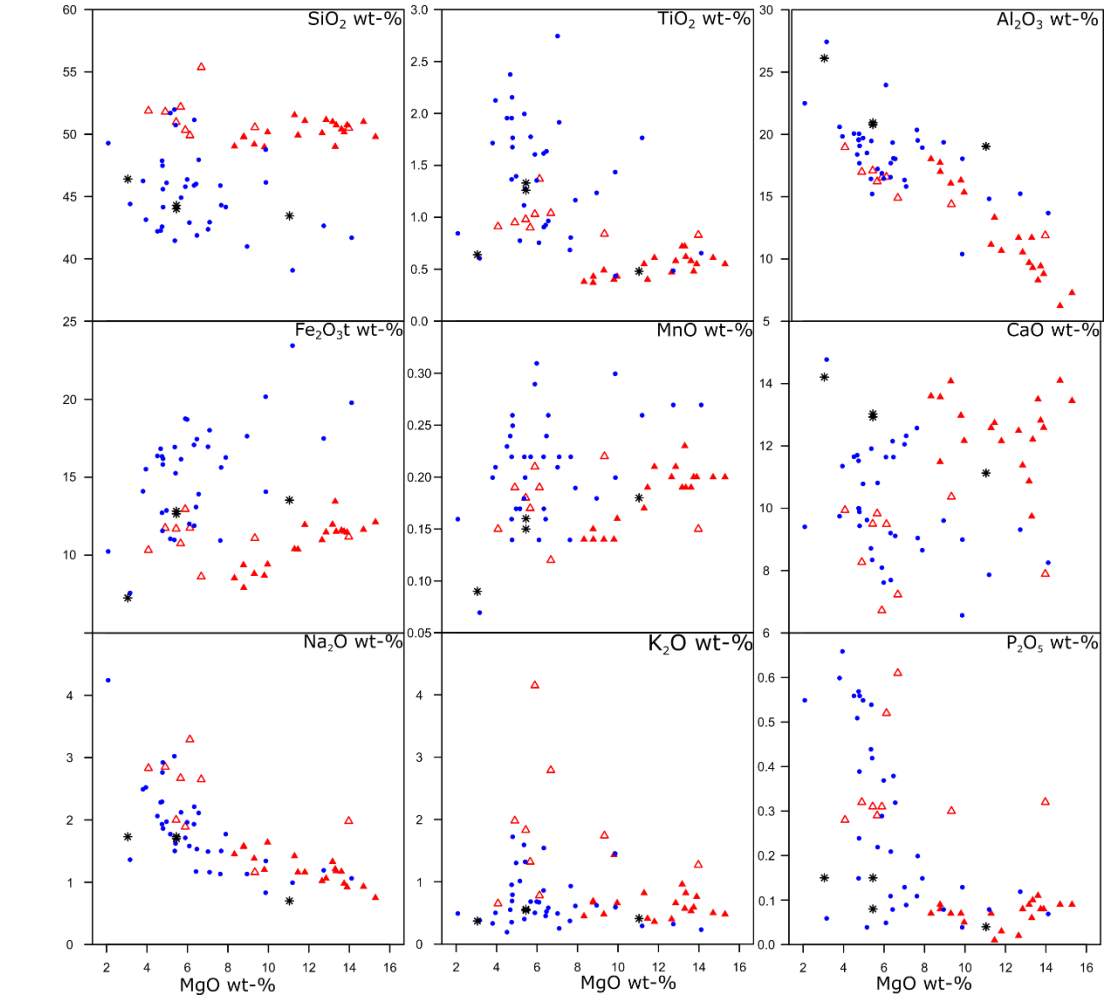

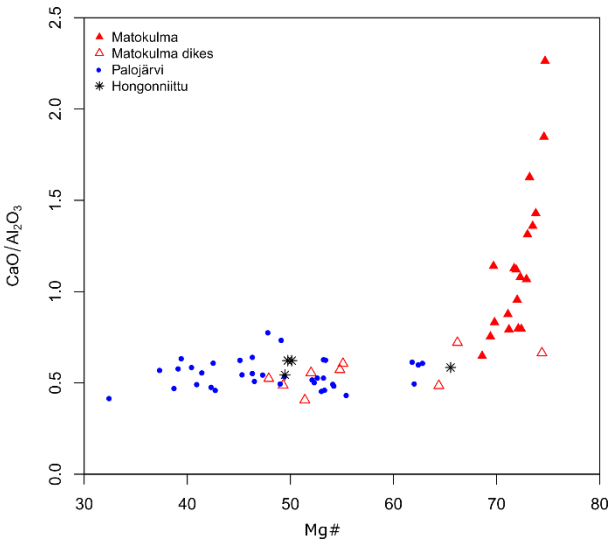

Figure 26. (above). Whole-rock chemical data from the studied intrusions with MgO against other major components. All data presented is normalized (volatile-free).

(left) Mg# versus CaO/Al_2O_3. The different composition of the studied intrusions is apparent. Matokulma gabbros are the most magnesian (Mg# > 70) and have the highest CaO/Al_2O_3 which decreases with decreasing Mg#. Palojärvi has a rather constant CaO/Al_2O_3 with generally low Mg# (<50), some of the amphibole-rich samples have Mg# >60. Hongonniittu samples are similar to Palojärvi.

Table 1. Whole-rock assays for the studied intrusions. Median PGEs for all intrusions are below detection limit and are not shown. Oxides are normalized to 100% (volatile-free). Oxides and unmarked elements are analyzed with XRF from powder pellets, 1 = Analyzed with ICP-OES, REE and elements with 2 with ICP-MS, n = number of analyzed samples, SD = standard deviation, <10 = below detection limit, C*= total carbon (combustion analysis), Mg# = 100*MgO/(MgO+0.85*FeO_{tot})

Intrusion	**Matokulma**		**Matokulma dykes**		**Palojärvi**		**Hongonniittu**	
n (XRF)	19	**SD**	9	**SD**	36	**SD**	4	**SD**
n (ICP)	6		6		9		1	
wt-%								
SiO_2	50.16	0.77	50.97	1.56	45.29	3.16	44.43	1.29
TiO_2	0.55	0.10	0.95	0.15	1.39	0.57	0.93	0.43
Al_2O_3	11.16	3.60	16.53	1.89	18.49	2.89	21.67	3.05
Fe_2O_3t	11.46	1.46	11.18	1.13	16.02	3.21	11.54	2.89
MnO	0.19	0.03	0.18	0.03	0.21	0.05	0.15	0.04
MgO	12.65	2.11	5.89	2.85	5.97	2.52	6.23	3.39
CaO	12.59	1.09	9.49	1.23	9.70	1.74	12.79	1.27
Na_2O	1.18	0.24	2.65	0.62	1.78	0.68	1.46	0.51
K_2O	0.59	0.24	1.74	1.02	0.60	0.41	0.47	0.09
P_2O_5	0.08	0.03	0.31	0.11	0.22	0.20	0.11	0.05
ppm								
Ba	120	96	450	299	180	160	108	40
Cl	300	56	200	94	300	96	290	50
Co[1]	56	5	44		50	23	66	-
Cr	880	395	140	327	40	26	104	42
Cu	60	16	45	21	50	13	48	19
Hf[2]	0.73	0.06	1.96	1.18	1.53	1.30	2.04	-
Ni	90	64	50	119	35	14	42	9
Rb[1]	16.75	5.72						-
S	900	516	200	266	550	404	528	375
Sc[1]	58.30	5.06	34.40	2.98	18.90	15.63	15.8	-
Sr	310	146	577	134	590	166	718	100
V[1]	364.5	33.64	221	26	355	143	372	170
Ta[2]	<1	-	<1	-	1.28	0.00	<1	-
Th[2]	<2	-	2.28	0.14	2.36	4.06	<2	-
U[2]	0.39	0.07	0.67	0.41	0.47	0.56	0.22	-
Y[1]	11.10	1.15	26	7	20	10	10	0
Zn	80	14.96	110	15	130	30	87	18
Zr	50	10.04	90	31	60	21	63	8
La	5.56	1.74	14.10	3.87	8.70	6.04	3.3	-
Ce	14.35	3.76	31.70	9.90	18.60	16.61	8.85	-
Pr	2.10	0.46	4.30	1.46	2.40	2.43	0.84	-
Nd	10.07	1.83	18.98	6.59	10.40	10.94	3.54	-
Sm	2.63	0.35	4.17	1.34	2.57	2.54	0.76	-
Eu	0.73	0.05	1.40	0.37	0.91	0.68	0.41	-
Gd	2.73	0.36	4.10	1.16	2.41	2.50	0.79	-
Tb	0.44	0.05	0.64	0.16	0.34	0.40	0.13	-
Dy	2.70	0.32	3.78	0.88	2.02	2.46	0.79	-
Ho	0.53	0.06	0.75	0.17	0.40	0.49	0.15	-
Er	1.49	0.18	2.15	0.48	1.19	1.44	0.45	-
Tm	0.20	0.03	0.30	0.06	0.18	0.20	<0.1	-
Yb	1.25	0.15	1.86	0.40	1.10	1.26	0.42	-
Lu	0.18	0.02	0.28	0.06	0.18	0.20	<0.1	-
C* wt-%	0.09	0.02	0.06 (6)	0.01	0.10	0.03	0.09	0.02
Mg#	72	2	55	8.00	49	7	54	8
Al_2O_3/CaO	0.93	0.29	1.70	1.50	1.84	0.25	1.69	0.09

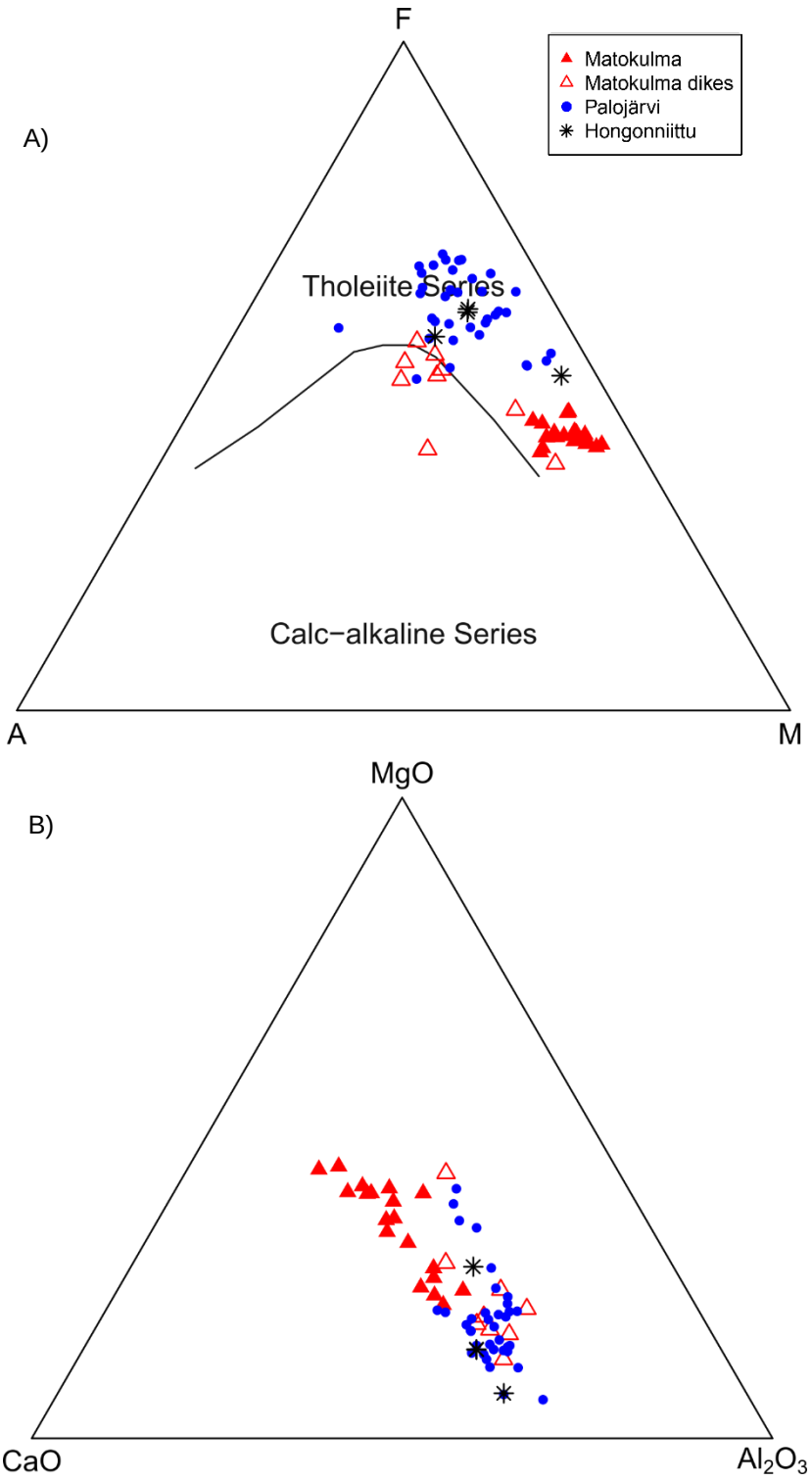

Figure 27. A) AFM diagram (Irvine and Baragar 1971). Samples from Matokulma plot into a group on the tholeiite side of the line, halfway between FeOt and MgO vertices in the AFM diagram. The Matokulma dikes are more alkali-rich and they mostly plot into the calc-alkaline area, except for the more MgO rich ones. Palojärvi and Hongonniittu samples are more evolved and display scatter. They plot higher on the tholeiite series, towards the FeOt vertex. Alkali-rich sample (SIKA-2017-156.1) plots into the Calc-alkaline side of the line. Leucogabbro dike (SIKA-2017-17.1) plots further from the rest of the Palojärvi samples. B) CaO-MgO-Al2O3 (CMA) diagram.Samples from Matokulma are more magnesian and display a clinopyroxene-dominated evolution in the CMA diagram, whereas Palojärvi, Matokulma dikes, and Hongonniittu are more plagioclase-dominated, with some of the more MgO-rich samples behaving differently, plotting closer to the MgO vertex.

Trace elements

Concentration of Ni and Cu are low, with median values of 90 and 60 ppm, respectively. S values have a median of 900 ppm, with the highest value being 2500 ppm. Barium has a median concentration of 120 ppm. The concentration of barium correlates positively with K_2O. The median concentrations of Cr and V are 880 ppm and 250, respectively. Both Cr and V correlate negatively with Al_2O_3 and positively with MgO and Mg#. Sr behaves conversely by showing negative correlation to MgO and positive to Al_2O_3. Sr concentrations range from 140–630 ppm and have a median of 310 ppm.

La, Ce, Pr, Eu show a strong (r>0.95), positive correlation with Ti, Zr, P. Nd, Gd show a positive correlation with Ti and P. Most samples have LREEs 8 to 12 times the concentration of primitive mantle (Sun and McDonough 1995). In primitive mantle (Sun and McDonough 1995) normalized spider diagram (Figure 28), most samples are enriched in LREE compared to HREE. The samples have gentle slopes from LREE to HREE. The median value for La_N/Yb_N is 3.16. All samples display a slight negative Eu anomaly (Eu*/Eu < 1), with a median ratio of 0.84.

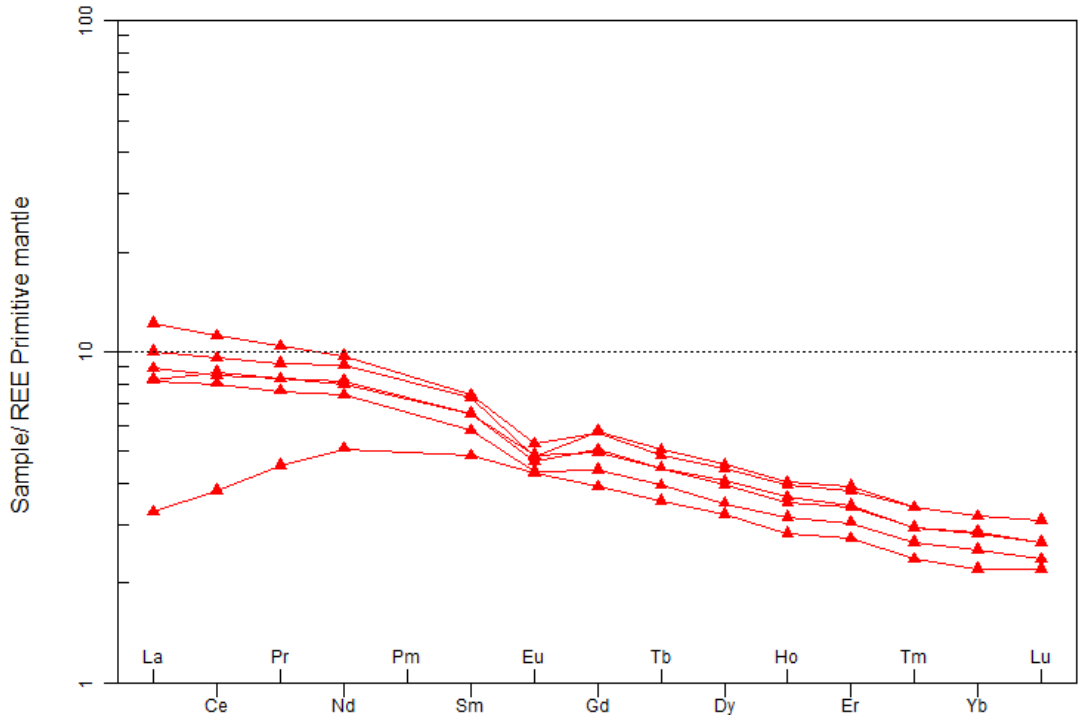

Figure 28. Gabbroic samples in a Primitive Mantle (McDonough and Sun 1995) normalized spider diagram. Most sample display similar element ratios, LREE enrichment and a negative Eu anomaly. Sample SIKA-2017-6.4, however, displays lower LREE.

The sample with the lowest REE concentration is SIKA-2017-6.4, a sample from the fine-grained, thin, ultramafic layer from an outcrop where magmatic lamination is visible. This sample differs from the other samples by having lower concentrations of total REEs and depletion in LREE. The La_N/Yb_N, LaN/SmN, Sm_N/Yb_N, ratios of the sample are 1.49, 0.67, and 2.21, respectively. The median values of all gabbroic samples are 3.16, 1.37, and 2.29, respectively.

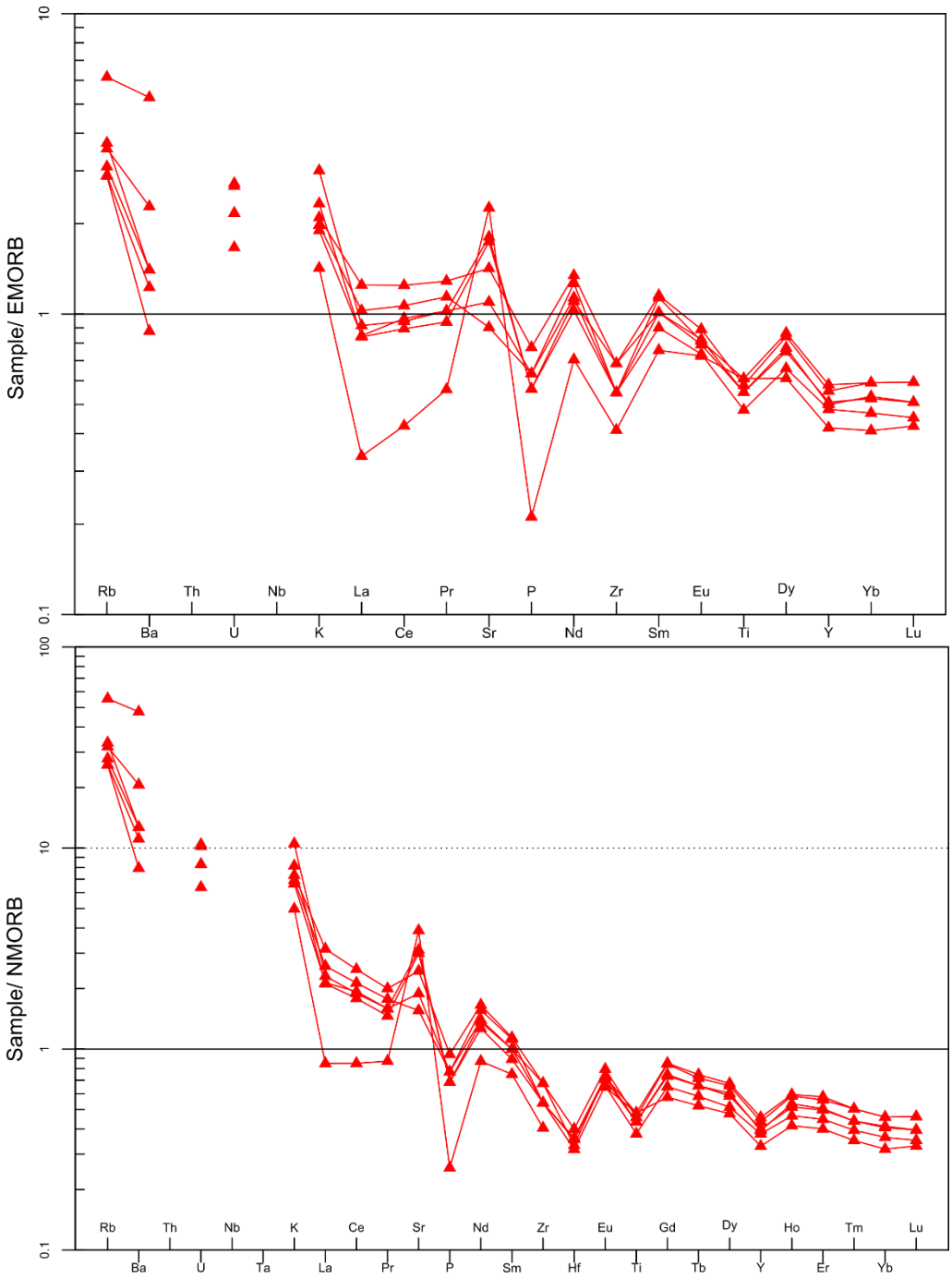

Figure 29. Matokulma samples on EMORB (above) and NMORB (below) normalized spider diagrams. Normalization values from Sun and McDonough (1989).

In NMORB and EMORB normalized diagrams (Sun and McDonough 1989), the samples have a ‘spiky’ appearance, with enrichment in large ion lithophile elements (LILE – Rb, Ba, K, Sr) and some samples enriched in U but depletion in other high field-strength elements (HFSE – P, Th, Zr, Ti, HREE) (Figure 29). Nb and Ta concentrations are below detection limits (<3 ppm and <1 ppm, respectively).

Dike rocks

The dike rocks are basic, on the basis of the median SiO_2 value of 50.97 wt-%. Sample SIKA-2017-121.1, which contains macroscopically visible quartz, has the highest silica concentration of 55.37 wt-%. SiO_2 correlates negatively with Fe_2O_3t. TiO_2 concentration is 0.95 wt-%. Al_2O_3 has a median concentration of 16.53 wt-%, with a range of 11.89–18.97 wt-%. Al_2O_3 correlates negatively with MgO. Fe_2O_3t and MnO correlate positively and their median concentrations are 11.18 wt-% and 0.18 wt-%, respectively. Median MgO concentration is 5.89 wt-%. Sample SIKA-2017-119.1, however has 13.97 wt-% MgO. Median concentration of CaO is 9.49 wt-%. K_2O and Na_2O concentrations are 1.74 wt-% and 2.65 wt-%, respectively. Median concentration for P_2O_5 is 0.31 wt-%.

CIPW norms

All samples are Hy and Di normative, with 4 out of 9 samples being Q normative and 5 out of 9 being Ol normative. En, Fo, and An percentages are 50, 48, and 56, respectively. All samples are Or normative with a median concentration of 10 % and a wide range of 4–25 %. Mt and Il are present in all samples, with median concentrations of ~ 2 %. Ap is also present in all samples with a median concentration of 0.7 %.

Trace elements

Ni and Cr show strong positive correlation with MgO and negative to Al_2O_3. Median concentration for Ni is 50 ppm. The highest Ni value of 400 ppm is found in sample SIKA-2017-119.1, which also has the highest (13.97 wt-%) MgO concentration. The highest Cr concentration, 1010 ppm, is also found in this sample. The median Cr concentration is, however much less – 140 ppm. Cu concentration is 45 ppm in median and 70 ppm in maximum. Ba has a median concentration of 450 ppm and it correlates positively with K_2O. Zr concentration is 90 ppm and it strongly correlates positively with P_2O_5. Zn concentration is 110 ppm in median and it strongly correlates positively with MnO and also with Fe_2O_3t, albeit less so. Median V concentration is 210 ppm. S concentrations range from 100 to 900 ppm, with a median of 200 ppm.

The Matokulma dikes display similar REE trends as the gabbroic samples, although they are more enriched in REEs, especially LREEs (Figure 30). LREE to MREE show a strong positive correlation with P_2O_5. The LREE concentrations are 15 to 34 times the primitive mantle values. The slope from LREE to MREE to HREE changes from a steeper to a gentler. The La_N/Yb_N, La_N/Sm_N, Sm_N/Yb_N values are 5.13, 1.98, 2.56, respectively. Median Eu*/Eu is 0.99.

The samples display similar LILE enrichment and HFSE depletion (Ta, Nb, Zr, and HREE) to the gabbroic samples on NMORB and EMORB normalized spider diagrams (Figure 31).

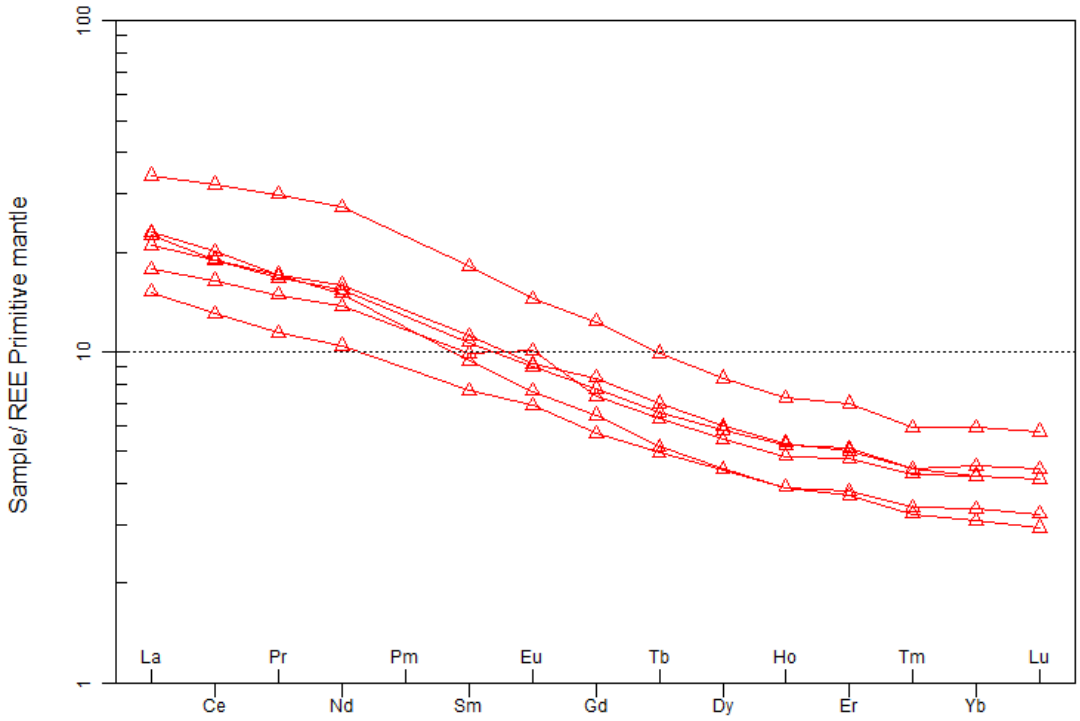

Figure 30. Dike rock samples in a primitive mantle (McDonough and Sun 1995) normalized spider diagram.

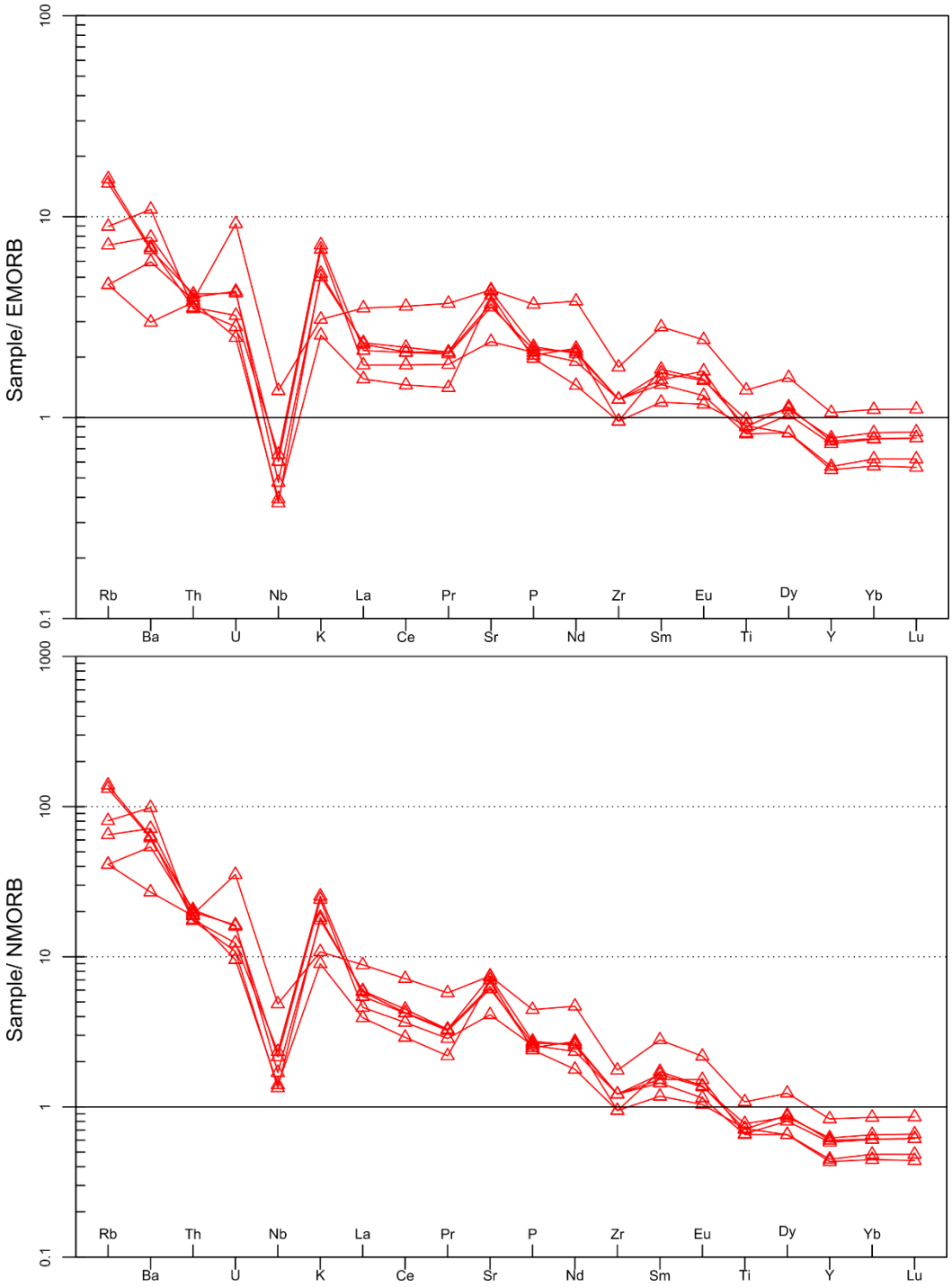

Figure 31. Matokulma mafic dike samples plotted on EMORB (top) and NMORB (bottom) spider diagrams (Sun and McDonough 1989).

4.3.2 Palojärvi

The gabbroic samples from Palojärvi have a wide composition range from ultrabasic to ~basic (39.12–52.02 wt-% SiO_2), with a median value of 45.29 wt-%. Other major element oxides show a wide range and scatter when plotted against other element oxides. Samples from Palojärvi are more evolved than Matokulma, based on the higher concentrations of especially Fe_2O_{3t} and Al_2O_3, TiO_2 and lower concentrations of MgO. There are, however some MgO-rich cumulate samples, where the concentration of MgO is up to 14.15 wt-%. The highest Fe_2O_{3t} and Al_2O_3 values are 23.48 wt-% and 27.47 wt-%, respectively.

TiO_2 values range from 0.44–2.74 wt-%, with a median of 1.39 wt-%. Al_2O_3 has a median value of 18.49 wt-%, with a wide range of 10.44–27.47 wt-%. Fe_2O_{3t} values have a median of 16.02 wt-%, also with a wide range of 7.60–23.48 wt-%. MnO has a median of 0.21, with a range of 0.07–0.31 wt-%. MnO shows a positive correlation with Fe_2O_{3t}. MgO has a wide range from 2.12 to 14.15 wt-%, with a median of 5.97 wt-%. CaO ranges from 6.58 to 14.79 wt-%, with a median of 9.70 wt-%. Na_2O content has a median of 1.78 wt-%, with a range of 0.84–4.25 wt-%. K_2O has a median value of 0.60 wt-% and a range of 0.20–1.73 wt-%. P_2O_5 ranges from 0.04–0.66 wt-%, with a median of 0.22 wt-%. All samples plot into the metaluminous field in the A-CNK/A-NK diagram. When plot into the AFM diagram (Irvine and Baragar 1971), most samples are situated in the tholeiitic field, near the apex of the calc-alkaline line. Sample SIKA-2017-156.1 plots into the calc-alkaline field. In the CMA diagram, the samples plot closer to the orthopyroxene-plagioclase dominated trend than the Matokulma samples.

CIPW norms

The samples from Palojärvi have varying normative compositions. Four of the samples are quartz (Q) and Hy normative, fourteen are nepheline (Ne) and Ol normative, and one is corundum (C), Hy, and Ol normative. Median Plg, Hy, Ol, Di concentrations are 55, 7, 5, and 18. The median An, Fo, En, and Di percentages are 74, 41, 47, and 47 respectively. All of the samples contain normative Mt, Il, Or with median concentrations of 3 %, 3 %, and 4 %, respectively.

Trace elements

The more evolved nature of Palojärvi can also be seen in the concentrations of trace elements. The median concentration of Ba and Sr are 185 ppm and 590 ppm. Highest

values are 750 ppm and 1020 ppm, respectively. Ba correlates positively with K_2O. Zn has a median concentration of 130 ppm. Zn correlates positively with MnO. V concentrations are elevated, up to 780 ppm, with a median concentration of 360 ppm. Concentrations of Ni,Cr, and Cu are 30 ppm, 40 ppm, and 50 ppm, respectively.

Among the analyzed gabbro samples, also a mafic inclusion from within a granite (sample SIKA-2017-22.1) and a leucogabbro (SIKA-2017-17.1, age determination sample) were analyzed. Samples from Palojärvi display more variance in REEs as well (Figure 32). Most samples display a similar LREE enrichment, slightly positive Eu anomaly, and a shallow slope from MREE to an almost flat HREE pattern but a few samples behave differently. One sample (SIKA-2017-62.1) has a rather flat LREE/MREE ratio and a positive Eu anomaly. Another sample (SIKA-2017-54.1) has higher REEs in general, a gentle slope from Ce to Nd, and a negative Eu anomaly and strong enrichment in Th. The leucogabbro sample displays a strong positive Eu anomaly. The median La_N/Yb_N, La_N/Sm_N, Sm_N/Yb_N ratios for all samples are 4.49, 2.07, 2.27, respectively. Median Eu*/Eu is 1.19. The samples display more scatter in EMORB and NMORB-normalized diagrams (Figure 33). Most samples display positive Sr and K and negative Nb, Zr, and Y anomalies.

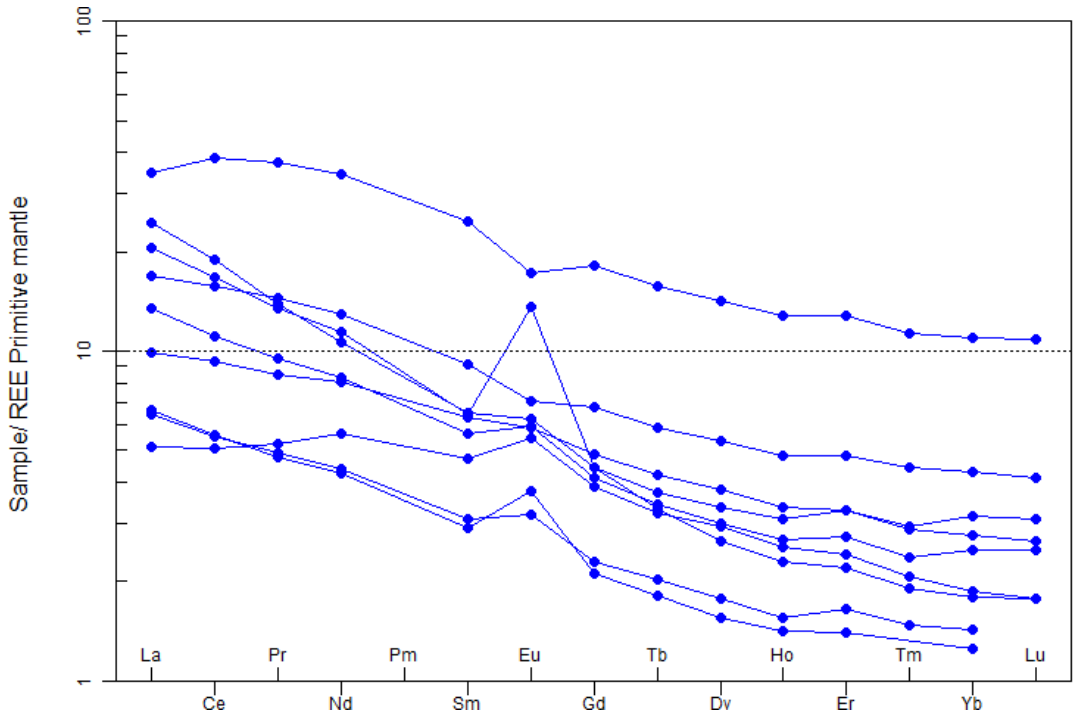

Figure 32. Samples from Palojärvi plotted into REE spider diagram, normalized against Primitive Mantle (McDonough and Sun 1995). Most samples display a positive Eu anomaly and LREE enrichment, flat HREE, and with a gentle slope from LREE to HREE.

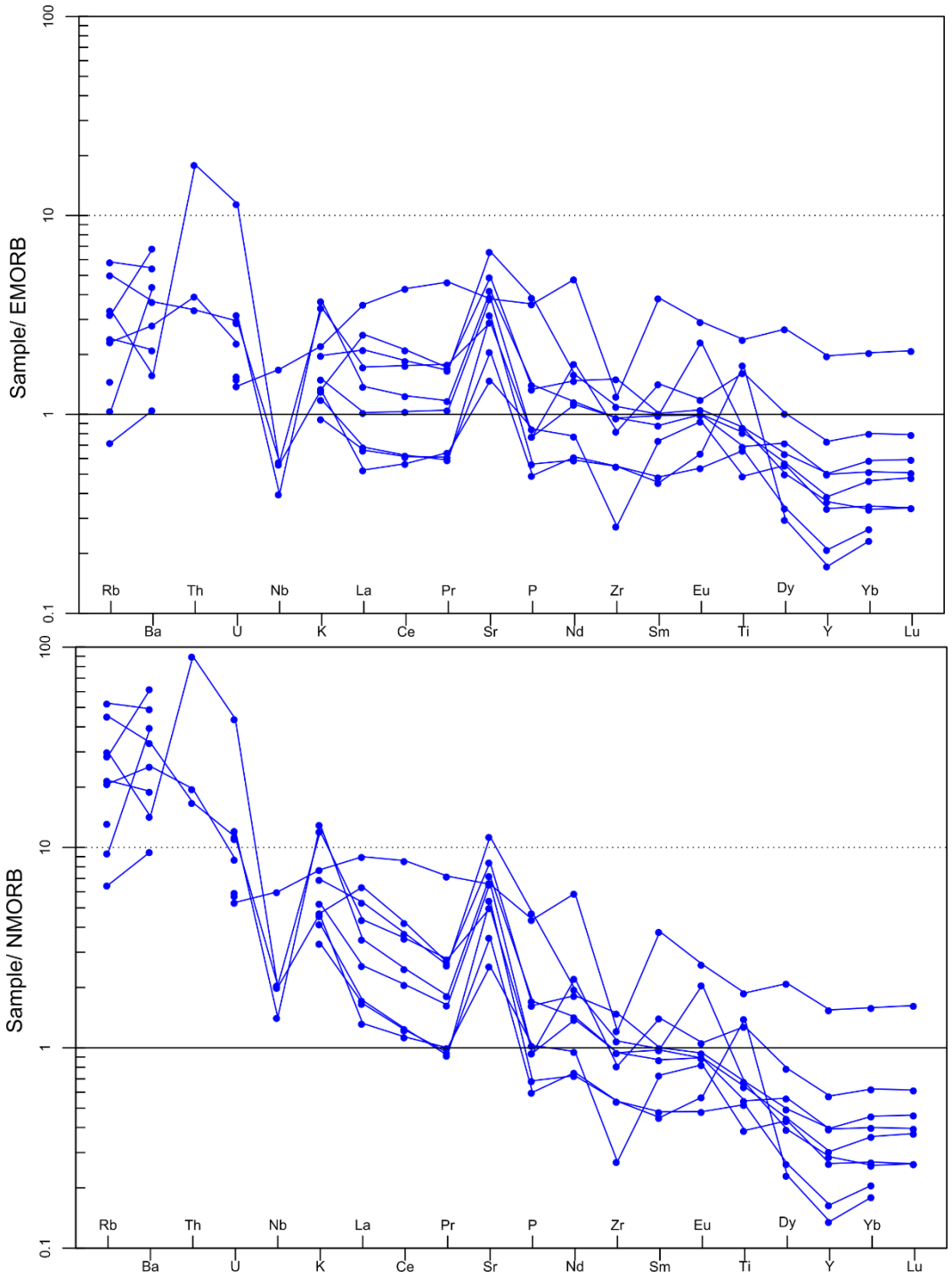

Figure 33. Samples from Palojärvi plotted into EMORB (above) and NMORB (below) normalized spider diagrams (Sun and McDonough 1989).

4.3.3 Hongonniittu

The four samples from Hongonniittu are taken from observation points next to each other. This, and the fact that there are only four samples, means that they cannot be used to estimate the overall composition of the intrusion. They rather serve as an indication of the composition of the rock types and can be used as a comparison to the samples from Matokulma and Palojärvi and Hongonniittu is not discussed further in this study.

Major elements

The samples are ultrabasic in general, based on the median of 44.43 wt-% SiO_2. Minimum and maximum silica values are 43.37 wt-% and 46.30 wt-%, respectively. The range of TiO_2 is from 0.48 wt-% to 1.32 wt-%, with a median of 0.93 wt-%. Al_2O_3 values are the highest of the studied intrusions at 21.67 wt-% median values, with a range from 19.00 wt-% to 26.06 wt-%. Fe_2O_{3t} ranges from 7.24 wt-% to 13.51 wt-% with a median value of 11.54 wt-%. MnO ranges from 0.09 wt-% to 0.18 wt-%, with a median value of 0.15 wt-%. MgO values range from 3.04 wt-% to 11.02 wt-%, with a median value of 6.23 wt-%, similar to Palojärvi. CaO has a median value of 12.79 wt-% and a range from 11.11 wt-% to 14.18 wt-%. Median value of Na_2O is 1.46 wt-% and minimum and maximum values of 0.70 wt-% and 1.73 wt-%,

CIPW norms

All four samples from Hongonniittu are Ol normative, with two of them being Ne normative and the other two Hy normative. Mean An, Fo, and En percentages are 83, 46, and 52, respectively

Trace elements

Trace element concentrations from Hongonniittu are mostly similar to those of Palojärvi, with some differences; Cr and Sr concentrations are higher – 100 and 720 ppm and Zn concentration is lower, 90 ppm. Ni concentration is 40 ppm on median.

One sample from Hongonniittu was analyzed for trace elements. The sample (SIKA-2017-9.1) is enriched in LREEs, displays a positive Eu anomaly, enrichment in LREE and MREE, primitive mantle like HREE concentrations (Figure 34). The sample displays depleted concentrations in MORB-normalized immobile elements spider diagram (Figure 35).

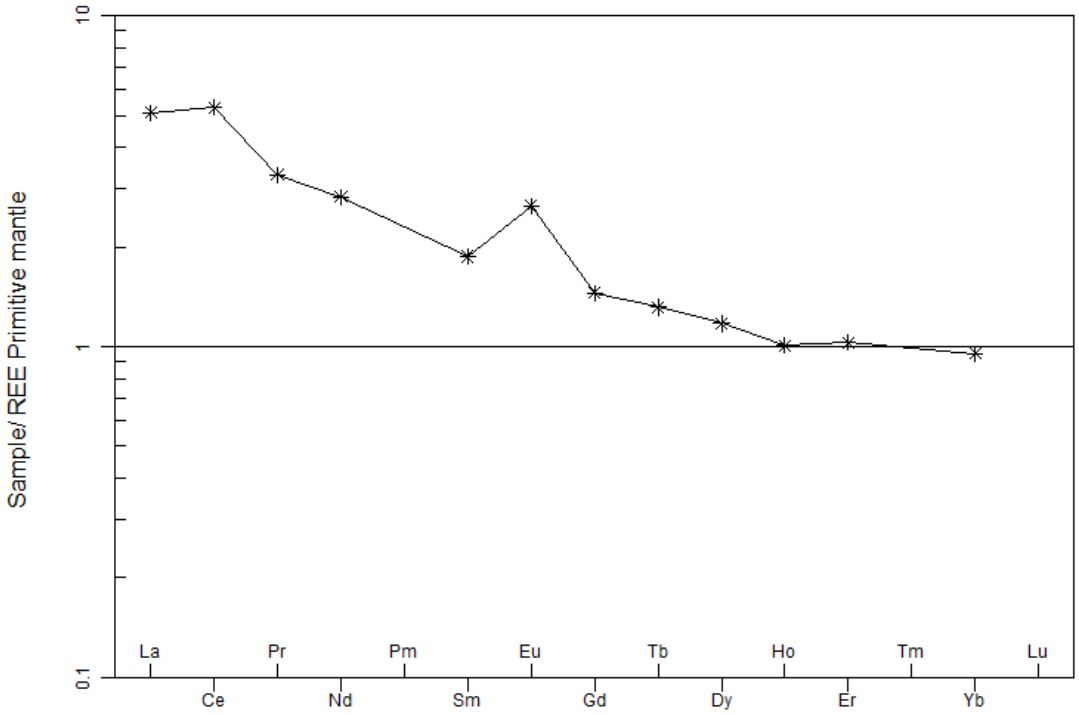

Figure 34. Hongonniittu sample plotted into a REE spider diagram, normalized against Primitive Mantle (McDonough and Sun 1995). The sample displays slight LREE enrichment, a positive Eu anomaly and primitive mantle-like HREE values.

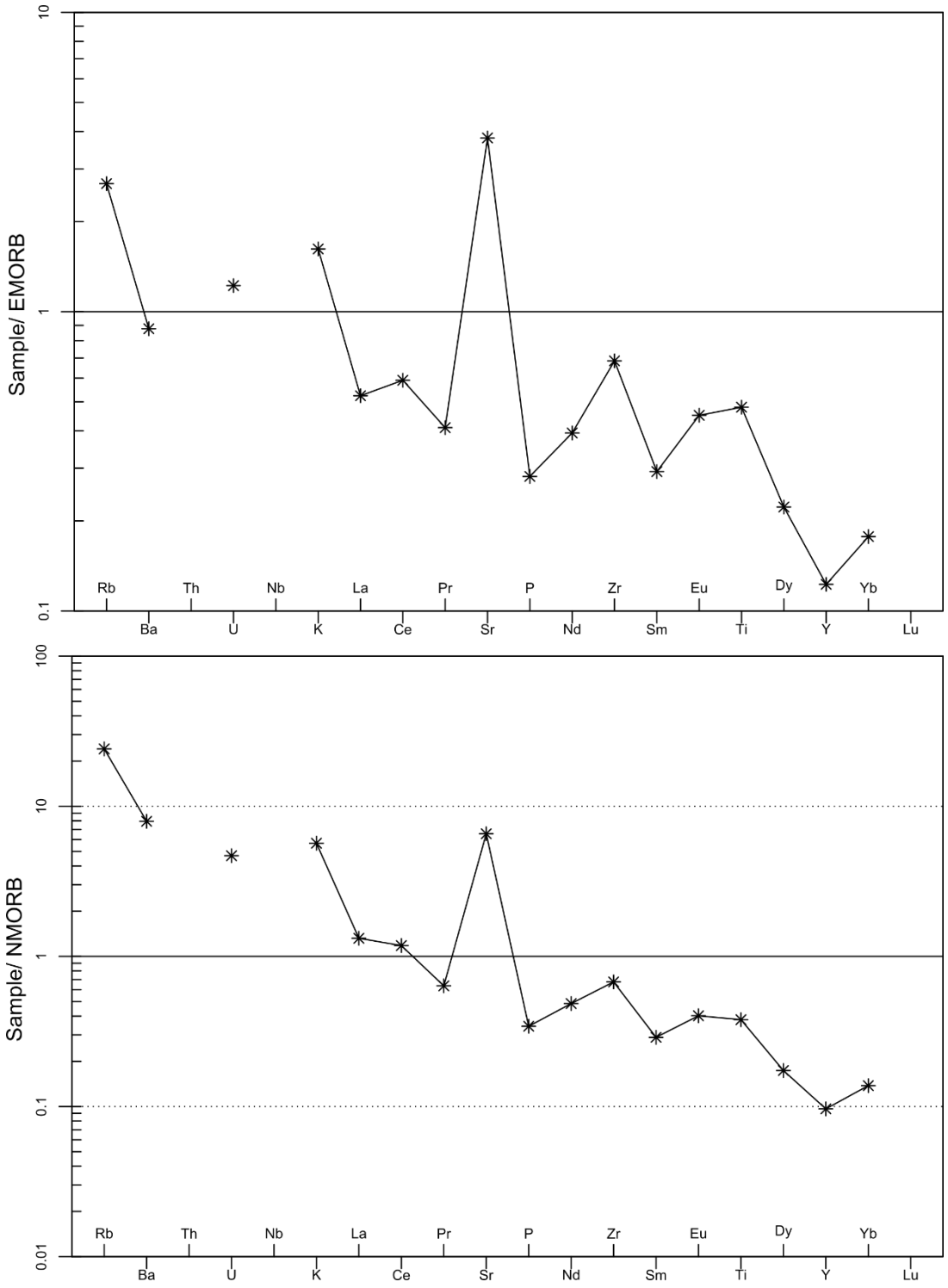

Figure 35 The sample from Hongonniittu, normalized to EMORB (top) and NMORB (bottom) (Sun and McDonough 1989). The sample displays slight enrichment in LILE and depletion in HFSE. Missing symbols indicate concentrations below detection limit.

4.4 Mineral chemistry

The analyzed pyroxenes belong to the Ca-Mg-Fe group and they are classified with the ternary endmember diagram – enstatite, wollastonite, ferrosilite (En, Wo, Fs), following the nomenclature and calculation principles of the International Mineralogical Association (IMA) (Morimoto et al. 1988). En and Wo are calculated on basis of the MgO and CaO concentrations, respectively, and Fs with both FeO_{total} and MnO. Amphiboles were classified with an Excel spreadsheet (ACES, Locock 2014), that follows the latest nomenclature and classification scheme of IMA (Hawthorne et al. 2012). The spreadsheet was also used to approximate the valence of Fe and Mn, and to estimate the hydroxyl content in the amphibole with OH^{-}=2-2Ti per atomic formula unit (apfu). Estimating hydroxyl content this way also raises the $Fe^{3+}/\Sigma Fe$ used in the normalization of the formula and consequently, affects the mineral name.

For example, the difference between pargasite ($NaCa_2(Mg_4\mathbf{Al})(Si_6Al_2)O_{22}(OH)_2$) and magnesio-hastingsite ($NaCa_2(Mg_4\mathbf{Fe^{3+}})(Si_6Al_2)O_{22}(OH)_2$) is the occupancy of C site by Al^{3+} or Fe^{3+}, respectively. Because of this, many of the amphiboles classified below as magnesio-hastingsite could also be classified as pargasite.

4.4.1 Matokulma

Orthopyroxene

The orthopyroxenes from Matokulma are enstatites. The compositions have a range of En_{65-74}, with a median of En_{69}. The concentration of Wo varies from 2 to 3 %. Mg# varies from 67 to 76. Al_2O_3 concentrations range from 0.4 up to 2.1 wt-% and correlate positively with TiO_2, which is on median 0.21 wt-% and range from 0.03–0.32 wt-%. Ni concentration is on median 50 ppm, with a range from below detection limit up to 110 ppm. Cr content varies largely between samples.

Orthopyroxene in sample SIKA-2017-115.2 have the highest median concentration of 870 ppm Cr, with some grains up to 1180 ppm Cr. The concentration of Ni ranges from below detection limit up to 110 ppm, and on median 40 ppm. The median V concentration is 1240 ppm. The sample has the highest median En and Mg#, 71 and 74, respectively.

Sample SIKA-2017-173.1 is similar to the previous sample where the median En and Mg# are 68 and 70.5, respectively. Median Ni is higher, 100 ppm, as is V, at 1360 ppm.

SIKA-2017-20.1 is markedly different from the other samples. Mg# and En values are lower, at 67 and 65, respectively. MgO, TiO_2, Al_2O_3, CaO values are lower than in the other two samples as well. SiO_2, FeO and MnO are higher. Highest Ni concentration from a single spot is 62 ppm.

All pyroxene analyses from Matokulma are plotted to an En-Wo-Fs diagram in Figure 36.

Clinopyroxene

Clinopyroxene compositions in Matokulma range from diopside to augite, based on the Wo component. Most of the analyzed grains are diopside, with a median Wo value of 46 %. The En component has a range of 40–48 %. The range of Fs component is 10–13 %. Wo component ranges from 42 to 48 %. Mg# of individual grains from all samples range from 77 to 83, with a median of 79. The median Mg# in any sample is rather uniform – 78–79.

As with orthopyroxene, TiO_2 and Al_2O_3 correlate positively. TiO_2 ranges from 0.01–0.48 wt-% and is on median 0.07 wt-%. Al_2O_3 concentration is on median 0.70 wt-% and has a range of 0.39 wt-% up to 3.01 wt-%. SiO_2 correlates negatively with TiO_2 and Al_2O_3.

Cr has a median concentration of 720 ppm, with a wide range from 80 up to 3100 ppm. V shows a similar, wide range of concentration, from 60–3800 ppm. Ni concentrations are low, on median 20 ppm. Zn and Co concentrations are on median 70 ppm and 55 ppm, respectively.

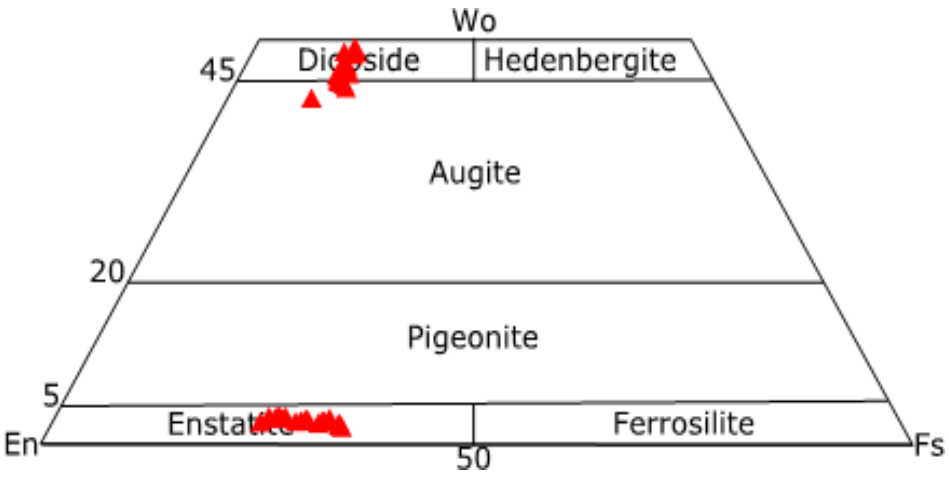

Figure 36. En-Wo-Fs pyroxene diagram. The diagram is cut off at Wo 50 m-%. All of the analyzed orthopyroxene plot into the enstatite field and most of the clinopyroxene plot into the diopside field.

The clinopyroxene in samples SIKA-2017-20.1 and SIKA-2017-112.1 are diopside (45–50 % Wo). In SIKA-2017-115.2, one of the grains is classified as augite (< 45 % Wo), the others as diopside. Sample SIKA-2017-173.1 contains both diopside and augite. In the sample, there is a grain with an augitic center and a rim of diopside, representing either an inclusion or zoned growth. The augite part contains more Al_2O_3 and TiO_2, slightly more MgO and FeO, and less CaO than the surrounding diopside.

Augites from SIKA-2017-173.1 have the highest Mg#, Cr, V concentrations, at 83.4, 3100 ppm, and 3800 ppm, respectively. The highest Al_2O_3 and TiO_2 concentrations (3.01 wt-% and 0.45 wt-%, respectively) are also found from this sample. The diopsides in the sample have lower Cr concentrations than the augites.

Amphibole

The analyzed poikilitic amphiboles belong mainly to the Ca-amphibole subgroup and they are classified as magnesio-hastingsites, magnesio-hornblendes, magnesio-ferri-hornblendes, and pargasites. Actinolite is also present in some samples, usually within or as rims around previously mentioned poikilitic amphiboles or pyroxenes. Primary, poikilitic amphiboles are magnesio-hastingsites and pargasites that have $^{A}(Al+Fe^{3+}+2Ti) > 1.2$ and $^{C}(Na+K+2Ca) > 0.5$ (Figure 37). Hornblendes are mostly present as uralitic rims around clinopyroxene and between the clinopyroxene and surrounding poikilitic amphibole or as fully altered grains within poikilitic amphibole.

The poikilitic amphiboles have, on median, higher concentrations of Ni, Cr, V when compared to pyroxenes. Cr and V concentrations are several times higher than those of the pyroxenes in the same sample.

The magnesio-hastingsites have median Mg#, MgO, and FeO values of 70, 13.72 wt-%, and 10.59 wt-%, respectively. Al_2O_3, CaO, Na_2O, K_2O are 12.33 wt-%, 11.64 wt-%, 2.01 wt-%, 0.91 wt-%, respectively. Ni concentration is on median 60 ppm, with the highest values up to 100 ppm. Cr concentration is on median 2640 ppm. TiO_2 and V_2O_3 are 1.77 wt-% and 0.93 wt-%, respectively.

The magnesio-hornblendes and magnesio-ferri-hornblendes have median values Mg#, MgO, and FeO of 72, 15.61 wt-%, and 10.69 wt-%, respectively. Al_2O_3, CaO, Na_2O, K_2O are 8.62 wt-%, 11.70 wt-%, 1.11 wt-%, 0.56 wt-%, respectively. Ni and Cr concentrations on median 75 ppm, with the highest values up to 130 ppm, and 960 ppm, respectively. TiO_2 and V_2O_3 are 0.72 wt-% and 0.53 wt-%, respectively.

The two analyzed pargasite grains have median Mg#, MgO, and FeO values of 65, 12.31 wt-%, and 11.68 wt-%, respectively. Al_2O_3, CaO, Na_2O, K_2O are 12.61 wt-%, 11.78 wt-%, 1.52 wt-%, 0.98 wt-%, respectively. Ni and Cr have median concentrations of 20 ppm and 1050 ppm, respectively. TiO_2 and V_2O_3 are 1.46 wt-% and 0.65 wt-%, respectively.

Feldspars

Plagioclase was analyzed from samples SIKA-2017-115.2 and -173.1. The plagioclase from sample SIKA-2017-115.2 are stained by a reddish-brown pigment and they are An_{83} in composition. Alkali feldspar was also found from sample SIKA-2017-115.2, with a composition of $Or_{85–90}$-$Ab_{10-15}An_0$. Slightly more Ca-rich plagioclase is found in sample SIKA-2017-173.1, where the plagioclase is $An_{85–86}$ in composition.

Other phases

Cl-rich (median 2.53 wt-% Cl) apatite was analyzed from sample SIKA-2017-115.2. The apatite is enclosed within interstitial amphibole.

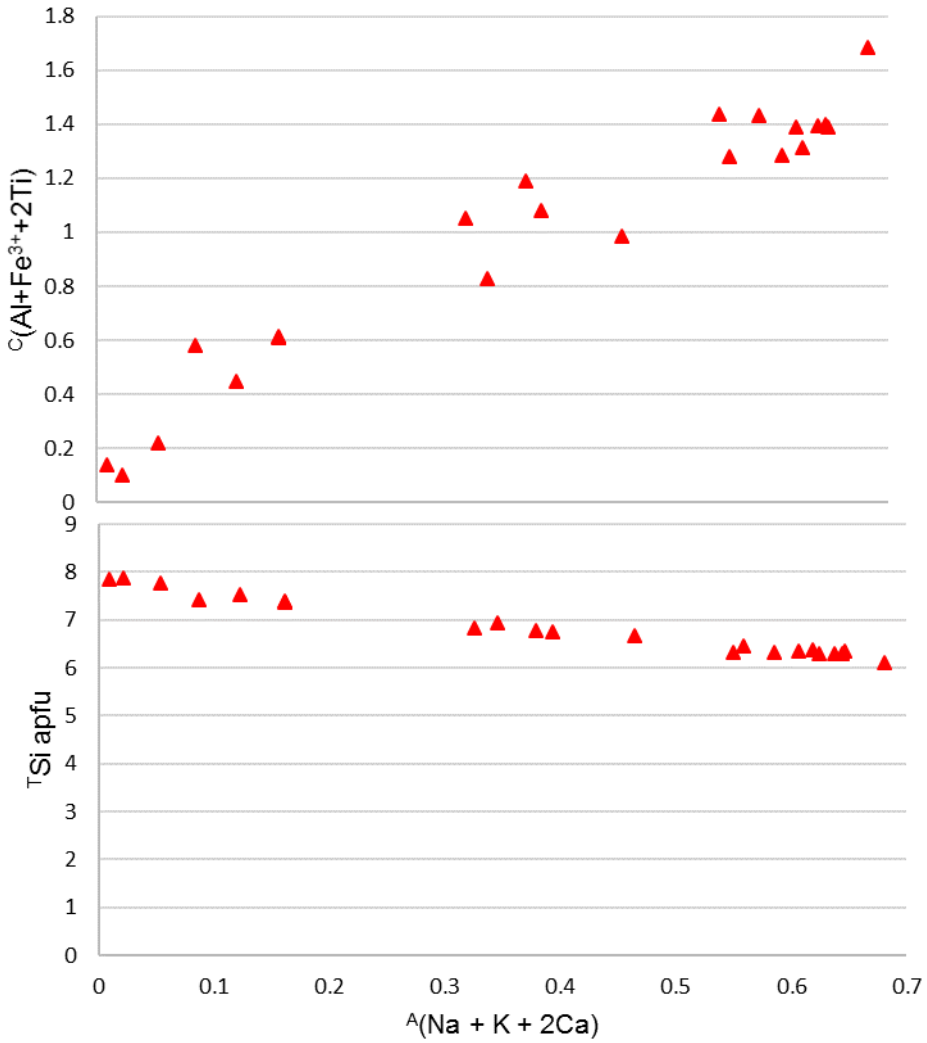

Figure 37. Amphibole compositions from Matokulma on (Na+K+2Ca) versus (Al+$^{Fe3+}$+2Ti) (above) and versus Si (below). Primary, poikilitic amphiboles have high, > 1.2 (Al+$^{Fe3+}$+2Ti) and >0.5 (Na+K+2Ca) and lower Si than metamorphic phases. Uppercase A, T, C denote amphibole structural sites. All values are apfu.

4.4.2 Palojärvi

Orthopyroxene

During the setting of analysis spots for EPMA analysis, orthopyroxene grains in samples SIKA-2017-1.1 and 1.2 were observed to display lamellar, exsolution textures, when observed in back-scattered electron image. The lamellae are CaO-rich based on qualitative EDS analyses. Sample SIKA-2017-88.2 display similar, but thinner lamellae. These lamellae are not visible in optical petrographic examination.

The orthopyroxene compositions have a range of $En_{41–59}$, $Fs_{39–55}$, Wo is 3 % at maximum. The orthopyroxene in samples SIKA-2017-1.1 and -1.2 are mostly ferrosilite (Fs > 50 %) and, in samples SIKA-2017-80.1, -88.1, and -88.2, enstatite (En > 50 %). Mg# is, on median 54 and ranges from 44 to 61. The highest enstatite concentration is in sample SIKA-2017-80.1 (olivine norite), where the poikilitic orthopyroxene is more magnesian than the cumulus olivine ($Mg\#_{Opx}$ 58 and $Mg\#_{Ol}$ 45). Ni concentrations for all samples are on median 70 ppm and at maximum – 190 ppm. V concentrations range from below detection limit to 1200 ppm and on median, 530 ppm. All pyroxene analyses from Palojärvi are plotted to a ternary En-Wo-Fs diagram in Figure 38.

Clinopyroxene

Clinopyroxene was analyzed from three samples from Palojärvi. The range of Wo, En, and Fs compositions are 40–47 %, 34–44 %, and 13–21 %, respectively. The median values of Wo, En, and Fs components are 45 %, 38 % and 17 %, respectively. Mg# range from 62 to 77. V concentrations have a range from 600 up to 4400 ppm. Cr concentrations are generally low, median value of all samples is 90 ppm.

The clinopyroxene grains in sample SIKA-2017-88.1 contained both augite and diopside, with the lowest Wo % being 43. Most of the grains, however were classified as diopside and the median Wo of the analyses is 45 %. In sample SIKA-2017-88.2, all of the analyzed clinopyroxene grains were diopside (Wo > 45 %).

SIKA-2017-156.1 contains large, round grains of clinopyroxene, all of which are classified as augite (Wo < 45 %). The clinopyroxene in this sample are more primitive than in other samples. They have the highest Mg#, Cr, V, and Ni (median values of 75, 1300 ppm, 3000 ppm, respectively The Al_2O_3 concentration of the clinopyroxenes in the sample are also higher than in other samples (3.0–5.5 wt-%).

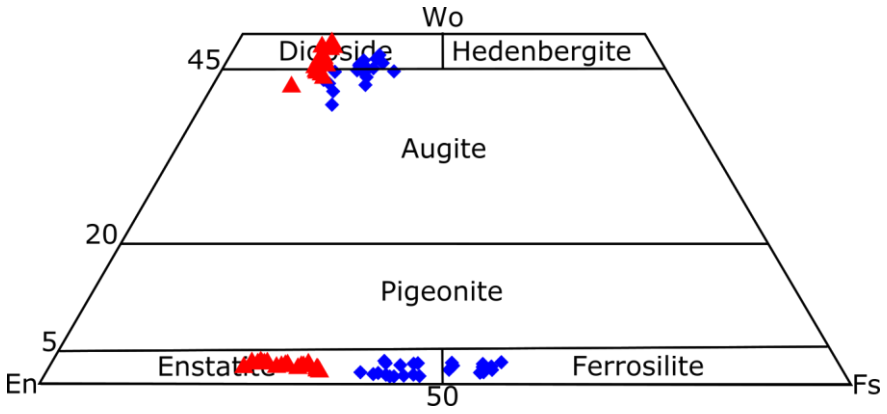

Figure 38. Pyroxene analyzes from Palojärvi (blue symbols) plotted into a ternary pyroxene En-Wo-Fs diagram, the diagram is cut at Wo 50 m-%. Pyroxene analyzes from Matokulma (red symbols) are shown for reference.

The clinopyroxene compositions fall into two groups, with lower En %, with lower Wo %, and higher Fs % with higher Wo %.

Amphibole

Most of the analyzed poikilitic amphiboles are classified as magnesio-hastingsite or magnesio-ferri-hornblende. In SIKA-2017-88.2, the amphiboles are classified as Ti-rich magnesio-hastingsite. Other amphibole species, cummingtonite and actinolite, were also analyzed. Primary amphiboles have higher have $^{A}(Al+Fe^{3+}+2Ti) > 1.2$ and $^{C}(Na+K+2Ca)$ over 0.5 (Figure 39). Hornblendes and actinolites are mostly present as uralitic rims around clinopyroxene and between the clinopyroxene and surrounding poikilitic amphibole or as fully altered grains within poikilitic amphibole.

Median chemical compositional values for magnesio-hastingsite analyses are Mg# of 56.7, MgO and FeO are 11.10 wt-% and 15.09 wt-%, respectively. CaO, Na_2O and K_2O are 10.80 wt-%, 2.20 wt-% and 0.62 wt-%, respectively. TiO_2 and V_2O_3 are 2.21 wt-% and 0.67 wt-%, respectively. Ni concentrations are on median 16 ppm, but some grains have higher Ni concentrations, with values up to 147 ppm Ni. Magnesio-hastingsites have $^{C}(Na+K+2Ca)$ over 0.5

Magnesio-ferri-hornblende and one magnesio-hornblende grains have median chemical compositions of Mg# 48.3. MgO and FeO are 9.67 wt-%, 18.75 wt-%, respectively. CaO, Na_2O and K_2O are 11.12 wt-%, 1.22 wt-%, and 0.89 wt-%, respectively. TiO_2 and V_2O_3 are 1.53 wt-%, 0.66 wt-%, respectively. Ni concentrations are on median 21 ppm, but concentrations up to 225 ppm are found in single grains. Hornblendes have $^{C}(Na+K+2Ca)$ below 0.5, from 0.497 down to 0.276.

In sample SIKA-2017-156.1, large, round clinopyroxene phenocrysts are partly or completely uralitized to dark, green pleochroic amphibole. The amphibole, magnesio-hastingsite, magnesio-hornblende, and magnesio-ferri-hornblende, is noticeably richer in Cl, 0.20–0.30 wt-%, than the other Palojärvi amphiboles, which have ≤0.08 wt-% Cl.

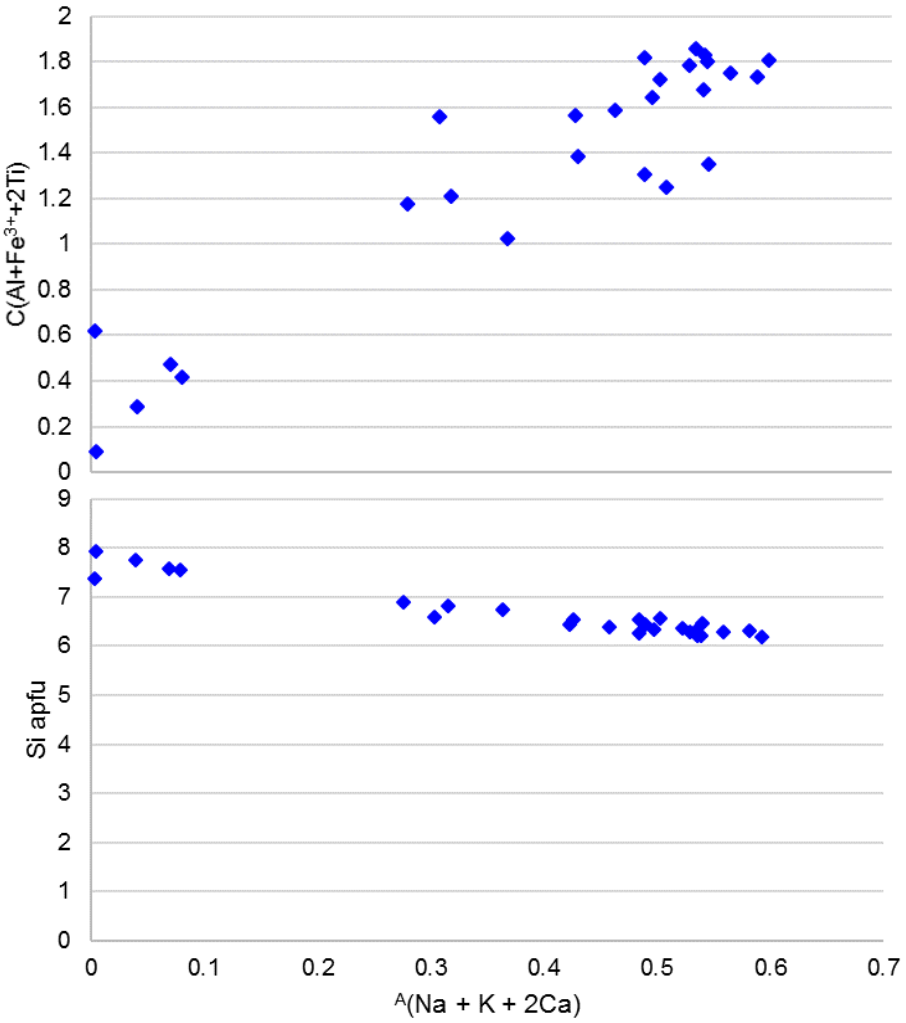

Figure 39. Amphibole compositions from Palojärvi on (Na+K+2Ca) versus (Al+$^{Fe3+}$+2Ti) (above) and versus Si (below). Primary, poikilitic amphiboles have high, > 1.2 (Al+$^{Fe3+}$+2Ti) and ~>0.5 (Na+K+2Ca) and lower Si than metamorphic phases. Uppercase A, T, C denote amphibole structural sites. All values are apfu

Plagioclase

Plagioclase was analyzed from samples SIKA-2017-88.2 and -156.1. The plagioclase in sample 88.2 is $An_{67–70}$ in composition. A normally zoned plagioclase crystal from sample SIKA-2017-156.1 was analyzed. The center of the crystal is An_{50} and the rim An_{41} in composition, respectively.

Olivine

Only one sample (SIKA-2017-80.1) contained olivine. The olivine crystals are in the cumulate phase together with plagioclase and they are enclosed in poikilitic orthopyroxene, amphibole, and phlogopite. The olivine is fayalitic in composition ($Fo_{42–49}$). Ni concentrations are on median 105 ppm, ranging from below detection limit up to 250 ppm, depending on the analysis spot. MnO content is 0.60–0.75 wt-%, resulting in

an Mn-endmember (tephroite) component of 0.75–0.95 m-%. Al_2O_3 content is mostly below detection limit but in some grains up to 0.02 wt-%. CaO content is 0.01–0.02 wt-% in all of the analyzed grains. The concentrations of both Na_2O and K_2O are similar, with a range from below detection limit up to 0.02 wt-%. P_2O_5 has a median concentration of 0.01 wt-%, with concentrations up to 0.07 wt-%.

Opaque

The few analyzed oxide minerals were ilmenite and magnetite. Both magnetite and ilmenite were analyzed from samples SIKA-2017-88.2. and -156.1 In sample SIKA-2017-88.2, magnetite is vanadiferous, containing up to 1.37 wt-% V_2O_3 (~9300 ppm V) and contains 0.29–0.54 wt-% TiO_2. Ilmenite contains 0.12–0.17 wt-% V_2O_3. The magnetite and the ilmenite in sample SIKA-2017-156.1 contain 0.95 wt-% and 0.20 wt-% V_2O_3, respectively. The magnetite contains 0.05 wt-% TiO_2.

Mica

Sample SIKA-2017-156.1 contains biotite, which has Mg# of 50.5 and is rich in TiO_2 and V, 4.53 wt-% and 5500 ppm, respectively. The biotite contains 0.23 wt-% and 0.16 wt-% of F and Cl, respectively.

4.5 Geophysics

4.5.1 Petrophysics

All of the collected samples were measured for their petrophysical properties and the results were plotted and grouped based on the studied intrusion (Figure 40). The samples from Matokulma have notably lower magnetic susceptibilities and less variance than the Palojärvi samples. The median density and magnetic susceptibility of the mafic samples are 2960 kg/m^3 and $660 \cdot 10^{-6}$ SI, respectively. The median Q-ratio of the samples is 2.15, with a wide range from 0 to 11. The mafic samples from Palojärvi have a wide scatter in magnetic susceptibilities, median and highest values are $9100 \cdot 10^{-6}$ SI and 1,730,000 10^{-6}

SI, respectively. The median density and Q-ratio are 3020 kg/m^3 and 0.67, respectively. The magnetic susceptibility correlates positively with increasing density.

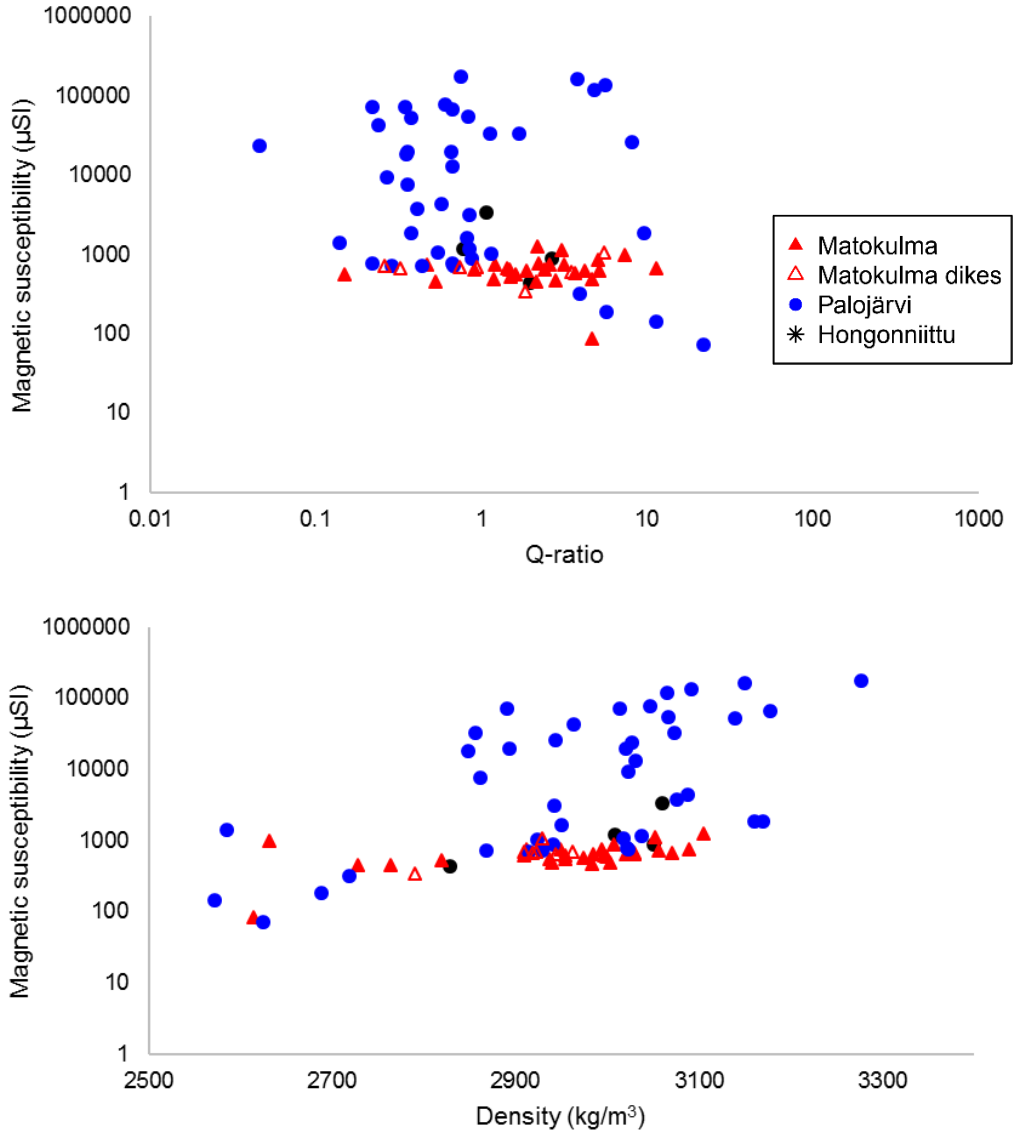

Figure 40. (above) Q-ratio against magnetic susceptibility. (below) Density versus magnetic susceptibility. Notice that also the more felsic, country rock samples (lower density) are plotted. Hongonniittu (black circles), Matokulma (red circles), Palojärvi (blue circles).

4.5.2 Gravity measurements

Palojärvi and Hongonniittu

The results of gravity measurements are presented as Bouguer anomaly profiles over modelled anomaly objects in figures 41 and 42. Figure 41 show the anomaly models for Palojärvi and Hongonniittu. The Palojärvi model shows a slightly irregular, steeply southwards dipping object, which continues into a depth of up to 850 m.

The Hongonniittu model dips northwards, with a more gentle dip. The anomaly object is modelled to be a simple rectangular slab, which continues to a depth of over 700 m.

Matokulma

Two survey profiles, lines 12 and 13, were measured over the eastern and western part of the Matokulma intrusion, respectively (Figure 42). The model for line 12 is exposed for some 300–350 m on the surface in N-S direction, after which it steeply plunges below the surface for some 60 m, after which the plunge becomes more shallow. Based on the model, the intrusion has depth extent of ca. 225 m.

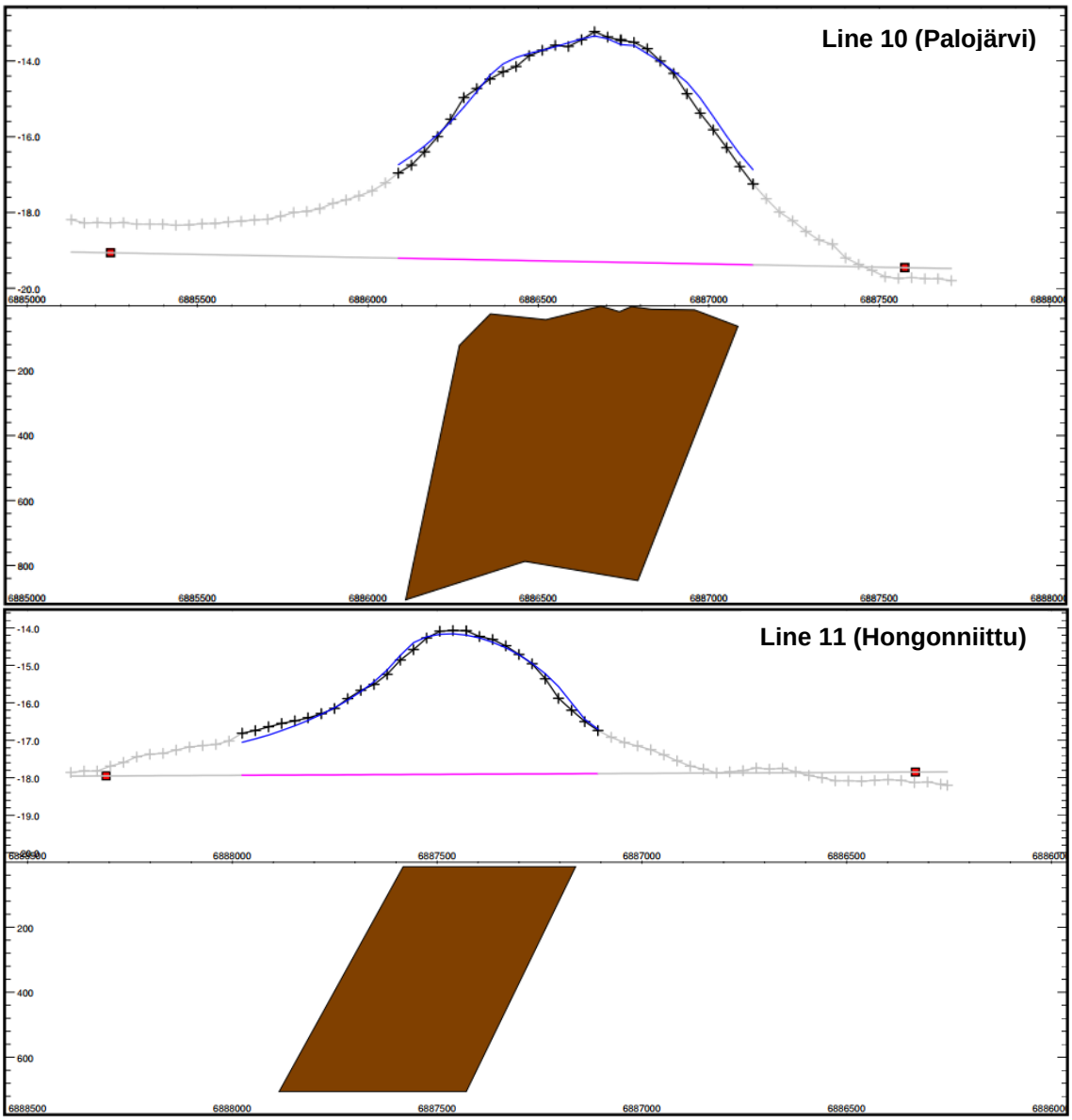

Figure 41. Bouguer anomaly measurements of lines 10 and 11, over Palojärvi (top) and Hongonniittu (bottom), respectively. Background density of 2670 kg/m^3 and intrusion densities of 3020 kg/m^3 and 2987 kg/m^3 were used for lines 10 and 11, respectively. North coordinate is on the X axis and Bouguer anomaly on the Y axis and the depth below, next to the anomaly model. Notice that the coordinates increase to the right i.e. go northwards on the Palojärvi profile, where as they decrease in the Hongnonniittu profile. All coordinates are in KKJ3 coordinate system.

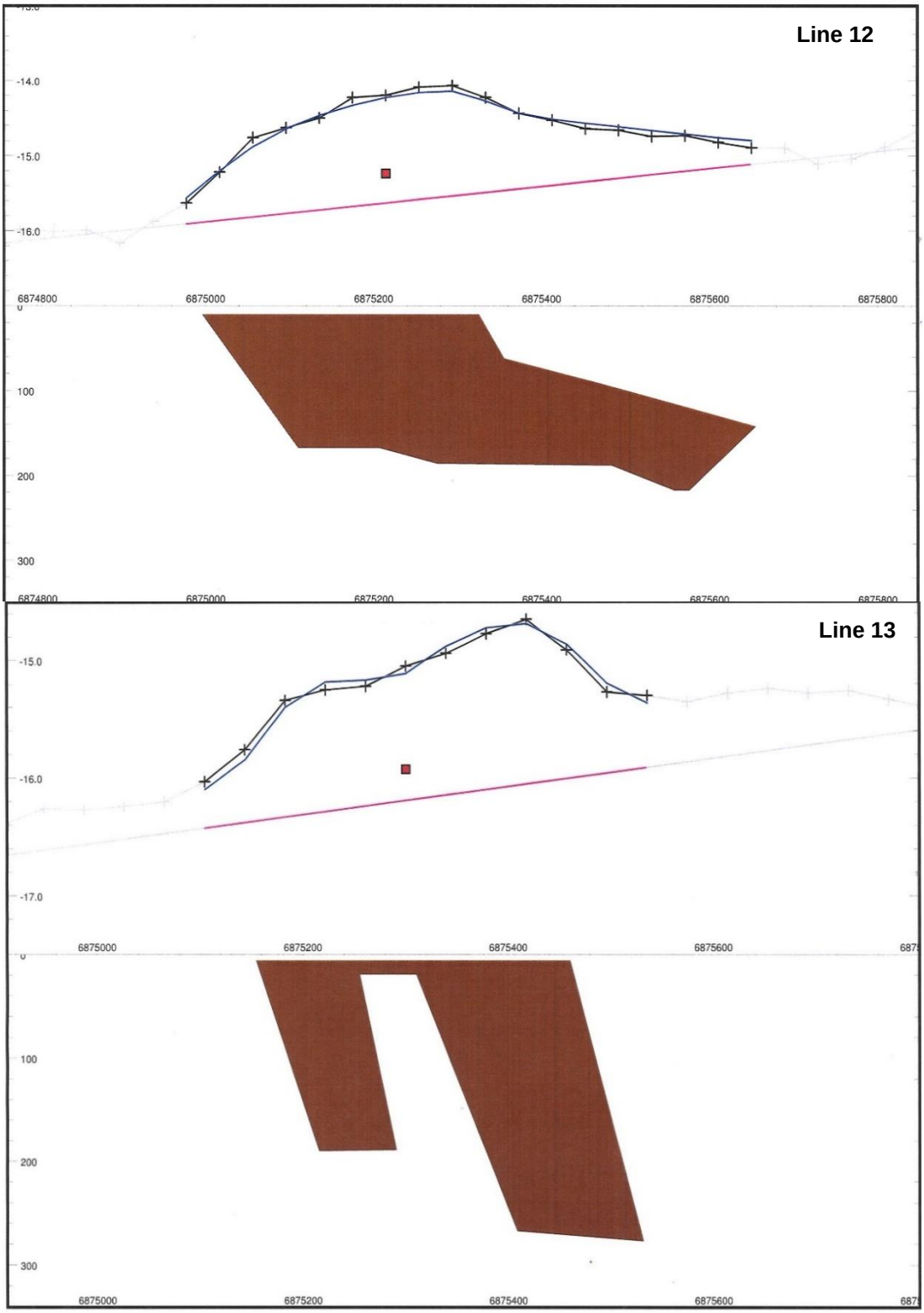

Figure 42. Bouguer anomaly profiles and models over Matokulma. Line 12 (top), line 13 (bottom). The Bouguer anomaly values are shown above a model of the anomaly. Densities used for the models are 2670 kg/m^3 for background, 2980 kg/m^3 for the westside and 2970 kg/m^3 for eastside of the line. North coordinate is on the X axis and Bouguer anomaly on the Y axis and the depth below, next to the anomaly model. All coordinates are in KKJ3 coordinate system.

The model for line 13 is a more complex object or two parallel objects. The model has two northwards plunging ‘plates’ to a depth of 200 m and 250 m with a shallow part between them. The object is exposed for some 300 m on or near surface.

4.6 Isotope geochemistry

4.6.1 U-Pb (zircon)

Sample description

Two samples for age determinations were taken from Palojärvi. One sample is from a leucogabbro dike (Sample SIKA-2017-17.1), which cuts the melanocratic gabbro dike in the center of the Palojärvi intrusion. The other is from a granite (sample SIKA-2017-101.1) which is located on the south side of Palojärvi, near the contact zone. The granite cuts the gabbro.

SIKA-2017-17.1 (A2463)

Sample SIKA-2017.17.1 is a leucocratic gabbro, which consists of zoned plagioclase, which exhibits undulatory extinction, pleochroic blueish-green to light brown amphibole and light to light green pleochroic amphibole, and biotite. Magnetite, apatite, and zircon are present as accessory phases. The composition of plagioclase is ~ An_{55}, based on the extinction angles of polysynthetic twinning of crystals, and An_{54}, based on the normative composition.

The zircons are fractured, occasionally broken crystals, which are mostly sub to euhedral grains which sometimes display zoned growth textures (Figure 43). The grains are 100–150 µm in length. 20 grains were analyzed in total.

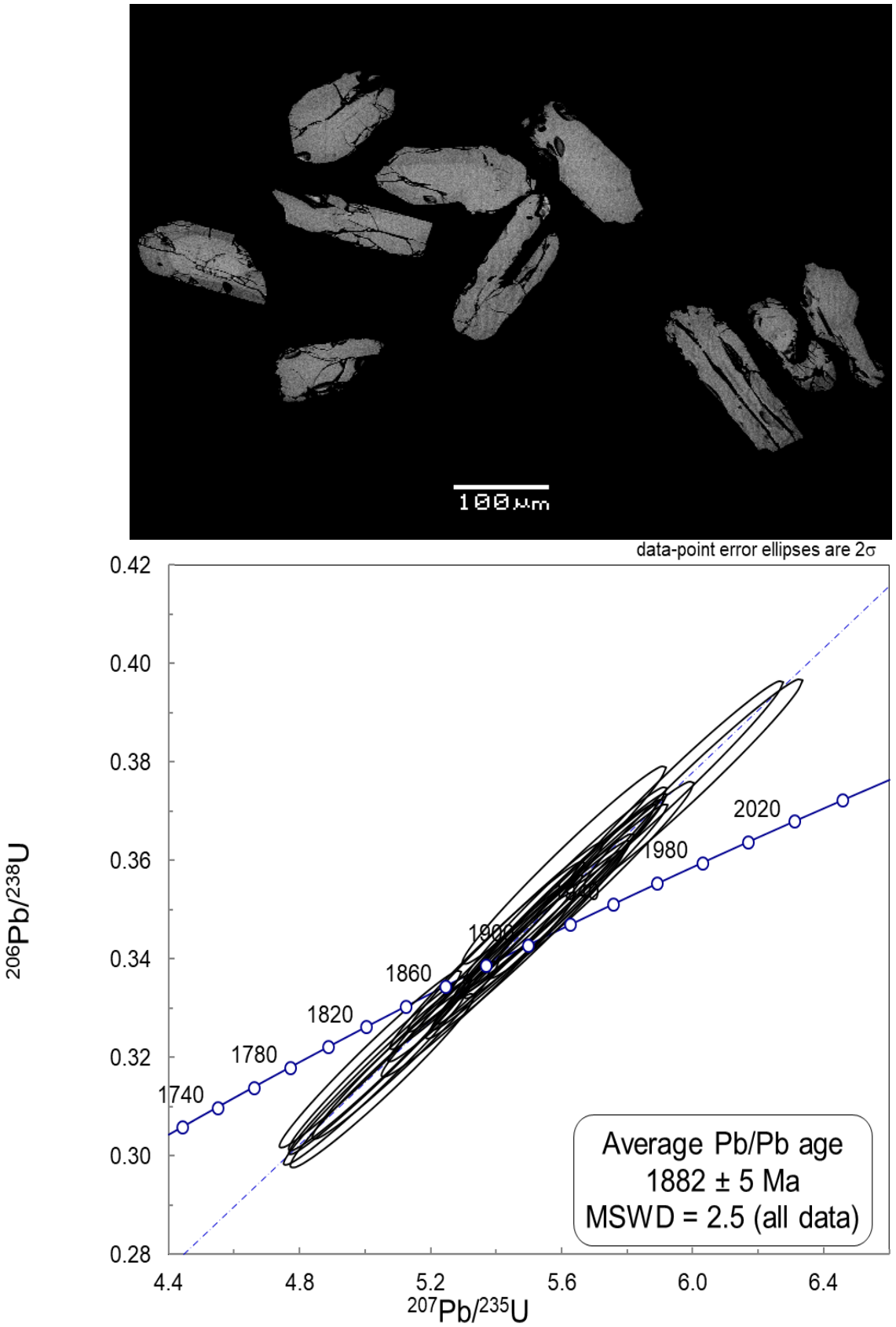

Figure 43. Top) BSE image of some of the zircon grains from sample SIKA-2017-17.1 (A2463). Most grains are fractured. Some of the grains display overgrowth textures. (bottom) Below) Concordia diagram for the analyzed zircons from sample SIKA-2017-17.1 (A2463), leucogabbro (Huhma 2018, written communication).

The concordia diagram (Figure 43, Huhma 2018, written communication) has all of the analyzed zircons plotted, resulting in an average Pb/Pb age of 1882±5 Ma. Removing the most inversely discordant zircons and then calculating the average $^{206}Pb/^{207}Pb$ ages using the weighted average of the analyses result in an average age of 1883±4.8 Ma (Meaned square weighted deviation (MSWD=1.9)) (Figure 44).

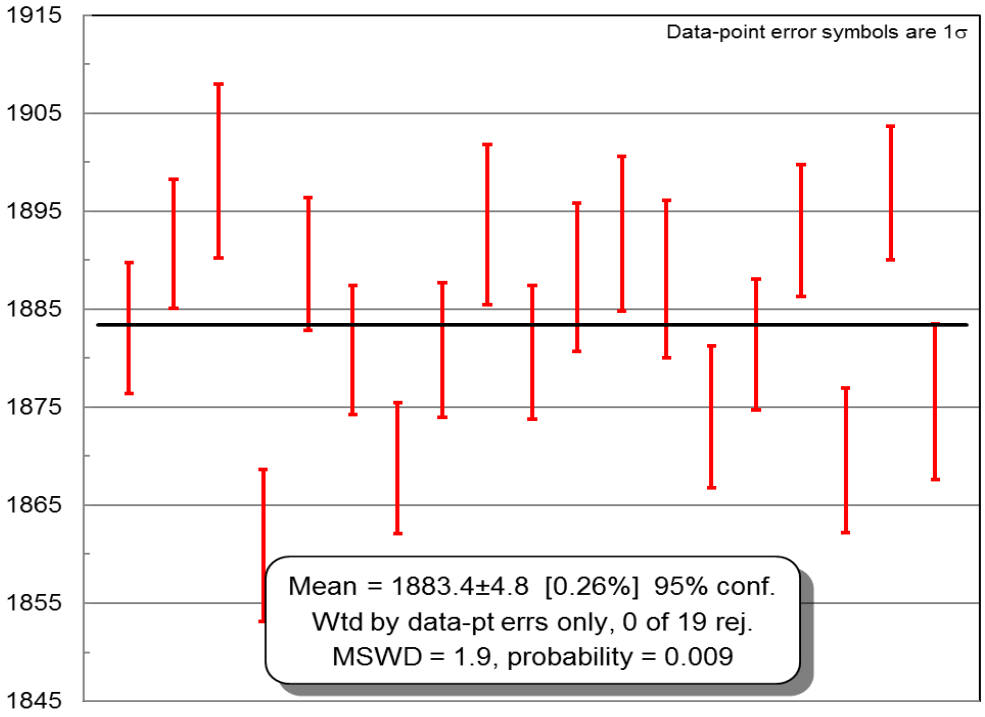

Figure 44. Weighted average $^{206}Pb/^{207}Pb$ age diagram of sample SIKA-2017-17.1 (A2463), leucogabbro. The weighted average age is 1883.4±4.8 Ma.

SIKA-2017-101.1 (A2464)

Sample SIKA-2017-101.1 is a leucocratic, foliated biotite-amphibole granite. Main minerals are plagioclase, K-feldspar, quartz, pleochroic amphibole, and biotite, with epidote, titanite, muscovite, zircon, and apatite as accessory phases. Quartz and plagioclase display undulatory extinction and quartz also has recrystallization textures, such as bulging. Plagioclase is sericitized. K-feldspar is perthitic and displays tartan twinning. Grain boundaries between quartz and K-feldspars show myrmekitic textures. The sample is metaluminous.

The zircons in the sample are usually rounded, euhedral grains, which are sometimes fractured and often display zoned growth textures (Figure 45). Many grains have metamict cores.

Figure 45. BSE image of some of the zircon grains from sample SIKA-2017-101.1 (A2464). Many grains have metamict cores and display overgrowth textures.

The concordia diagram in Figure 46 includes all of the analyzed zircons. Two of the clearly older, inherited zircons were excluded from the calculation of the average age. The average Pb/Pb age for the sample is 1897±7 Ma (MWSD=4.3).

Some of the zircons used in the calculations are inversely discordant. Removing the most inversely discordant zircons from the calculations and calculating the average $^{206}Pb/^{207}Pb$ ages using the weighted average of the analyses results in an average age of 1893±7.1 Ma (MSWD=3.2) (Figure 46).

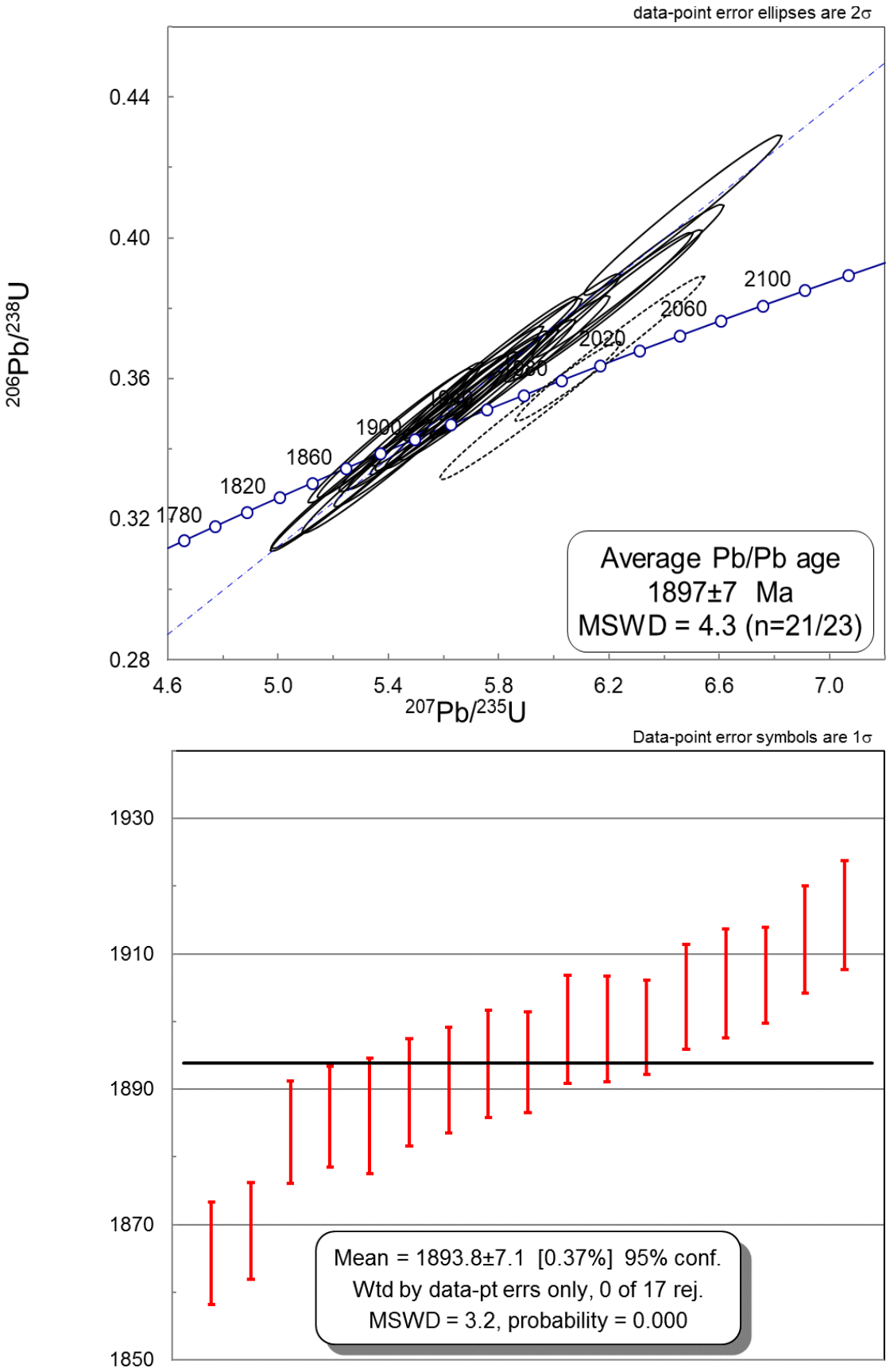

Figure 46. (Top) Concordia diagram for U-Pb analyzed from all but the two inherited zircons (dashed ellipses), with an average $^{206}Pb/^{207}Pb$ age of 1897±7 Ma (Huhma 2018, written communication). (Bottom) Removing the four inversely discordant zircons result in a weighted average $^{206}Pb/^{207}Pb$ age of 1893.8±7.1 Ma. Sample SIKA-2017-101.1 (A2464), leucogranite.

4.6.2 Sm-Nd (whole-rock)

The results of the Sm-Nd analyses are given in Table 2. Sm and Nd concentrations are 1.56 ppm, 8.78 ppm and 2.54 ppm and 17.87 ppm, for the leucogabbro and the granite, respectively. $^{147}Sm/^{144}Nd$ and $^{143}Nd/^{144}Nd$ values for the gabbro are 0.1076 and 0.511666 and 0.0858 and 0.511339 for the granite. Both samples have positive εNd values; 2.5 and 1.6, respectively.

Table 2. Result table of whole-rock Sm-Nd analysis of two samples from Palojärvi. Both samples have positive εNd values.

Sample	Sm (ppm)	Nd (ppm)	$^{147}Sm/^{144}Nd$	± 0.4%	$^{143}Nd/^{144}Nd$	2σ	T (Ma)	ε(T)	Age/U-Pb (Ma)	Age-error (±Ma)
A2463 SIKA-2017-17.1	1.56	8.78	0.1076	0.0011	0.511666	0.000009	1883	2.5	1883.4	4.8
A2464 SIKA-2017-101.1	2.54	17.87	0.0858	0.0009	0.511339	0.000007	1894	1.6	1893.8	7.1

5. DISCUSSION

5.1. Parental magmas

As the studied rocks are cumulates, they do not directly represent the composition of the parental magma from which they fractionated. Chilled margins or magmas quenched against country rock have been used to deduce parental magma compositions (e.g. Makkonen 1996, Forss et al. 1999). The use of chilled margins as vectors for the parental magma composition is not without pitfalls (e.g. Latypov et al. 2007). Chilled margins were not found from any of the intrusions studied in this thesis.

Mineral chemistry of primary, early crystallizing mafic minerals (i.e. olivine, orthopyroxene) can be used to deduce the parental magma composition, if the minerals were in equilibrium with the magma during crystallization. The MgO end members of olivine and orthopyroxene can be used to determine the ratio MgO/ FeO ratio of the magma from which the minerals crystallized from (Roeder and Emslie 1970). According to Roeder and Emslie (1970), the partitioning of iron and magnesium between melt and olivine can be described with distribution coefficient (K_D). For olivine K_D is

experimentally determined to be 0.30±0.03 and independent of temperature at a pressure of 1 atm (Roeder and Emslie 1970, Roeder 1974).

$$K_D = \frac{(X_{FeO}^{Ol})}{(X_{FeO}^{Liq})} \frac{(X_{MgO}^{Liq})}{(X_{MgO}^{Ol})} \qquad (eq.\,2)$$

The experimental work of Roeder and Emslie (1970) was done with basaltic samples with MgO up to 12 wt-% and experimental temperatures up to 1300º C. Therefore, these calculations cannot be used for melts with higher MgO concentrations or temperatures. The calculations can be used to determine both the MgO/FeO ratio of the parental melt or conversely, the mineral which would be in equilibrium with a melt of a certain MgO/FeO ratio.

The results of Roeder and Emslie (1970) have been widely applied in petrological studies, but not without critique (e.g. Herzberg and O'Hara 2002, Toplis 2005 and references therein). According to later studies (see the previously cited studies) the partition coefficient is affected not only by the MgO and FeO concentrations of the magma, but also the temperature and pressure of the system and the concentration of alkalis, SiO_2, H_2O, and P_2O_5. However, the K_D value of ~0.30 is often observed in natural samples, because the aforementioned parameters tend to cancel out (Toplis 2005). Thus, the partition coefficients of Roeder and Emslie (1970) still hold fairly well for tholeiitic basalts in pressures less than 2 GPa (See Figure 15a in Toplis 2005).

As the studied intrusions consist mostly of evolved, plagioclase-bearing cumulates with cpx ± opx and intercumulus amphibole, rather than olivine or orthopyroxene cumulates, the following calculations provide only a rough estimate on the MgO concentration of the parental magmas.

Makkonen (1996) combined the equations presented in Roeder and Emslie (1970) that describe the partitioning of MgO and FeO ratio between melt and olivine/orthopyroxene. The equations give out the concentration of MgO (wt-%) in melt for a given Fo or En composition, with a given distribution coefficient of MgO/FeO between the melt and the mineral. The equations conform to the MgO/FeO ratio of the Svecofennian tholeiites-picrites, which are considered to be comagmatic with the Svecofennian mafic-ultramafic intrusions (e.g. Makkonen and Huhma 2007, Barnes et al. 2009) and can be used only for magma types of similar MgO/FeO ratio.

The equation for Fo (K_D=0.33) is

$$\log MgO_{liq} = \frac{\log Fo - \log(252.7833 - 0.7825Fo)}{0.4602} + 1.795 \qquad (eq.3)$$

For En (K_D = 0.23);

$$\log MgO_{liq} = \frac{\log En - \log(36268.9182 - 188.1602En)}{0.4602} + 6.1409 \qquad (eq.4)$$

Makkonen (1996) presented ways how to approximate the MgO content of the parental magma based on whole-rock chemistry if no primary mafic minerals are present or cannot be analyzed due to alteration. First, the MgO/FeO ratios of Mg-Fe-silicates in equilibrium with the parental melt are calculated from the molar ratios of MgO and FeO_t with the following equations;

$$b = \frac{MgO\ m\text{-}\%}{FeO_t\ m\text{-}\%} \qquad (eq.5)$$

$$Fo,En = \frac{b}{1+b} \qquad (eq.6)$$

Pearce (1968) molar ratio diagrams of MgO and FeO_t against Al_2O_3 or TiO_2 can be used to determine the MgO/FeO ratio of the parental magma from the regression line of the plotted samples. As Al_2O_3 is not compatible into olivine or orthopyroxene, the ratio of MgO and FeO is dependent on the ratio of the elements in the magma. The slope of the regression line gives the molar ratio of MgO to FeO. If all iron is assumed to be Fe^{2+}, the slope gives the MgO/FeO ratio directly. This ratio is then used to calculate Fo or En content of the mineral that controls the fractionation. The Fo, En content is then input into equation 3 or 4, respectively, which gives the MgO concentration (wt-%) of the melt. Mg# of the magma can be calculated with the MgO/FeO ratio together with the partition coefficient K_D, which can then be used to calculate the FeO_t concentration.

5.1.1 Matokulma

The gabbroic cumulate samples from Matokulma were plotted to Pearce (1968) molar ratio diagrams where FeOt and MgO were divided with either Al_2O_3 or TiO_2. The FeOt and MgO versus Al_2O_3 diagram (Figure 47) proved to fit the regression line well (R^2>0.95) which made it usable for the calculations. The Fo, En content based on the regression line is 72. The MgO content of the magma (MgO_{liq}), calculated on the basis of the Fo content, assuming Fe^{2+}/Fe_{tot} =1, is 7.06±0.16 wt-%. Mg# of the magma is 46 and the FeO_t concentration based on the Mg# is 14.79 wt-%.

If orthopyroxene would have been the mineral first to crystallize, the MgO_{liq} is calculated to be 5.15±0.11 wt-% with a Mg# of 37 and a FeO_t concentration of 10.78 wt-%. The cumulative error of the MgO calculation is estimated from the R^2 value of the regression line. As the rock types in Matokulma contain no olivine, at least at the present erosional level, orthopyroxene is used for the calculation basis of the parental magma.

Orthopyroxene analyses were also used to estimate the parental magma composition. Enstatite concentrations were input into Equation 4. The highest value obtained was 5.58 wt-% MgO_{liq}, which was calculated from the composition of a poikilitic orthopyroxene grain from sample SIKA-2017-173 with En_{74}. The enstatite composition and the calculated MgO_{liq} is somewhat similar to the one calculated from whole-rock compositions, within 0.5 wt-%.

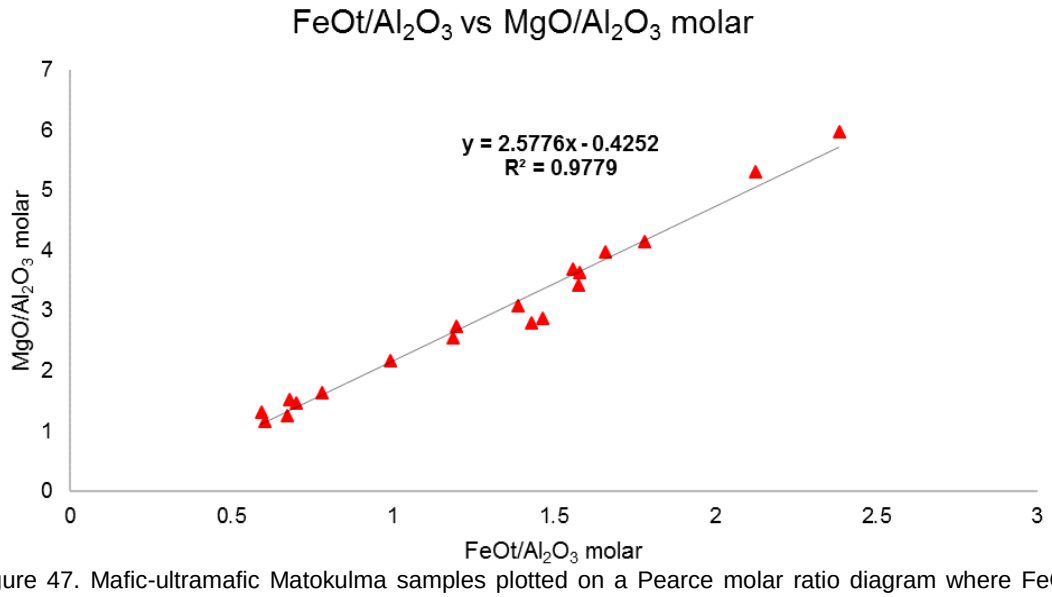

Figure 47. Mafic-ultramafic Matokulma samples plotted on a Pearce molar ratio diagram where FeOt is against MgO, normalized with Al2O3. The samples fit the regression line well (R^2=0.9779).

5.1.2 Palojärvi

The gabbroic, cumulate samples from Palojärvi were similarly plotted into a Pearce (1968) molar ratio diagram. The TiO_2 normalized samples fit the regression line well (R^2=0.9633) and were used for calculations (Figure 48). The Fo, En content of the based on the regression line is 62.

If forsterite was the controlling cumulus mineral, the MgO concentration of the magma would have been 4.75±0.17 wt-% and FeOt 15.48±0.17 wt-%, assuming Fe^{2+}/Fe_{tot} =1. The Mg# of the magma would have been 35.

If enstatite had been the cumulus mineral, the MgO and FeO concentrations of the magma would have been 3.18±0.12 wt-% and 10.36±0.12 wt-%, respectively. Mg# for would have been 28.

Olivine and orthopyroxene EPMA analyses were made from some Palojärvi samples. Sample SIKA-2017-80.1 from Palojärvi contains both olivine and orthopyroxene. The olivine compositions in the sample have a range of $Fo_{42–46}$ and the calculated equilibrium MgO concentration in the magma range from 1.75 wt-% to 2.27 wt-% at minimum and maximum, respectively, and 1.99 wt-% MgO in median. The orthopyroxene compositions in the same sample have a range of En_{5260} with the calculated MgO concentrations ranging from 1.86 wt-% to 2.73 wt-% MgO at extremes, and 2.31 wt-% MgO in median.

The orthopyroxene from other samples have lower En concentration and consequently lower calculated MgO_{liq} concentrations, which range from 0.94 wt-% up to 2.23 wt-%.

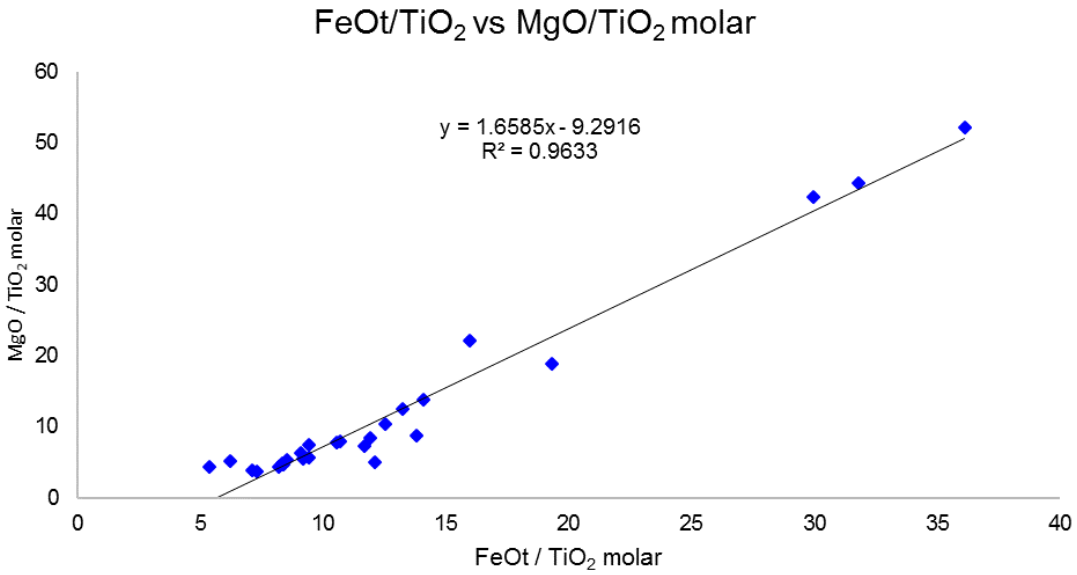

Figure 48. Mafic-ultramafic Palojärvi samples plotted on a Pearce molar ratio diagram where FeOt is against MgO, normalized with TiO_2. The samples fit the regression line well (R^2=0.9633). The three samples with high MgO and FeO are amphibole rich samples.

5.2 Whole-rock and mineral chemistry constraints on magmatic evolution

The parental magma calculations in the previous chapter show that the melts were not primary melts in equilibrium with mantle, as they were far too poor in MgO. A basalt melt in equilibrium with mantle peridotite has Mg# of ~70 (e.g. Roeder and Emslie 1970, Green et al. 1974), in contrast to the calculated parental magma Mg# values of 46 and 35, of Matokulma and Palojärvi, respectively.

When samples from all studied intrusions are plotted together into a primitive mantle-normalized REE spider diagram, they overlap and display similar patterns of enrichment and depletion (Figure 49). Notable differences are in Eu anomalies, the ratios of normalized La/Sm, and La/Yb. Many samples from Palojärvi and the Hongonniittu sample show positive Eu anomalies. The Hongonniittu sample has primitive mantle-like HREE concentrations and similar patterns but lower concentrations as the bulk of Palojärvi samples.

The evolution of the intrusions can be displayed by comparing Mg# and Cr with CaO/Al_2O_3 (Figure 50) Matokulma dikes have low CaO/Al_2O_3 ratios which slightly decrease with Mg#. Palojärvi and Hongonniittu have significantly lower Mg# and Cr concentrations and a narrow range and low CaO/Al_2O_3 ratio, suggesting clinopyroxene fractionation and resulting depletion of Cr has taken place earlier in the evolution of these intrusions. These and other geochemical trends and patterns in whole-rock and mineral chemistry are discussed in the next two subchapters.

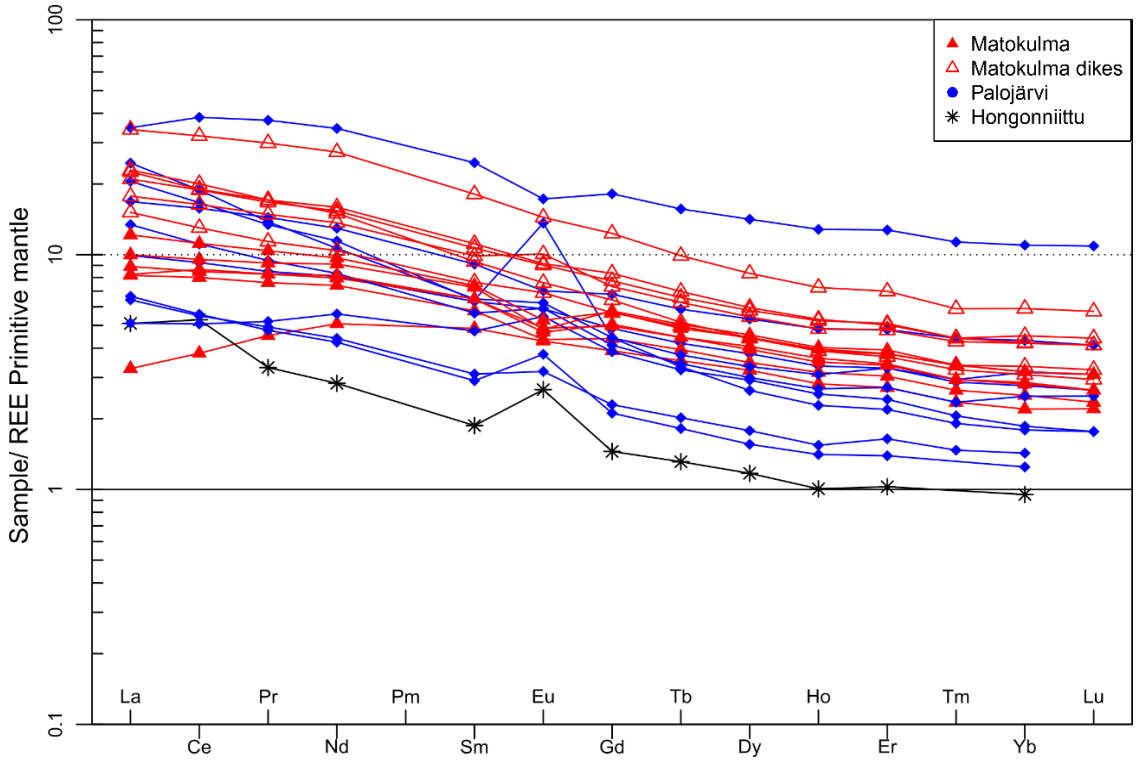

Figure 49. Primitive mantle normalized REE spider diagram. The intrusions have very similar patterns with some variation, related to magma evolution and fractional crystallization – Positive/negative Eu-anomalies and La_N/Sm_N ratios below and above 1. Samples normalized again primitive mantle (McDonough and Sun 1995).

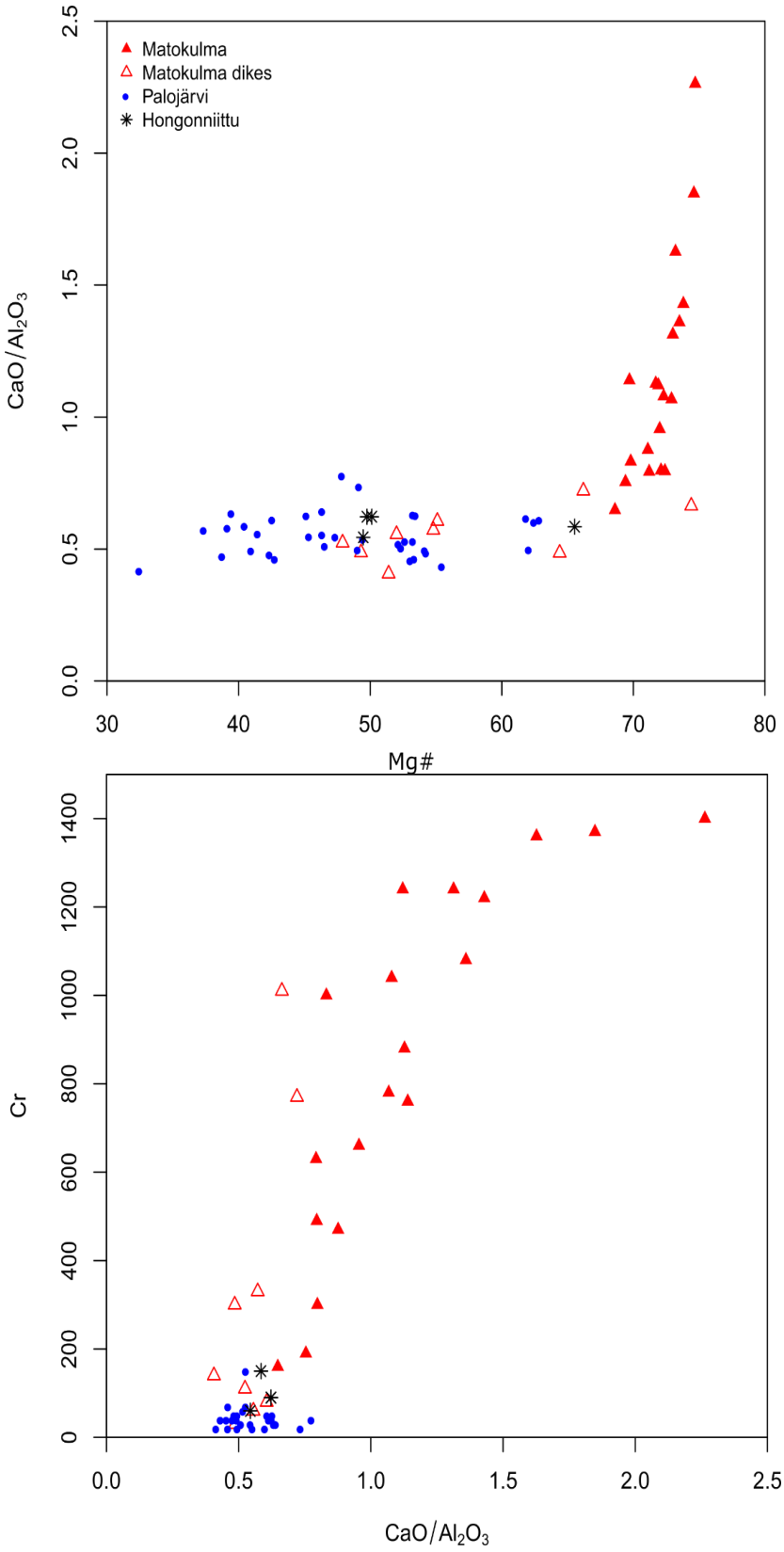

Figure 50. Diagrams illustrating the evolution and difference of the studied intrusions. Mg# vs CaO/Al_2O_3 (top) and CaO/Al_2O_3 vs Cr (below). The decrease of CaO/Al_2O_3 together with Cr is caused by the fractionation of clinopyroxene and chromite.

5.2.1 Matokulma

Gabbros and dikes show similar REE patterns, with partial overlap of the most and least REE-enriched samples, respectively. Most gabbros show a negative Eu-anomaly, whereas the dike rocks have a slight positive Eu-anomaly or no anomaly at all.

Most of the Matokulma gabbros and dikes display similar LILE enrichment and HFSE depletion (Figure 51). This, together with 'spiky' MORB-normalized signatures are often referred to as 'arc signature'(e.g. Tatsumi and Kogiso 2003, Li et al. 2015, Zellmer et al. 2015, Pearce 1982) caused by subduction-related fluid influence. A titanate phase (e.g. rutile, titanite) has high partition coefficients for HFSE which retains these elements and depletes them in the fluid formed from the dehydrating subducting slab (McCulloch and Gamble 1991, Green 1994, Saunders and Tarney 1984, Foley et al. 2000). The presence of amphibole in the dehydrating slab might also cause this signature (Woodhead et al. 1993). Early fractionation of Fe-Ti-oxides will also incorporate HFSE from the magma (Klemme et al. 2006).

It is worthwile noting that the detection limit for Nb and Ta in the ICP-MS analyzes for this thesis were 3 ppm and 1 ppm, respectively. In NMORB, the concentrations are lower than these – 2.33 and 0.133 ppm for Nb and Ta, respectively (Sun and McDonough 1989). However, the depletion of other HFSE together with other geochemical patterns discussed earlier suggest that the depletion of Nb and Ta are actual geochemical anomalies, rather than just the result of the limitations of the analysis method.

Sample SIKA-2017-6.4 has flat, slightly depleted, NMORB-like LREE concentrations and the lowest incompatible element concentrations of all of the samples. This might reflect the parental magma composition. The other gabbros and dikes are LREE-enriched, which can be explained with continued evolution from the parental magma composition. Overall, the samples have close to NMORB-like concentrations of trace elements. The gabbros and the dike rocks show a clear genetic relationship, based on the similar enrichment and depletion patterns and partial overlap between samples.

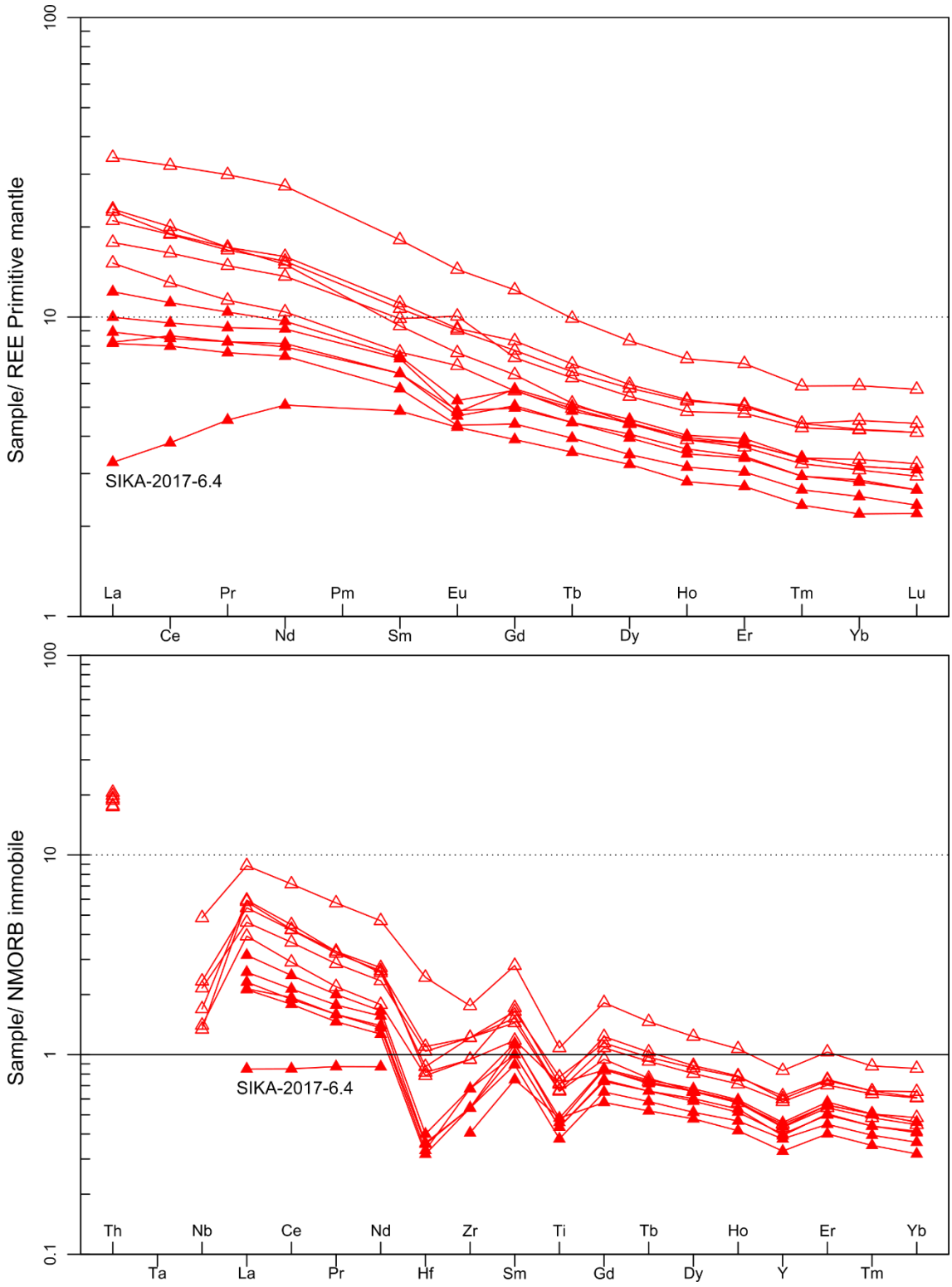

Figure 51. Spider diagrams of Palojärvi samples and Hongonniittu sample normalized against primitive mantle (above) and NMORB (below). Matokulma gabbro (filled triangles) and dike rocks (open triangles). Primitive mantle values from McDonough and Sun (1995), NMORB values from Sun and McDonough (1989).

Matokulma has a rather constant, high Mg# with a wide range of CaO/Al_2O_3, which decreases with decreasing Mg# and Cr. As CaO/Al_2O_3 decreases, so does the ratio of modal and normative clinopyroxene to plagioclase. The most primitive samples have the highest CaO/Al_2O_3, Mg#, and Cr. Based on petrography, clinopyroxene is the earliest cumulate phase. The clinopyroxene crystals have a similar median Mg# of ~79 in all samples analyzed. The concentration of Cr however, changes between samples. These trends are consistent with progressive fractionation and modal decrease of clinopyroxene ± chromite and increase of plagioclase, which indicates that clinopyroxene controlled the evolution of the parental magma (e.g. Bender et al. 1978).

Mineral chemistry

The pyroxenes in Matokulma have quite low Mg# and Ni, which is in agreement with the depleted nature of the parental magma.

Natural and experimental orthopyroxenes and clinopyroxenes crystallized from hydrous arc magma under high pressure conditions are enriched in Al if there are no Al-phases precipitating (Elthon et al. 1982, Müntener et al. 2001, DeBari and Coleman 1989). Increasing degree of crystallization also increases the concentration of Al_2O_3 and FeO in pyroxenes (Bender et al. 1978).

The analyzed clinopyroxenes are on median low in Al_2O_3 (0.70 wt-%) and TiO_2 (0.07 wt-%) but most grains in sample SIKA-2017-173.1 have higher concentrations (2–3 wt-% Al_2O_3 and 0.2–0.5 wt-% TiO_2) and also higher Cr and V (up to 3000 ppm, 3800 ppm, respectively) and Mg# (83). The clinopyroxenes in this sample may have fractionated deeper in the crust, based on the Al and Cr-rich composition, before the onset of plagioclase crystallization.

The cumulus clinopyroxene and plagioclase grains are often at least partially resorbed and display a reaction rim with the poikilitic amphibole, which indicates that the cumulus phases reacted with the residual melt to form amphibole (e.g. Powell 1978, Conrad and Kay 1984**)**. For example, in sample SIKA-2017-173.1, a cumulus diopside with 1300 ppm Cr has a rim of magnesio-hastingsite amphibole with 3900 ppm Cr. This is enclosed in magnesio-hornblende with 1490 ppm Cr, which is within a poikilitic enstatite with 150 ppm Cr.

5.2.2 Palojärvi

On average, the REE concentrations and trends of Palojärvi are not different from those of Matokulma, especially on primitive mantle normalized spider diagrams. There is more scatter in the NMORB normalized spider diagram, especially in MREE and HFSE (Figure 52).

LILE enrichment it similar to that of Matokulma. The depletion of HFSE is apparent with regard to Nb, Ta, and Y. Some samples also exhibit depletion of Ti whereas some are enriched or NMORB-like in Ti, which is caused by incorporation Ti into silicate phases, especially amphibole, and the abundant Fe-Ti-oxides.

The more evolved composition of Palojärvi is evident from the strong depletion of mantle-compatible elements (Ni, Cr, Cu). The median concentrations are < 70 ppm and 35 ppm, 50 ppm, respectively. Even in the olivine and orthopyroxene-bearing amphibole norite (SIKA-2017-80.1), whole-rock Ni concentration is 50 ppm. Sample SIKA-2017-156.1 contains more Cr (150 ppm) than all other samples and is further discussed later in this chapter.

The enrichment of Fe, Ti, Al, and V, is apparent both in whole-rock and mineral chemistry. Silica concentrations are, however not higher than in Matokulma. In Palojärvi, median SiO_2 is 45.3 wt-% and most samples are strongly olivine-normative, 18 % Ol on median and 42 % at maximum. The same sample (SIKA-2017-51.1) has the highest Fe-concentration at 23.5 wt-% Fe_2O_3t. The sample is very altered, rich in amphiboles and large grains of Fe-Ti-oxides and sulfides, and green spinel.

A mafic inclusion sample (SIKA-2017-22.1) from a garnet-bearing granite dike was included in trace element analyses of gabbroic samples. The inclusion is strongly enriched in U and Th, 90 times that of NMORB, but besides that, displays similar concentrations and trends in primitive mantle and NMORB-normalized spider diagrams to those of gabbroic samples.

Sample SIKA-2017-54.1 differs from other samples with noticeably higher REE and other trace elements. This sample is also the most TiO_2 and Y-rich (2.38 wt-%, 43.3 ppm, respectively) of the plotted samples. This is most likely caused by large amount of

amphibole + biotite (Claeson and Meurer 2004), and fine-grained magnetite dissemination.

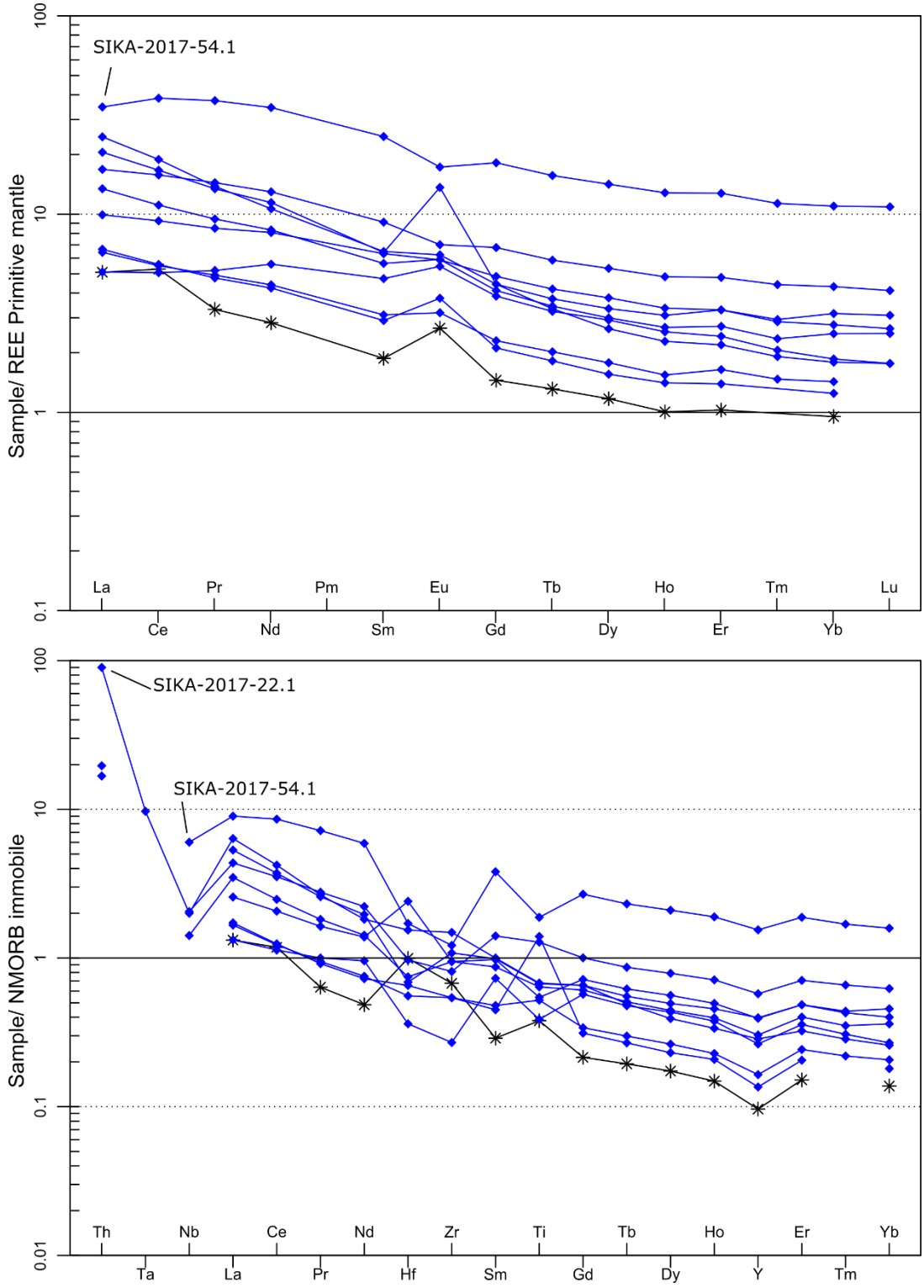

Figure 52. Spider diagrams of Palojärvi samples (blue) and Hongonniittu sample (black) normalized against primitive mantle and NMORB. Primitive mantle values from McDonough and Sun 1995, NMORB values from Sun and McDonough 1989.

The geochemical characteristics of Palojärvi are more common with other tholeiitic, highly Fe-Ti-P enriched mafic-ultramafic layered intrusions within the CFGC, such as Perämaa and Kälä (Nironen 2000, Peltonen 2005), than the ultrabasic Vammala-Kotalahti types. Nironen (2000) classifies Perämaa and Kälä intrusions as Type 2, post-kinematic, which are associated with crustal weakness zones. They are characterized by Fe and Ti-rich whole-rock and mineral chemistry. Palojärvi is not, however as far enriched as these intrusions. The concentration of P is also noticeably lower. An important difference with Palojärvi and, for example Perämaa intrusion is the absence of hydrous magmatic phases in Perämaa intrusion (Peltonen 2005).

Isotope geochemistry

The two age determination samples have weighted zircon U-Pb ages of 1883±4.8 Ma (MSWD=1.9) and 1893±7.1 Ma (MSWD=3.2), for the leucogabbro and the granite, respectively. This result is in contrast with the field observation that the granite cuts the gabbro. However, considering the margin of error of the results, the granite can be younger than the gabbro, 1887 Ma and 1888 Ma, respectively. The εNd values of the samples are 2.53 and 1.55, respectively. The positive values for both samples indicate a depleted mantle source.

The leucogabbro occurs as a dike in the more common melagabbro, which indicates that the dike is younger than the mafic gabbro. The leucogabbro is likely the late-stage product of the gabbroic magma. This is supported by the positive εNd, indicating a mantle source.

The granite magmatism seems to have been roughly coeval with the mafic magmatism, based on the magma mixing and mingling textures seen on many outcrops. Felsic rocks were not studied in detail and there are no trace element analyses from the few samples that were gathered. Therefore, the possible petrogenetic connection between mafic and felsic rocks in Palojärvi cannot be studied further in this thesis.

Mafic intrusions within the Svecofennian domain have positive εNd values (Makkonen and Huhma 2007). According to Makkonen and Huhma (ibid.), the εNd correlate with the εNd values of the country rocks. The oldest rocks within the Svecofennian domain (1.92 Ga, tonalitic gneisses) have εNd values up to +3 (Lahtinen and Huhma 1997). The mafic-ultramafic intrusions near the Archean boundary (Kotalahti belt) have mostly negative εNd, due to the assimilation of Archean rocks with strongly negative εNd.

Mineral geochemistry

The most striking difference in the mineralogy of the two intrusions is the presence of ilmenomagnetite and the iron-rich composition of other minerals (olivine, pyroxenes and amphiboles) in Palojärvi. Fayalitic olivine (Fo_{45}) is enclosed within orthopyroxene (En_{56}) and magnesio-hastite amphibole (Mg#=56). The minerals are generally extremely depleted in Cr and Ni but enriched in V. Palojärvi also has a conspicuous positive magnetic anomaly. This anomaly is caused by vanadium-bearing ilmenomagnetite, which is a common accessory phase in most samples. The analyzed minerals are enriched in Ti and V, such as Ti-rich pargasite and V-rich ilmenomagnetites in sample SIKA-2017-88.2.

Clinopyroxenes from Palojärvi are less magnesian and have higher Al, Ti, V than in Matokulma. The median Al_2O_3 is 2.3 wt-%. Sample SIKA-2017-156.1 has large, porphyric clinopyroxene grains which are higher in Al, Ti, Cr, and Ni than the other samples. The median Cr concentration from this sample is 1300 ppm, compared to the median value of 80 ppm of all samples. Ni concentration is on median 120 ppm Ni, up to 200 ppm, which is higher than the values from any olivine or orthopyroxene. The clinopyroxene grains in this sample have Al_2O_3 concentrations from 3.0 to 5.5 wt-%. Such high values are comparable to those clinopyroxene found in high pressure ultramafic cumulates, save for the lower Mg# (e.g. Debari and Coleman 1989). The groundmass of the sample consists of fine-grained plagioclase with overgrown grain boundaries. Based on EPMA, the plagioclase is zoned, with An_{50} cores and An_{41} rims. In arc-cumulates, the plagioclase although rare would be very An-rich in composition (Debari and Coleman 1989, Dessimoz et al. 2012).

Primary amphibole phases are similar to those of Matokulma – magnesio-hastingsite, pargasite to magnesio-hornblende or magnesio-ferri-hornblende.

5.3 Comparison to Vammala and Kotalahti type intrusions

The Ni-Cu mineralized intrusions of Vammala and Kotalahti types are hosted by ultrabasic rock types, formed from tholeiitic basalt parental melts with 10–15 wt-% MgO, which assimilated crustal material that led to the fractionation of sulfide melts form which the ores formed (Peltonen 2005, Makkonen 2015).

The intrusions studied in this thesis are markedly different from those of mineralized Vammala and Kotalahti type intrusions. The studied intrusions are gabbroic in composition and mostly olivine-free, in contrast to the olivine-pyroxene-dominated ultrabasic cumulates of the mineralized intrusions. This reflects the evolved nature of the parental melts from which the studied intrusions crystallized from.

The differences to ore potential Vammala and Kotalahti type intrusions are clearly demonstrated on CMA and AFM diagrams (Figure 53). The ore potential intrusions plot near the MgO vertices due to their ultrabasic, olivine-rich composition. Note the ore potential Kotalahti-type intrusions that are more Al-rich due to the assimilation of crustal material (Makkonen et al. 2008). The intrusions studied here, as well as Kaipola layered intrusion (Peltonen and Elo 1999, Nironen 2000, Peltonen 2005) are clearly less magnesian and more iron-rich and contain more alkalis and aluminum and are gabbroic in bulk composition. The more evolved compositions indicate a further magma evolution.

One conspicuous similarity is the presence of magmatic interstitial amphibole, which is present both in Vammala and Kotalahti type intrusions, Kaipola gabbro (Makkonen 1996, Peltonen 2005, Lamberg 2005) and Matokulma and Palojärvi.

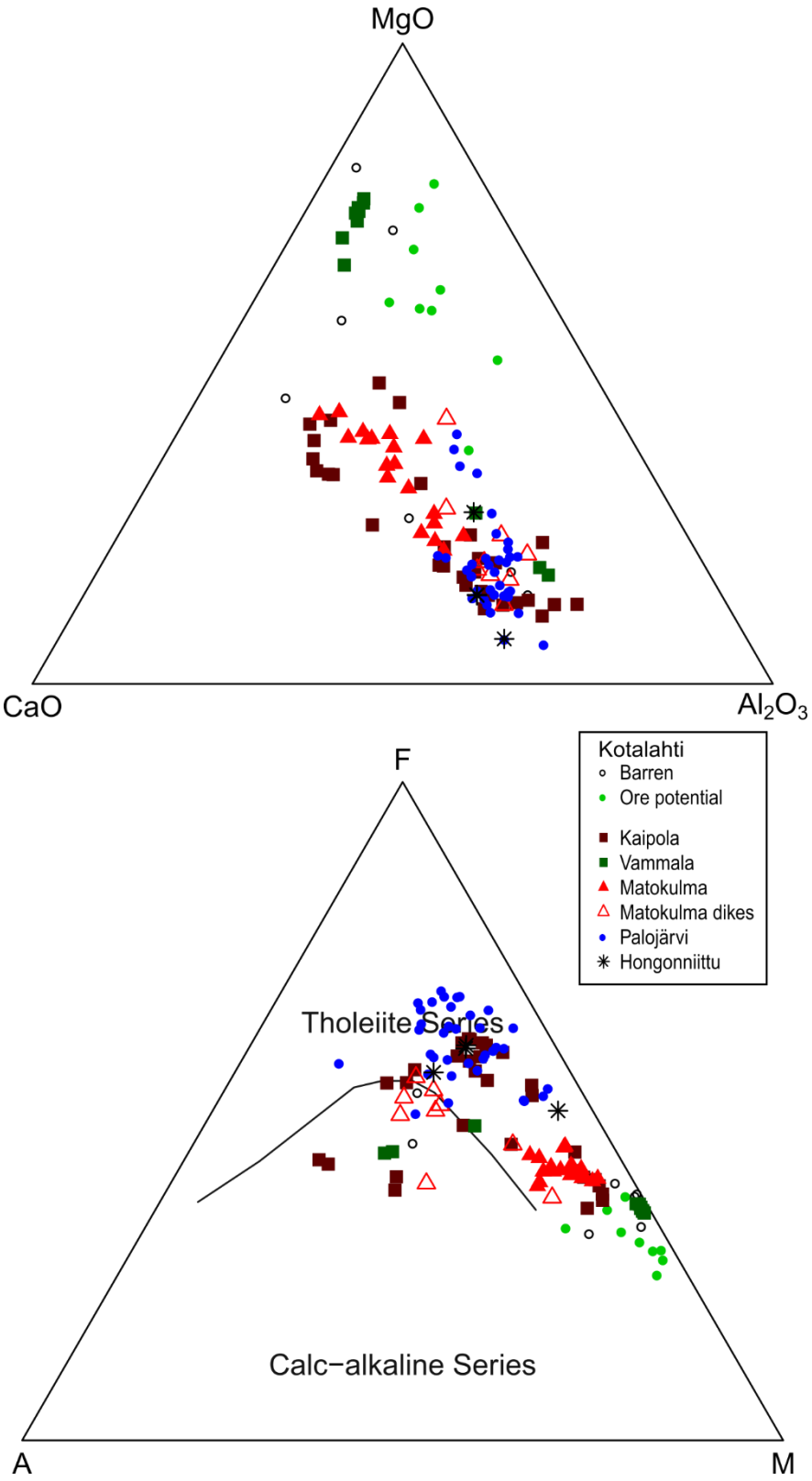

Figure 53. CMA and AFM diagram of studied intrusions together with intrusions from Vammala and Kotalahti belts and Kaipola gabbro. Ore potential intrusions plot near the MgO vertex, because of their ultrabasic composition. The intrusions studied here are less magnesian and more evolved. Kotalahti intrusions are divided to barren and ore potential intrusions. The ore potential intrusions contain more Al due to the assimilation of Archean rocks. Kaipola and Vammala data from P. Peltonen (unpublished data.), Kotalahti data from Makkonen and Mäkinen (2003).

5.4 Ore potential

The pre-requisites for economic Ni-Cu mineralizations are that they form from mantle-derived, MgO-rich magmas with sufficient metal concentrations, that can attain sulfur saturation through crustal contamination at the late-stages of ascent in the crust (Naldrett 1999, Ardnt et al. 2005, Lamberg 2005, Maier and Groves 2011).

The ore potential of the studied intrusions can be evaluated by whole-rock and mineral geochemistry by examining the magnesium content (Mg#) and Ni, Cr, Cu content of early crystallizing minerals olivine, orthopyroxene, spinel (e.g. Häkli 1971, Makkonen 1996, Lamberg 2005.

MgO versus Ni diagram (Figure 54) is a way to evaluate the Ni mineralization potential of an intrusion. If the samples plot beneath the line, they are depleted in nickel (Makkonen et al. 2017). According to Makkonen et al. (2008, 2017), the most potential intrusions have samples that plot both above and beyond the line, indicating in-situ depletion of nickel, within the current erosional level of the intrusion.

Olivine is absent from all Matokulma samples. The Mg# range of orthopyroxenes is 67–76 and the mean Ni concentrations in orthopyroxene (58 ppm) is similar to that of average Svecofennian quartz diorites (60 ppm, Häkli 1971).

The low whole-rock and mineral Ni and Mg#, and the rarity of sulfide phases indicate that the concentration of MgO and Ni in the melt was low.

Due to the evolved nature of Matokulma and Palojärvi intrusions, they have very low potential for Ni-Cu-PGE mineralizations. Sulfide saturation has probably taken place at some point of the evolution of the intrusions, prior to emplacement to the depth of the current erosional level, as indicated by the very strong depletion of Ni and PGE.

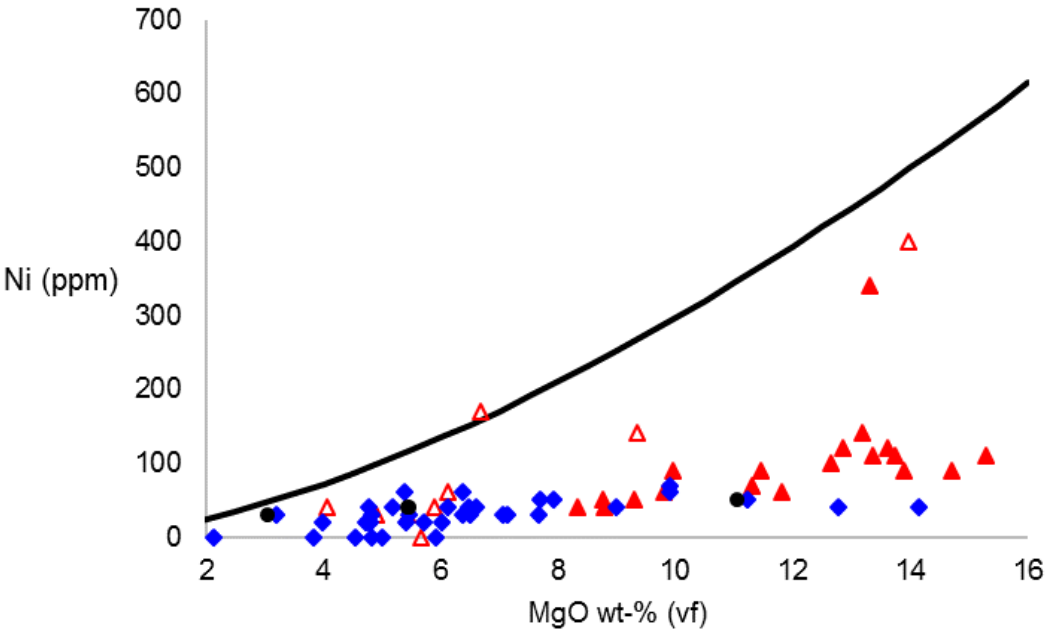

Figure 54. MgO (volatile-free) vs Ni. The line represents nickel depletion. Except for one Matokulma dike sample, all the samples are below the line. The samples with higher Ni are strongly altered and sheared. The equation for the line is $8.36*MgO^{1.55}$ (Makkonen et al. 2017).

As Palojärvi is further evolved than Matokulma, it has even lower potential for Ni-Cu-PGE mineralizations.

Palojärvi could, however potentially host Ti-V mineralizations as the few analyzed magnetites have elevated concentrations of V (1.2–1.4 wt-% V_2O_3). As magmatic layering is seen on the current erosional level, it is possible that there are Fe-Ti-V spinel-rich layers deeper in the intrusion, as the gravity survey and resulting modelling suggests that the intrusion continues to a depth of some 800 m. Gabbros with such mineralizations are known within the CFGC (e.g. Kärkkäinen and Appleqvist 1999, Kärkkäinen and Bornhorst 2003, Peltonen 2005). Kauhajärvi and Koivusaarenneva form two clusters of similar, Ti-Fe-P gabbros, which are Svecofennian, synorogenic and located within the CFGC (Peltonen 2005).

The enrichment of V into magnetites happen at a narrow fO_2 range, between NNO and NNO-1.5 (Reynolds 1985, Cawthorn and Molyneux 1986, Toplis and Corgne 2002). The concentration of V in the melt decreases rapidly as V-rich magnetite continues to fractionate (Toplis and Corgne 2002, Cawthorn 2005). This phenomenon is observed in the magnetitite (monomineralic magnetite) layers of the Bushveld intrusion (e.g. Cawthorne et al. 2005). Thus, the most vanadian magnetites are most likely found deeper in stratigraphic height of a layered intrusion where the earliest magnetites accumulate, assuming the right fO_2 was attained.

5.5 Petrogenesis

Olivine is a ubiquitous phase in primitive arc environment cumulates, where it is the first liquidus phase together with spinel and later also with clinopyroxene (e.g. Gaetani et al. 1993, DeBari and Coleman 1989, DeBari and Sleep 1991, Elthon et al. 1982, Pichavant and Macdonald 2007). Plagioclase fractionation is suppressed in arc environments, due to both high total pressure and partial water pressure, which leads to the enrichment of Al in the residual melt (Müntener et al. 2001, Dessimoz et al. 2012, Pichavant and Macdonald 2007). Orthopyroxene stability also decreases with increasing water pressure (Kushiro 1969, Sisson and Grove 1993).

Large, interstitial amphibole oikocrysts, which are present in both Matokulma and Palojärvi cumulates occur in Vammala and Kotalahti type intrusions as well. They are thought to be formed by late magmatic peritectic reactions (Makkonen 1996, Lamberg 2005, Peltonen 2005). Magmatic amphiboles are common in arc cumulates (Debar and Coleman 1989, Davidson et al. 2007). The magmatic amphiboles that are found in arc cumulates belong to the Ca-amphibole group and are commonly magnesio-hastingsite, pargasite or magnesio-hornblende (Krawczynski et al. 2012).

5.5.1 Matokulma

Olivine is noticeably absent in the Matokulma gabbros, despite it being a normative mineral in all samples and the first liquidus phase in the crystallization of both MORB and arc-type basalts (e.g. Kushiro 1969, Sisson and Grove 1993). Even though olivine is not present at the current erosional level, olivine ± spinel may have fractionated earlier during the evolution of the magma and decreased the concentration of MgO and Ni and increased the SiO_2 in the evolving magma (Crawford et al. 1987, Nicholls and Ringwood 1972, Straub et al. 2008). The increasing silica decreases the solubility of sulfur which would eventually cause the exsolution of a sulfide melt (e.g. Ripley and Li 2013), which would deplete the melt of PGEs due to the extremely high partition coefficients of these elements to the sulfide melt (Mitchell and Keays 1981, Naldrett 1999, Rehkämper et al. 1999, Cawthorn et al. 2005).The orthopyroxene that is present in many samples could have been formed by peritectic reactions between olivine and residual melt (Dessimoz et

al. 2012, Müntener et al. 2001, Straub et al. 2008) or by basaltic magma that has assimilated silica (Ripley and Li 2013). These would however result in high Mg# and Ni concentration in the resulting orthopyroxene, which is not the case in Matokulma. The crystallization of forsterite would efficiently reduce the MgO and Ni content of the magma and increase all the other components not incorporated into olivine.

The fractionation and accumulation of olivine would also reduce the density of the residual magma and allow it to ascend in the crust (Gust and Perfit 1987). Clinopyroxene fractionation followed and further depleted the magma of MgO and started the decrease of Cr, together with the crystallization of chromite. Magnetite fractionation happened early on the evolution based on the lack of iron enrichment and Fe-Ti oxides in the gabbros, which is apparent also as low magnetic susceptibilities.

The depletion of MgO and enrichment of SiO_2 move the magma composition towards more evolved basaltic andesite to andesitic compositions where orthopyroxene is stabilized as the liquidus phase after clinopyroxene (Pichavant and Macdonald 2007). Orthopyroxene may also be stabilized by the assimilation of silica (Ripley and Li 2013). For example, in observation point SIKA-2017-115, mingling textures are seen between a leucogranite and melagabbro. In the melagabbro sample (SIKA-2017-115.2), orthopyroxene is a euhedral cumulus phase. Some of the clinopyroxene were transported to the current erosional level where they were in disequilibrium and were partially resorbed and incorporated into magmatic amphibole, as indicated by the high Cr concentration of amphiboles surrounding cumulus clinopyroxene (Conrad and Kay 1984).

The evolution of the magma took place in relatively high fO_2 based on the modest enrichment of iron and the liquid line of descent from the tholeiitic, magnesium-rich gabbros to the mostly calc-alcaline dike rocks. The shift from tholeiitic to calc-alcaline compositions may be caused by high concentration of water in the magma (Grove et al. 2003). The dike rocks intruded the country rock around the gabbro. They are related to the gabbros and probably represent the residual magma from which the gabbros fractionated. The trace element characteristics and the presence of magmatic amphibole implies that the parental melt was a hydrous NMORB-type basalt, with arc-type enrichment and depletion patterns, related to the alteration by volatiles released by dehydration reactions in the subducting slab (LILE enrichment, HFSE depletion).

5.5.2 Palojärvi

Based on the results and discussion in previous chapters, it is clear that Palojärvi intrusion did not evolve the same way Matokulma did. The depletion of Cr and Ni is even larger than in Matokulma, which indicates a longer evolution history, assuming a similar source for the parental magma.

The most primitive, least altered samples are composed of cumulus olivine or pyroxenes and plagioclase, enclosed in large, poikilitic amphibole, orthopyroxene, or phlogopite. The parental magma calculations based on the cumulus olivine and enclosing orthopyroxene show that the magma was very depleted in MgO. Magmatic, poikilitic amphibole and, to lesser extent phlogopite is common in Palojärvi intrusion, which indicates that the Palojärvi parental magma was hydrous.

Palojärvi fractionated from an evolved tholeiitic basalt magma, which further evolved under low fO_2, which prevented Fe-Ti-oxides from precipitating deeper in the crust and led to the enrichment of Fe in the tholeiitic trend (e.g. Irvine and Baragar 1971). In a closed system, the fractional crystallization of olivine and plagioclase will raise the relative fO_2 in the melt as FeO is preferentially incorporated into the olivine structure (Snyder et al. 1993). This rise of oxygen fugacity started the precipitation of ilmenomagnetite, which causes the strong positive magnetic anomaly of the intrusion.

Mixing and mingling textures and unclear cutting relations between felsic and mafic rocks seen on many observation points in Palojärvi indicate possible immiscibility between the two melt types. The roughly coeval ages of the leucogabbroic dike and granite also suggest bimodal magmatism. The nearby Kaipola layered intrusion is associated with syn- and post-kinematic granitoids with similar features indicating immiscibility between the gabbroic and granitic melts (Nironen 2000, Peltonen 2005). The geochemical and mineralogical similarity to the Kaipola layered intrusion, together with the close spatial relation suggests a similar magmatic source.

6. CONCLUSIONS AND FURTHER STUDIES

The studied gabbro intrusions formed from NMORB-type, tholeiitic basalts that were hydrous on the account of magmatic amphiboles. The NMORB-signature is modified by subduction-related fluid metasomatism. The parental magmas of Matokulma and Palojärvi, contained approximately 5 wt-% and 2 wt-% MgO, respectively, based on approximations calculated from whole-rock and mineral chemistry. The studied intrusions show similarities to the known Ni-Cu mineralized Vammala and Kotalahti type intrusions in trace element chemistry and magmatic amphibole composition, but they are are more evolved – gabbros instead of ultramafic, olivine-rich cumulates, which host the Ni-Cu mineralizations in Vammala and Kotalahti belts.

Due to the evolved nature of the studied intrusions, they have low potential for Ni-Cu mineralizations. Matokulma is the least evolved of the intrusions, based on the larger concentration of MgO, Cr, and Ni in whole-rock and mineral chemistry. Palojärvi is more evolved and enriched, especially in Fe and Ti, and depleted in MgO, Cr, and Ni. Palojärvi intrusion might host a Fe-Ti-V mineralization based on the abundance of V-bearing ilmenomagnetite, which causes the strong, positive magnetic anomaly. Based on field observations, the intrusion is layered, and gravity survey models suggest that the intrusion has a depth extent of ca. 800 m. Therefore, it is possible that there are magnetite-rich mineralized layers somewhere within the intrusion.

Two age determination samples from Palojärvi (leucogabbro dike, 1883±4.8 Ma and leucogranite 1893±7.1 Ma) Ma suggest that the intrusion was formed early in the main stage of Svecofennian mafic-ultramafic magmatism, ca. 1.89 Ga.

The relationship between the gabbro and the surrounding and transecting granite in Palojärvi intrusion is complicated and magma mixing and mingling textures are visible on many outcrops. Based on field observations, the granite cuts the gabbro, which is in contrast with the results of the age determination. However, considering the margin of error of the results, the granite can be younger than the gabbro. A more detailed mapping and sampling study, focusing on the felsic rocks and especially the cutting relationships between mafic and felsic rocks, utilizing trace element chemistry and more isotope geochemistry could elucidate this issue.

The Hongonniittu intrusion was not investigated in detail in this thesis due to time constraints. The available data suggests similarity to Palojärvi intrusion, but the similarities or differences need to be confirmed with detailed mapping.

7. ACKNOWLEDGEMENTS

I would like to express my gratitude towards my supervisors Dr. Tapani Rämö and Dr. Hannu Makkonen for their vast knowledge and guidance throughout this project. I deeply am grateful for Dr. Perttu Mikkola for providing me a chance to work on this project and for providing me with ample resources that made this thesis highly interesting to work on. Dr. Mikkola is also thanked for being an efficient facilitator, *de facto* supervisor, and editor. The Geological Survey of Finland and everyone in the mineral chemistry and isotope laboratories are thanked for their guidance, help, and work effort that supplied crucial data. The kind help and company of Antti Mäkelä during field studies allowed sampling with a mini drill and was much appreciated. Lastly, I would like to thank Paula for supporting me throughout this work and for enduring my incessant geochemistry ramblings.

8 REFERENCES

Airo, M. L., Säävuori, H. 2013. Petrophysical characteristics of Finnish bedrock. Geological Survey of Finland. Report of investigation, 205, 33.

Arndt, N., Lesher, C.M., Czamanske. G.K., 2005. Mantle-derived magmas and magmatic Ni-Cu-(PGE) deposits. Economic geology, 100th Anniversary volume, .5-24.

Barnes, S.J., Makkonen, H.V., Dowling, S.E., Hill, R.E.T., Peltonen, P. 2009. The 1.88 Ga Kotalahti and Vammala nickel belts, Finland: Geochemistry of the mafic and ultramafic metavolcanic rocks. Bulletin of the Geological Society of Finland 81, 103–141.

Bender, J.F., Hodges, F.N., Bence, A.E. 1978. Petrogenesis of basalts from the project FAMOUS area: experimental study from 0 to 15 kbars. Earth and Planetary Science Letters 41, 277–302.

Belousova, E.A., Griffin, W.L., O'Reilly, S.Y. 2005. Zircon crystal morphology, trace element signatures and Hf isotope composition as a tool for petrogenetic modelling: examples from Eastern Australian granitoids. Journal of Petrology 47, 329–353.

Cawthorn, R.G., Molyneux, T.G. 1986. Vanadiferous magnetite deposits of the Bushveld Complex. Mineral deposits of southern Africa 2, 1251–1266.

Conrad, W.K., Kay, R.W., 1984. Ultramafic and Mafic Inclusions from Adak Island: Crystallization History, and Implications for the Nature of Primary Magmas and Crustal Evolution in the Aleutian Arc. Journal of Petrology 25, 88–125.

Crawford, A.J., Falloon, T.J., Eggins, S., 1987. The origin of island arc high-alumina basalts. Contributions to Mineralogy and Petrology 97, 417–430.

Davidson, J., Turner, S., Handley, H., Macpherson, C., Dosseto, A. 2007. Amphibole “sponge” in arc crust? Geology 35, 787–790.

DeBari, S.M., Coleman, R.G. 1989. Examination of the deep levels of an island arc: Evidence from the Tonsina ultramafic-mafic assemblage, Tonsina, Alaska. Journal of Geophysical Research: Solid Earth 94, 4373-4391.

Dessimoz, M., Müntener, O., Ulmer, P. 2012. A case for hornblende dominated fractionation of arc magmas: the Chelan Complex (Washington Cascades). Contributions to Mineralogy and Petrology 163, 567-589.

Eilu, P., Lahtinen, R. 2013. Fennoscandian metallogeny and supercontinent cycles in Mineral Deposit Research for a High-tech World, 1630–1634.

Ekdahl, E.1993. The evolution and metallogenesis of the Raahe–Ladoga zone in Global Geoscience Transect/SVEKA: Proceedings of the Kuopio seminar, Finland, 25–26.

Elthon, D., Casey, J.F., Komor, S. 1982. Mineral chemistry of ultramafic cumulates from the North Arm Mountain Massif of the Bay of Islands ophiolite: Evidence for high-pressure crystal fractionation of oceanic basalts. Journal of Geophysical Research: Solid Earth 87, 8717-8734.

Foley, S.F., Barth, M.G., Jenner, G.A. 2000. Rutile/melt partition coefficients for trace elements and an assessment of the influence of rutile on the trace element characteristics of subduction zone magmas. Geochimica et Cosmochimica Acta 64, 933–938.

Forss, H., Kontoniemi, O., Lempiäinen, R., Luukas, J., Makkonen, H. Mäkinen, J., 1999. Ni-vyöhyke ja 1. 9 Ga magmatismi-hankkeen (12204) toiminta vuosina 1992-1998 Tervo-Varkaus-alueella. Geological Survey of Finland, Archive report, M 19/3241/99/1/10, 152 p.

Gaál G. 1972. Tectonic control of some Ni-Cu deposits in Finland. In: Gill JE (ed.) International Geological Congress, 24th session, Montreal 1972: Section 4, Mineral deposits, 215–224

Gaetani, G.A., Grove, T.L., Bryan, W.B. 1993. The influence of water on the petrogenesis of subduction related igneous rocks. Nature 365, 332–334.

Green, D.H., Edgar, A.D., Beasley, P., Kiss, E., Ware, N.G. 1974. Upper mantle source for some hawaiites, mugearites and benmoreites, Contributions to Mineralogy and Petrology 48, 33–43.

Green, T. H. 1994. Experimental studies of trace-element partitioning applicable to igneous petrogenesis—Sedona 16 years later. Chemical Geology 117, 1-36.

Grove, T.L., Elkins-Tanton, L.T., Parman, S.W., Chatterjee, N., Muntener, O., Gaetani, G. A. 2003. Fractional crystallization and mantle-melting controls on calc-alkaline differentiation trends. Contributions to Mineralogy and Petrology 145, 515–533.

Gust, D.A., Perfit, M.R. 1987. Phase relations of a high-Mg basalt from the Aleutian island arc: implications for primary island arc basalts and high-Al basalts. Contributions to Mineralogy and Petrology 97, 7-18.

Hawthorne, F.C., Oberti, R., Harlow, G.E., Maresch, W.V., Martin, R.F., Schumacher, J.C., Welch, M.D. 2012. Nomenclature of the amphibole supergroup. American Mineralogist 97, 2031-2048.

Hutchison, C.S. 1974. Laboratory handbook of petrographic techniques: John Wiley & Sons Inc., New York, 527p.

Hutchison, C.S. 1975. The norm its variations, their calculation and relationships. Schweizerische Mineralogische und Petrographische Mitteilungen 55, 243–256

Häkli, T.A., 1971. Silicate nickel and its application to the exploration of nickel ores. Bulletin of the Geological Society of Finland 43, 247–263.

Häkli, T.A., Vormisto, K., Hanninen, E., 1979. Vammala, a nickel deposit in layered ultramafite, southwest Finland. Economic Geology 74, 1166–1182.

Hölttä, P., Heilimo, E. 2017. Metamorphic map of Finland. Geological Survey of Finland, Special Paper 60, 77-128.

Herzberg, C., O'Hara, M.J. 2002. Plume-Associated Ultramafic Magmas of Phanerozoic Age. Journal of Petrology 43, 1857–1883.

Irvine, T. N. J., Baragar, W. R. A. 1971. A guide to the chemical classification of the common volcanic rocks. Canadian Journal of Earth Sciences 8, 523-548.

Kahma, A. 1973. The Main metallogenic features of Finland: With two tables and one appended map. Geologinen tutkimuslaitos.

Kahma, A. 1978. The main sulphide ore belt of Finland between Lake Ladoga and the Bothnian Bay. Bulletin of the Geological Society of Finland, 50, 39–43.

Klemme, S., Günther, D., Hametner, K., Prowatke, S., Zack, T., 2006. The partitioning of trace elements between ilmenite, ulvospinel, armalcolite and silicate melts with implications for the early differentiation of the moon. Chemical Geology 234, 251–263

Korsman, K., Glebovitsky, V. 1999. Raahe–Ladoga Zone structure-lithology, metamorphism and metallogeny: a Finnish–Russian cooperation project 1996–1999.

Korsman, K., Korja, T., Pajunen, M., Virransalo, P., GGT/SVEKA working group. 1999. The GGT/SVEKA Transect: Structure and evolution of the continental crust in the Paleoproterozoic Svecofennian Orogen in Finland. International Geology Review 41, 287–333.

Krawczynski, M.J., Grove, T.L., Behrens, H. 2012. Amphibole stability in primitive arc magmas: effects of temperature, H 2 O content, and oxygen fugacity. Contributions to Mineralogy and Petrology 164, 317-339.

Kähkönen, Y., 1987. Geochemistry and tectonomagmatic affinities of the metavolcanic rocks of the early proterozoic tampere schist belt, Southern Finland. Precambrian Research 35, 295–311.

Kähkönen, Y. 2005. Svecofennian supracrustal rocks. Developments in Precambrian Geology 14, 343–405. Elsevier

Kähkönen, Y., Huhma, H., Aro, K., 1989. U-Pb zircon ages and Rb-Sr whole-rock isotope studies of early Proterozoic volcanic and plutonic rocks near Tampere, southern Finland. Precambrian Research 45, 27–43.

Kärkkäinen, N.K., Bornhorst, T.J. 2003. The Svecofennian gabbro-hosted Koivusaarenneva magmatic ilmenite deposit, Kälviä, Finland. Mineralium Deposita 38, 169-184.

Lahtinen, R., Huhma, H., 1997. Isotopic and geochemical constraints on the evolution of the 1.93-1.79 Ga Svecofennian crust and mantle in Finland. Precambrian Research 82, 13–34.

Lahtinen, R., Johnston, S.T., Nironen, M. 2014. The Bothnian coupled oroclines of the Svecofennian Orogen: a Palaeoproterozoic terrane wreck. Terra Nova 26, 330–335.

Lahtinen, R., Korja, A., Nironen, M. 2005. Paleoproterozoic tectonic evolution. In Developments in Precambrian Geology 14, 481–531. Elsevier.

Lahtinen, R., Korja, A., Nironen, M., Heikkinen, P. 2009. Palaeoproterozoic accretionary processes in Fennoscandia. Geological Society, London, Special Publications 318, 237–256.

Lamberg, P. (2005). From genetic concepts to practice: lithogeochemical identification of Ni-Cu mineralised intrusions and localisation of the ore 402. Geological Survey of Finland.

Latypov, R., Chistyakova, S., Alapieti, T. 2007. Revisiting problem of chilled margins associated with marginal reversals in mafic–ultramafic intrusive bodies. Lithos 99, 178–206.

Li, C., Arndt, N.T., Tang, Q., Ripley, E.M. 2015. Trace element indiscrimination diagrams. Lithos 232, 76–83.

Locock, A. J. 2014. An Excel spreadsheet to classify chemical analyses of amphiboles following the IMA 2012 recommendations. Computers and Geosciences 62, 1-11.

Ludwig, K.R. 2003. User's manual for Isoplot/Ex, Version 3.00. A geochronological toolkit for Microsoft Excel. Berkeley Geochronology Center Special Publication 4.

Janousek, V. Farrow, C.M., Erban, V. 2006. Interpretation of whole-rock geochemical data in igneous geochemistry: introducing Geochemical Data Toolkit (GCDkit). Journal of Petrology 47, 1255–1259.

Maier, W.D. 2015. Geology and Petrogenesis of Magmatic Ni-Cu-PGE-Cr-V Deposits, in: Mineral Deposits of Finland. Elsevier, pp. 73–92.

Maier, W.D., Groves, D.I. 2011. Temporal and spatial controls on the formation of magmatic PGE and Ni–Cu deposits. Miner Deposita 46, 841–857.

Makkonen, H.V. 1996. 1.9 Ga tholeiitic magmatism and related Ni-Cu deposition in the Juva area, SE Finland. Geological Survey of Finland, Bulletin 386, 101 pp.

Makkonen, H.V. 2015. Nickel Deposits of the 1.88 Ga Kotalahti and Vammala Belts, in: Mineral Deposits of Finland. Elsevier, pp. 253–290.

Makkonen, H.V., Huhma, H., 2007. Sm-Nd data for mafic-ultramafic intrusions in the Svecofennian (1.88 Ga) Kotalahti Nickel Belt, Finland - Implications for crustal contamination at the Archaean/Proterozoic boundary. Bulletin of the Geological Society of Finland 79, 175–201.

Makkonen, H.V., Mäkinen, J., Kontoniemi, O., 2008. Geochemical discrimination between barren and mineralized intrusions in the Svecofennian (1.9 Ga) Kotalahti Nickel Belt, Finland. Ore Geology Reviews 33, 101–114.

Makkonen, H., Halkoaho, T., Tiainen, M., Iljina, M., Ahtonen, N., Toropainen, E. 2009. FINNICKEL-a public database on nickel deposits in Finland. Geological Survey of Finland. Version 1.0.

Makkonen, H.V., Halkoaho, T., Konnunaho, J., Rasilainen, K., Kontinen, A., Eilu, P. 2017. Ni-(Cu-PGE) deposits in Finland – Geology and exploration potential. Ore Geology Reviews 90, 667–696.

McCulloch, M.T., Gamble, J.A. 1991. Geochemical and geodynamical constraints on subduction zone magmatism. Earth and Planetary Science Letters 102, 358-374.

McDonough, WF., Sun, SS. 1995. The composition of the Earth. Chemical geology 120, 223-253.

Mitchell, R.H., Keays, R.R. 1981. Abundance and distribution of gold, palladium and iridium in some spinel and garnet lherzolites: implications for the nature and origin of precious metal-rich intergranular components in the upper mantle. Geochimica et Cosmochimica Acta 45, 2425-2442.

Müller, W., M. Shelley, Miller, P., Broude, S. 2009. Initial performance metrics of a new custom-designed ArF excimer LA-ICPMS system coupled to a two-volume laser-ablation cell. Journal of Analytical Atomic Spectrometry 24, 209–214

Müntener, O., Kelemen, P.B., Grove, T.L. 2001. The role of H_2O during crystallization of primitive arc magmas under uppermost mantle conditions and genesis of igneous pyroxenites: an experimental study. Contributions to Mineralogy and Petrology 141, 643–658.

Mäkinen, J. 1987. Geochemical characteristics of Svecokarelidic mafic-ultramafic intrusions associated with Ni-Cu occurrences in Finland. Geological Survey of Finland, 342. 109 pp.

Mäkinen, J., Makkonen, H.V. 2004. Petrology and structure of the Palaeoproterozoic (1.9 Ga) Rytky nickel sulphide deposit, Central Finland: a comparison with the Kotalahti nickel deposit. Mineralium Deposita 39, 405–421.

Naldrett, A.J. 1989. Magmatic sulfide deposits. Oxford university press. 186 p.

Naldrett, A.J., 1999. World-class Ni-Cu-PGE deposits: key factors in their genesis. Mineralium Deposita 34, 227–240.

Nicholls, I.A., Ringwood, A.E. 1972. Production of silica-saturated tholeiitic magmas in island arcs. Earth and Planetary Science Letters 17, 243–246.

Nironen, M. 1997. The Svecofennian Orogen: a tectonic model. Precambrian Research 86, 21–44.

Nironen, M., Elliott, B.A., Rämö, O.T. 2000. 1.88–1.87 Ga post-kinematic intrusions of the Central Finland Granitoid Complex: a shift from C-type to A-type magmatism during lithospheric convergence. Lithos 53, 37–58.

Nironen, M. 2003. Keski-Suomen granitoidikompleksi–kallioperäkartan selitys. Central Finland Granitoid Complex–Explanation to the bedrock map. Geological Survey of Finland, Report of Investigation, 157, 1-45.

Papunen, H., Koskinen, J. 1985. Geology of the Kotalahti nickel-copper ore. Nickel-copper deposits of the Baltic Shield and Scandinavian Caledonides. Geological Survey of Finland, Bulletin 333, 228–240.

Papunen, H., Gorbunov, I. (Eds) 1985. Nickel-copper deposits of the Baltic Shield and Scandinavian Caledonides. Geological Survev of Finland, Bulletin 333.

Papunen, H., 1986. Platinum-group elements in Svecokarelian nickel-copper deposits, Finland. Economic Geology 81, 1236–1241.

Pearce, T. H. 1968. A contribution to the theory of variation diagrams. Contributions to Mineralogy and Petrology, 19(2), 142-157.

Peltonen, P. 1995a. Petrogenesis of ultramafic rocks in the Vammala Nickel Belt: Implications for crustal evolution of the early Proterozoic Svecofennian arc terrane. Lithos 34, 253–274.

Peltonen, P. 1995b. Magma-country rock interaction and the genesis of Ni-Cu deposits in the Vammala Nickel Belt, SW Finland. Mineralogy and Petrology 52, 1–24.

Peltonen, P., Elo, S. 1999. Petrology of the Kaipola layered intrusion, southern Finland. Geological Survey of Finland, Special Paper 27, 21-24.

Peltonen, P. 2005. Mafic-Ultramafic intrusions of the Svecofennian orogen. In: Lehtinen, M., Nurmi, P.A., Rämö, O.T. (eds.). Precambrian of Finland – a key to the evolution of the Fennoscandian shield. Amsterdam: Elsevier, 413–447.

Pichavant, M., Macdonald, R. 2007. Crystallization of primitive basaltic magmas at crustal pressures and genesis of the calc-alkaline igneous suite: experimental evidence from St Vincent, Lesser Antilles arc. Contributions to Mineralogy and Petrology 154, 535–558.

Powell, M. 1978. Crystallisation conditions of low-pressure cumulate nodules from the Lesser Antilles island arc. Earth and Planetary Science Letters 39, 162–172.

Rehkämper, M., Halliday, A.N., Alt, J., Fitton, J.G., Zipfel, J., Takazawa, E. 1999. Non-chondritic platinum-group element ratios in oceanic mantle lithosphere: petrogenetic signature of melt percolation? Earth and Planetary Science Letters 172, 65–81.

Reynolds, I.M. 1985. The nature and origin of titaniferous magnetite-rich layers in the upper zone of the Bushveld Complex; a review and synthesis. Economic Geology 80, 1089–1108.

Ripley, E.M., Li, C., 2013. Sulfide saturation in mafic magmas: Is external sulfur required for magmatic Ni-Cu-(PGE) ore genesis? Economic geology 108, 45–58.

Roeder, P.L., Emslie, R.F., 1970. Olivine-liquid equilibrium. Contributions to Mineralogy and Petrology 29, 275–289.

Roeder, P.L., 1974. Activity of iron and olivine solubility in basaltic liquids. Earth and Planetary Science Letters 23, 397–410.

Rämö, T. 1986. The petrography, mineralogy, and petrology of the Perämaa mafic intrusion with special reference to the gabbroic rocks, Honkajoki. Unpublished M.Sc. thesis, Department of Geology, University of Helsinki.

Rämö, O.T., Vaasjoki, M., Mänttäri, I., Elliott, B.A., Nironen, M. 2001. Petrogenesis of the post-kinematic magmatism of the Central Finland Granitoid Complex I; Radiogenic isotope constraints and implications for crustal evolution. Journal of Petrology 42, 1971–1993.

Saunders, A.D., Tarney, J. 1984. Geochemical characteristics of basaltic volcanism within back-arc basins. Geological Society, London, Special Publications 16, 59–76.

Sisson, T.W., Grove, T L. 1993. Temperatures and H_2O contents of low-MgO high-alumina basalts. Contributions to Mineralogy and Petrology 113, 167–184.

Sjöblom, B. 1990. Mäntän kartta-alueen kallioperä, Suomen geologinen kartta 1 : 100 000, lehti 2231. Geologian tutkimuskeskus.

Snyder, D., Carmichael, I.S., Wiebe, R.A. 1993. Experimental study of liquid evolution in an Fe-rich, layered mafic intrusion: constraints of Fe-Ti oxide precipitation on the T-fo_2 and T- ρ paths of tholeiitic magmas. Contributions to Mineralogy and Petrology 113, 73-86.

Stacey, J.S., Kramers, J.D. 1975. Approximation of terrestrial lead isotope evolution by a two-stage model. Earth and Planetary Science Letters 26, 207–221.

Straub, S.M., LaGatta, A.B., Martin-Del Pozzo, A.L., Langmuir, C.H. 2008. Evidence from high-Ni olivines for a hybridized peridotite/pyroxenite source for orogenic andesites from the central Mexican Volcanic Belt. Geochemistry, Geophysics, Geosystems 9.

Sun, S.S., McDonough, WF. 1989. Chemical and isotopic systematics of oceanic basalts: implications for mantle composition and processes. Geological society, London, Special Publications 42, 313–345.

Tatsumi, Y., Kogiso, T. 2003. The subduction factory: its role in the evolution of the Earth's crust and mantle. Geological society, London, Special Publications 219, 55–80.

Toplis, M.J. 2005. The thermodynamics of iron and magnesium partitioning between olivine and liquid: criteria for assessing and predicting equilibrium in natural and experimental systems. Contributions to Mineralogy and Petrology 149, 22–39.

Toplis, M.J., Corgne, A. 2002. An experimental study of element partitioning between magnetite, clinopyroxene and iron-bearing silicate liquids with particular emphasis on vanadium. Contributions to Mineralogy and Petrology 144, 22–37.

Van Achterbergh, E., Ryan C., Jackson, S. and Griffin W. 2001. Data reduction software for LA-ICP-MS, in: Laser-Ablation ICPMS in the Earth Sciences – Principles and applications, Mineralogical Association of Canada short course series, 29, St John, Newfoundland, Sylverster P. Ed., 239– 243.

Woodhead, J., Eggins, S., Gamble, J. 1993. High field strength and transition element systematics in island arc and back-arc basin basalts: Evidence for multi-phase melt extraction and a depleted mantle wedge. Earth and Planetary Science Letters 114, 491–504.

Zellmer, G.F., Edmonds, M., Straub, S.M., 2015. Volatiles in subduction zone magmatism. Geological Society, London, Special publications 410, 1–17.

APPENDICES

Appendix 1. Whole-rock chemistry results. Detection limits are displayed below the analyzed oxide/element and above the unit. Analyzed with XRF, carbon analyzer(*) and ICP-OES(**). Coordinates in ETRS-TM35FIN.

Sample	Group	X	Y	SiO_2	TiO_2	Al_2O_3	Fe_2O_3t	MnO	MgO	CaO	Na_2O	K_2O	P_2O_5		As	Ba	Bi	Ce	Cl	Cr	Cu	Ga	La	Mo	Nb	Ni	Pb	Rb	S	Sb	Sc	Sn	Sr	Th	U	V	Y	Zn	Zr	C*	Au**	Pd**	Pt**
				0.01	0.003	0.01	0.01	0.005	0.02	0.003	0.03	0.003	0.006		10	20	30	30	100	20	20	30	30	10	20	20	30	10	100	50	20	30	10	30	10	10	10	20	10	0.05	5	5	5
				wt-%	wt-%	wt-%	wt-%	wt-%	wt-%	wt-%	wt-%	wt-%	wt-%		ppm	ppm	ppm	ppm	ppm	ppm	ppm	ppm	ppm	ppm	ppm	ppm	ppm	ppm	ppm	ppm	ppm	ppm	ppm	ppm	ppm	ppm	ppm	ppm	ppm	wt-%	ppb	ppb	ppb
SIKA-2017-6.1	Matokulma	390666	6872212	47.69	0.44	11.14	10.44	0.19	12.04	11.89	0.97	0.38	0.02	95.20	<10	50	<30	<30	300	780	20	<30	<30	<10	<20	100	<30	<10	200	<50	30	<30	350	<30	<10	260	20	80	40	0.09	<5	<5	<5
SIKA-2017-6.2	Matokulma	390668	6872212	47.61	0.41	14.57	8.93	0.16	9.45	11.55	1.56	0.62	0.05	94.91	<10	70	<30	<30	300	630	60	<30	<30	<10	<20	90	<30	<10	1200	<50	30	<30	570	30	<10	220	10	70	50	0.1			
SIKA-2017-6.3	Matokulma	390668	6872212	47.35	0.38	12.65	9.84	0.18	10.87	12.08	1.10	0.39	0.01	94.85	<10	30	<30	<30	300	660	40	<30	<30	<10	<20	90	<30	<10	500	<50	40	<30	400	<30	<10	240	<10	80	30	0.07			
SIKA-2017-6.4	Matokulma	390668	6872212	48.35	0.57	10.10	11.31	0.20	11.17	11.51	1.10	0.34	0.03	94.68	<10	50	<30	<30	300	760	50	<30	<30	<10	<20	60	<30	<10	1100	<50	40	<30	350	<30	<10	320	<10	90	30	<0.05	<5	<5	<5
SIKA-2017-7.1	Matokulma	390639	6872190	47.22	0.46	8.88	10.84	0.19	12.93	12.07	0.92	0.55	0.08	94.14	<10	80	<30	<30	300	1080	70	<30	<30	<10	<20	110	<30	<10	400	<50	40	<30	270	<30	<10	260	20	90	40	0.14	<5	<5	<5
SIKA-2017-18.1	Matokulma	389685	6872220	47.61	1.99	19.23	10.82	0.13	3.53	9.03	3.01	1.49	0.36	97.20	<10	250	<30	40	400	<20	20	<30	<30	<10	<20	20	<30	<10	900	<50	20	<30	660	<30	10	380	20	100	80	0.06			
SIKA-2017-20.1	Matokulma	389855	6872265	46.99	0.47	15.35	8.42	0.14	8.89	13.45	1.32	0.46	0.06	95.54	<10	120	<30	<30	300	470	60	<30	<30	<10	<20	50	<30	<10	900	<50	30	<30	500	30	<10	250	10	60	60	0.09	<5	<5	<5
SIKA-2017-21.1	Matokulma	389707	6872383	46.43	0.36	17.07	8.08	0.13	7.88	12.88	1.37	0.43	0.07	94.69	<10	120	<30	<30	300	190	30	<30	<30	<10	<20	40	<30	<10	800	<50	30	<30	590	<30	<10	190	<10	70	60	<0.05			
SIKA-2017-27.1	Matokulma	390401	6872097	54.07	0.63	15.03	8.37	0.13	6.25	8.36	1.75	1.34	0.09	96.02	<10	350	<30	<30	200	30	40	<30	<30	<10	<20	40	<30	<10	1100	<50	40	<30	420	30	<10	240	20	70	100	0.09			
SIKA-2017-27.2	Matokulma	390397	6872096	45.95	1.04	15.16	14.30	0.13	7.57	3.23	2.38	2.02	0.05	91.83	<10	290	<30	30	200	420	20	<30	<30	<10	<20	200	<30	<10	600	<50	40	<30	300	40	<10	280	20	220	110	0.06			
SIKA-2017-42.1	Matokulma	389589	6872260	47.90	0.52	8.32	10.82	0.19	13.11	11.89	0.87	0.71	0.08	94.41	<10	300	<30	<30	300	1220	60	<30	<30	<10	<20	90	<30	<10	900	<50	50	<30	280	30	<10	300	10	90	50	0.08	<5	<5	<5
SIKA-2017-44.1	Matokulma	389445	6872414	46.54	0.38	15.51	8.26	0.14	9.31	12.34	1.14	1.36	0.07	95.04	<10	380	<30	<30	300	490	50	<30	<30	<10	<20	60	<30	<10	900	<50	30	<30	410	<30	<10	230	10	60	50	0.09	<5	<5	<5
SIKA-2017-60.1	Matokulma	390217	6871917	60.69	0.47	18.07	5.38	0.05	0.90	4.02	3.88	3.04	0.29	96.79	<10	1360	<30	90	200	20	<20	<30	<30	<10	<20	30	<30	<10	100	<50	<20	<30	530	30	<10	40	30	90	320	0.1			
SIKA-2017-104.1	Matokulma	389130	6872325	48.32	0.55	9.96	10.83	0.20	12.14	10.75	1.00	0.62	0.08	94.45	<10	160	<30	<30	300	1040	60	<30	<30	<10	<20	120	<30	<10	1000	<50	50	<30	250	30	<10	280	20	90	40	0.06			
SIKA-2017-105.1	Matokulma	389033	6872307	47.74	0.58	8.75	10.83	0.18	12.56	11.49	1.11	0.77	0.09	94.11	<10	110	<30	<30	400	1240	60	<30	<30	<10	<20	110	<30	<10	1100	<50	40	<30	230	<30	<10	250	10	90	60	0.1			
SIKA-2017-107.1	Matokulma	388999	6872356	57.57	0.67	18.42	6.66	0.09	1.97	2.08	3.56	3.93	0.33	95.28	<10	1460	<30	60	100	40	80	<30	30	<10	<20	30	<30	<10	<100	<50	<20	<30	300	30	<10	70	30	110	310	0.1			
SIKA-2017-108.1	Matokulma	389210	6872461	47.90	0.68	9.11	11.24	0.18	12.37	10.21	1.25	0.90	0.08	93.92	<10	270	<30	<30	300	1240	60	<30	<30	<10	<20	140	<30	<10	400	<50	30	<30	280	<30	<10	240	20	90	60	<0.05	<5	<5	<5
SIKA-2017-111.1	Matokulma	390559	6872099	47.62	0.42	16.26	7.56	0.13	8.39	12.97	1.51	0.64	0.08	95.58	<10	190	<30	<30	200	300	40	<30	<30	<10	<20	40	<30	<10	900	<50	40	<30	580	<30	<10	230	<10	60	60	0.09	<5	<5	<5
SIKA-2017-112.1	Matokulma	390362	6872176	46.49	0.51	6.80	11.32	0.19	14.28	12.56	0.70	0.45	0.08	93.38	<10	70	<30	30	200	1370	80	<30	<30	<10	<20	110	<30	<10	1700	<50	50	<30	170	30	<10	310	20	90	40	<0.05	<5	<5	<5
SIKA-2017-115.1	Matokulma	390362	6872156	70.49	0.17	13.65	1.38	0.01	0.56	1.46	3.87	4.33	0.11	96.03	<10	430	<30	90	100	30	<20	<30	<30	<10	<20	<20	50	<10	<100	<50	<20	<30	190	40	<10	20	30	30	110	<0.05			
SIKA-2017-115.2	Matokulma	390353	6872244	47.56	0.57	5.81	10.85	0.18	13.71	13.15	0.87	0.47	0.09	93.25	<10	80	<30	30	400	1400	90	<30	<30	<10	<20	90	<30	<10	2500	<50	60	<30	140	<30	<10	360	10	80	40	<0.05	<5	<5	<5
SIKA-2017-167.1	Matokulma	390162	6872382	48.80	0.52	10.57	9.84	0.16	10.69	11.91	1.34	0.78	0.07	94.68	<10	120	<30	<30	300	880	60	<30	<30	<10	<20	70	<30	<10	800	<50	40	<30	290	30	<10	270	10	60	50	0.07			
SIKA-2017-169.1	Matokulma	390162	6872381	56.13	0.76	18.14	7.21	0.10	2.40	5.29	3.54	2.17	0.37	96.10	<10	960	<30	60	300	50	40	<30	30	<10	<20	40	<30	<10	400	<50	<20	<30	730	30	<10	100	20	100	230	0.05			
SIKA-2017-173.1	Matokulma	390072	6872118	47.31	0.55	7.79	10.88	0.18	12.77	12.67	1.10	0.50	0.10	93.85	<10	130	<30	30	400	1360	60	<30	<30	<10	<20	120	<30	<10	900	<50	50	<30	220	<30	<10	310	10	80	50	0.06	<5	<5	<5
SIKA-2017-174.1	Matokulma	390095	6872246	45.32	0.67	10.83	12.43	0.21	12.30	9.01	1.12	0.53	0.05	92.47	<10	120	<30	30	200	1000	<20	<30	<30	<10	<20	340	<30	<10	<100	<50	30	<30	310	30	<10	210	<10	110	40	0.09	<5	<5	<5
SIKA-2017-174.2	Matokulma	390097	6872243	47.63	0.36	16.96	8.96	0.14	8.39	10.99	1.50	0.66	0.09	95.67	<10	150	<30	<30	300	160	40	<30	<30	<10	<20	50	60	<10	400	<50	20	<30	630	30	<10	170	10	110	60	<0.05			
SIKA-2017-188.1	Matokulma	389004	6872330	49.43	0.78	18.76	8.67	0.07	3.81	1.86	2.49	6.93	0.08	92.87	<10	1850	<30	80	200	150	<20	<30	50	<10	<20	100	30	<10	<100	<50	30	<30	330	40	<10	130	30	150	150	<0.05			
SIKA-2017-27.3	Matokulma dikes	390454	6872085	48.65	0.94	16.31	11.16	0.18	5.19	9.07	1.91	1.75	0.30	95.44	<10	400	<30	40	200	60	50	<30	<30	<10	<20	30	<30	<10	900	<50	30	<30	550	<30	<10	220	30	110	90	0.06			
SIKA-2017-28.1	Matokulma dikes	390335	6872091	48.05	0.99	15.78	12.36	0.20	5.62	6.42	1.80	3.97	0.29	95.48	<10	1290	<30	<30	200	140	<20	<30	<30	<10	<20	40	<30	<10	100	<50	30	<30	310	30	<10	230	30	130	70	<0.05			
SIKA-2017-28.2	Matokulma dikes	390333	6872092	49.22	0.90	16.14	11.16	0.19	4.66	7.86	2.71	1.88	0.31	95.02	<10	570	<30	40	300	30	<20	<30	<30	<10	<20	30	<30	<10	<100	<50	30	<30	480	30	<10	210	30	130	100	0.06			
SIKA-2017-55.1	Matokulma dikes	390283	6872088	49.51	0.85	15.39	10.20	0.16	5.37	9.33	2.53	1.26	0.28	94.87	<10	620	<30	<30	300	80	40	<30	<30	<10	<20	<20	<30	<10	200	<50	30	<30	570	<30	<10	210	30	100	70	0.05			
SIKA-2017-58.1	Matokulma dikes	390167	6872152	50.73	0.89	18.55	10.09	0.15	3.98	9.72	2.77	0.64	0.27	97.78	<10	170	<30	<30	100	110	70	<30	<30	<10	<20	40	<30	<10	400	<50	20	<30	630	30	<10	240	20	100	70	0.05			
SIKA-2017-61.1	Matokulma dikes	389263	6872318	47.40	0.79	13.49	10.40	0.21	8.75	9.72	1.09	1.63	0.28	93.77	<10	390	<30	60	200	770	<20	<30	<30	<10	<20	140	<30	<10	<100	<50	30	<30	370	30	<10	210	20	120	90	0.07			
SIKA-2017-119.1	Matokulma dikes	390288	6872330	47.59	0.78	11.21	10.54	0.15	13.17	7.44	1.87	1.20	0.30	94.24	<10	450	<30	40	400	1010	70	<30	<30	<10	<20	400	<30	<10	200	<50	30	<30	660	<30	<10	190	10	100	90	0.06			
SIKA-2017-121.1	Matokulma dikes	390145	6872359	53.41	1.00	14.37	8.31	0.12	6.44	6.97	2.56	2.69	0.59	96.46	<10	630	<30	100	100	300	20	<30	<30	<10	<20	170	<30	<10	600	<50	<20	<30	730	30	<10	150	30	90	170	<0.05			
SIKA-2017-169.2	Matokulma dikes	390162	6872381	47.19	1.30	15.69	11.11	0.18	5.79	8.97	3.11	0.74	0.49	94.57	<10	340	<30	90	300	330	20	<30	<30	<10	<20	60	<30	<10	200	<50	30	<30	670	<30	<10	240	20	130	130	0.08			
SIKA-2017-1.1	Palojärvi	380806	6883770	45.71	1.61	16.87	18.74	0.29	5.91	8.09	1.72	0.51	0.29	99.73	<10	180	<30	40	200	40	20	<30	<30	<10	<20	<20	<30	<10	300	<50	20	<30	560	30	10	370	10	180	50	0.14			
SIKA-2017-1.2	Palojärvi	380801	6883763	46.16	1.72	20.58	14.09	0.20	3.83	9.73	2.49	0.34	0.60	99.73	<10	160	<30	<30	200	<20	40	30	<30	<10	<20	<20	<30	<10	500	<50	<20	<30	860	40	<10	350	<10	140	60	0.11			
SIKA-2017-3.1	Palojärvi	379713	6883761	44.15	0.66	19.61	10.55	0.14	7.36	12.10	1.10	0.36	0.10	96.14	<10	160	<30	<30	200	40	50	<30	<30	<10	<20	30	<30	<10	400	<50	30	<30	600	30	<10	290	<10	70	70	0.06	<5	<5	<5
SIKA-2017-4.1	Palojärvi	379492	6884258	44.75	1.58	16.18	16.67	0.22	6.20	8.98	1.89	0.85	0.11	97.43	<10	210	<30	50	300	20	40	<30	<30	<10	<20	30	<30	<10	300	<50	20	<30	450	30	<10	450	20	130	60	0.12			
SIKA-2017-5.1	Palojärvi	379379	6883371	40.93	1.83	15.10	17.19	0.21	6.79	11.75	1.11	0.24	0.08	95.23	<10	90	<30	<30	200	40	80	<30	<30	<10	<20	30	<30	<10	900	<50	50	<30	610	30	<10	780	10	150	50	0.15	<5	<5	<5
SIKA-2017-8.1	Palojärvi	382046	6883802	45.97	2.09	19.43	11.21	0.14	4.64	9.67	2.68	0.67	0.24	96.74	<10	180	<30	70	300	50	<20	<30	<30	<10	<20	20	<30	<10	<100	<50	30	<30	540	<30	<10	490	20	100	90	0.1			
SIKA-2017-11.1	Palojärvi	380113	6883503	45.42	1.33	16.15	18.34	0.30	5.89	7.47	1.93	0.68	0.36	97.87	<10	240	<30	40	300	20	40	<30	<30	<10	<20	20	<30	<10	600	<50	<20	<30	570	<30	<10	280	10	180	70	0.1			
SIKA-2017-11.2	Palojärvi	380114	6883503	41.74	1.67	18.06	15.32	0.24	4.56	8.93	1.77	1.64	0.53	94.46	<10	750	<30	50	300	<20	50	<30	<30	<10	<20	30	<30	<10	500	<50	30	<30	530	<30	<10	240	30	180	70	0.07			
SIKA-2017-13.1	Palojärvi	379478	6883827	43.83	0.42	17.17	13.38	0.19	9.41	8.55	1.28	0.57	0.12	94.92	<10	160	<30	40	300	20	<20	<30	<30	<10	<20	60	<30	<10	<100	<50	<20	<30	520	30	<10	100	10	110	70	<0.05			
SIKA-2017-14.1	Palojärvi	379867	6883696	39.10	0.62	12.86	18.56	0.25	13.26	7.75	1.00	0.22	0.07	93.69	<10	60	<30	<30	400	20	40	<30	<30	<10	<20	40	<30	<10	700	<50	<20	<30	320	30	<10	280	10	140	40	0.08	<5	<5	<5
SIKA-2017-17.1	Palojärvi	379220	6884107	47.64	0.82	21.77	9.92	0.16	2.05	9.10	4.10	0.48	0.54	96.58	<10	390	<30	<30	300	20	50	<30	<30	<10	<20	<20	<30	<10	400	<50	<20	<30	1020	<30	<10	90	<10	100	80	<0.05			
SIKA-2017-22.1	Palojärvi	379090	6883938	54.19	0.84	19.23	8.67	0.10	2.53	7.62	3.53	0.33	0.19	97.22	<10	90	<30	40	200	20	<20	<30	<30	<10	<20	30	<30	<10	100	<50	<20	<30	760	40	<10	130	10	90	110	<0.05			
SIKA-2017-30.1	Palojärvi	383110	6883898	50.16	1.07	14.87	11.69	0.16	4.52	7.75	3.14	1.65	0.14	95.15	<10	500	<30	<30	300	<20	50	<30	<30	<10	<20	30	<30	<10	600	<50	40	<30	310	30	<10	390	30	100	90	0.06			
SIKA-2017-49.1	Palojärvi	379465	6883459	39.16	1.53	16.93	16.33	0.22	6.07	10.89	1.44	0.50	0.35	93.42	<10	120	<30	<30	100	30	40	<30	<30	<10	<20	30	<30	<10	1000	<50	40	<30	680	<30	<10	480	10	130	40	0.14	<5	<5	<5
SIKA-2017-49.2	Palojärvi	379285	6883349	40.11	2.60	15.49	16.07	0.20	6.67	11.41	1.42	0.47	0.13	94.57	<10	130	<30	<30	300	20	70	<30	<30	<10	<20	30	<30	<10	1100	<50	60	<30	550	30	<10	520	<10	120	60	0.08			
SIKA-2017-51.1	Palojärvi	379359	6883573	37.94	1.72	14.42	22.77	0.26	10.89	7.64	0.97	0.29	0.08	96.98	<10	120	<30	<30	300	70	60	<30	<30	<10	<20	50	<30	<10	800	<50	<20	<30	490	30	<10	400	<10	170	40	0.1	<5	<5	<5
SIKA-2017-53.1	Palojärvi	379229	6883664	43.88	0.89	18.47	12.50	0.16	6.16	11.60	1.12	0.44	0.07	95.28	<10	120	<30	<30	200	40	50	<30	<30	<10	<20	40	<30	<10	400	<50	20	<30	510	<30	<10	440	10	90	40	0.1			
SIKA-2017-54.1	Palojärvi	379104	6883714	40.46	2.28	17.63	16.13	0.23	4.51	11.21	2.19	0.54	0.49	95.66	<10	250	<30	70	400	30	50	<30	<30	<10	<20	20	<30	<10	500	<50	50	<30	590	30	<10	400	40	170	90	0.13			
SIKA-2017-62.1	Palojärvi	390612	6872324	39.59	0.45	14.17	16.25	0.25	11.84	8.65	1.11	0.31	0.11	92.73	<10	<20	<30	<30	400	50	40	<30	<30	<10	<20	40	<30	<10	1400	<50	<20	<30	230	<30	<10	90	<10	140	20	0.06			
SIKA-2017-67.1	Palojärvi	379463	6883458	42.92	0.59	26.53	7.34	0.07	3.09	14.28	1.32	0.38	0.06	96.58	<10	120	<30	<30	200	<20	40	<30	<30	<10	<20	30	<30	<10	400	<50	<20	<30	820	30	<10	250	<10	60	70	0.09			
SIKA-2017-69.1	Palojärvi	380180	6883822	48.56	1.23	14.60	14.62	0.19	5.21	8.00	1.56	1.27	0.40	95.64	<10	260	<30	40	300	30	50	<30	<30	<10	<20	30	<30	<10	800	<50	<20	<30	470	<30	<10	280	20	110	100	0.11			
SIKA-2017-69.2	Palojärvi	380031	6883578	74.14	0.11	13.93	1.15	0.01	0.31	1.50	3.48	4.80	0.04	99.47	<10	780	<30	30	100	<20	<20	<30	<30	<10	<20	<20	50	<10	<100	<50	<20	<30	380	40	<10	20	20	20	120	0.11			
SIKA-2017-70.1	Palojärvi	380030	6883578	71.16	0.12	13.44	1.55	0.03	0.26	1.95	3.89	3.16	0.06	95.61	<10	670	<30	<30	200	<20	<20	<30	<30	<10	<20	<20	40	<10	<100	<50	<20	<30	250	<30	<10	10	<10	30	90	0.07			
SIKA-2017-75.1	Palojärvi	380084	6883456	42.59	1.69	16.36	15.34	0.21	5.42	10.26	2.02	0.65	0.21	94.75	<10	380	<30	<30	200	<20	60	<30	<30	<10	<20	20	<30	<10	1500	<50	40	<30	730	30	<10	500	20	130	80	0.11			
SIKA-2017-80.1	Palojärvi	381890	6883818	42.75	0.78	18.85	15.09	0.21	7.42	8.73	1.46	0.91	0.19	96.38	<10	310	<30	<30	200	70	30	<30	<30	<10	<20	50	<30	<10	300	<50	<20	<30	650	<30	<10	210	<10	120	70	0.12			
SIKA-2017-81.1	Palojärvi	379206	6884314	43.51	1.60	16.91	15.11	0.25	4.60	9.44	2.79	0.77	0.37	95.35	<10	380	<30	50	400	<20	40	<30	30	<10	<20	<20	<30	<10	700	<50	20	<30	590	<30	10	360	50	150	110	0.11			
SIKA-2017-82.1	Palojärvi	379122	6884336	42.64	2.11	19.63	15.36	0.20	3.93	11.23	2.50	0.51	0.65	98.76	<10	280	<30	60	300	<20	40	40	<30	<10	<20	20	<30	<10	200	<50	40	<30	760	<30	10	300	30	140	90	<0.05			
SIKA-2017-88.1	Palojärvi	379045	6884306	42.11	1.96	20.04	16.35	0.23	4.53	11.63	2.06	0.20	0.56	99.67	<10	160	<30	50	200	<20	50	30	<30	<10	<20	<20	<30	<10	1200	<50	40	<30	750	30	<10	410	20	160	60	0.11			
SIKA-2017-88.2	Palojärvi	379859	6883281	41.50	1.91	19.11	15.94	0.22	4.65	11.24	1.89	0.35	0.55	97.36	<10	140	<30	30	100	<20	50	<30	<30	<10	<20	20	<30	<10	1000	<50	40	<30	760	<30	<10	410	20	150	60	0.12			

Appendix 1. Continues

Sample	Group	X	Y	SiO_2	TiO_2	Al_2O_3	Fe_2O_3t	MnO	MgO	CaO	Na_2O	K_2O	P_2O_5	Sum	As	Ba	Bi	Ce	Cl	Cr	Cu	Ga	La	Mo	Nb	Ni	Pb	Rb	S	Sb	Sc	Sn	Sr	Th	U	V	Y	Zn	Zr	C*	Au**	Pd**	Pt**
				0.01	0.003	0.01	0.01	0.005	0.02	0.003	0.03	0.003	0.006		10	20	30	30	100	20	20	30	30	10	20	20	30	10	100	50	20	30	10	30	10	10	10	20	10	0.05	5	5	5
				wt-%	wt-%	wt-%	wt-%	wt-%	wt-%	wt-%	wt-%	wt-%	wt-%		ppm	ppm	ppm	ppm	ppm	ppm	ppm	ppm	ppm	ppm	ppm	ppm	ppm	ppm	ppm	ppm	ppm	ppm	ppm	ppm	ppm	ppm	ppm	ppm	ppm	wt-%	ppb	ppb	ppb
SIKA-2017-88.3	Palojärvi	379859	6883281	40.63	1.96	19.10	16.62	0.22	5.30	11.68	1.48	0.40	0.53	97.92	<10	100	<30	<30	100	<20	60	<30	<30	<10	<20	20	<30	<10	1300	<50	40	<30	830	30	<10	420	<10	150	60	0.06			
SIKA-2017-101.1	Palojärvi	379859	6883281	60.10	0.53	17.61	4.43	0.09	0.66	3.87	5.50	2.28	0.24	95.31	<10	560	<30	90	200	<20	<20	<30	40	<10	<20	20	40	<10	<100	<50	<20	<30	380	50	<10	40	30	80	420	0.12			
SIKA-2017-126.1	Palojärvi	379656	6883244	66.81	0.36	14.61	3.68	0.07	0.90	2.57	3.46	4.34	0.18	96.97	<10	970	<30	60	400	20	<20	<30	<30	<10	<20	30	30	<10	<100	<50	<20	<30	370	40	<10	40	30	50	150	<0.05			
SIKA-2017-130.1	Palojärvi	377719	6884746	43.92	1.41	18.07	14.16	0.26	3.41	8.87	3.03	1.41	0.65	95.18	<10	700	<30	70	400	<20	40	<30	<30	<10	<20	20	<30	<10	500	<50	40	<30	690	<30	<10	180	40	160	90	<0.05			
SIKA-2017-139.1	Palojärvi	377592	6881284	40.70	1.18	15.57	15.05	0.17	8.05	10.69	1.34	0.68	0.07	93.49	<10	190	<30	<30	300	50	70	<30	<30	<10	<20	40	<30	<10	1200	<50	30	<30	570	<30	<10	580	<10	100	60	0.1			
SIKA-2017-140.1	Palojärvi	377956	6881429	43.59	1.32	18.66	12.19	0.16	4.72	10.20	1.87	1.24	0.52	94.47	<10	330	<30	40	400	<20	40	<30	<30	<10	<20	<20	<30	<10	600	<50	<20	<30	680	30	<10	350	20	110	70	0.06			
SIKA-2017-142.1	Palojärvi	377594	6881527	39.42	1.20	18.65	16.98	0.18	8.63	9.24	1.10	0.61	0.07	96.08	<10	180	<30	<30	200	40	50	<30	<30	<10	<20	40	<30	<10	1600	<50	<20	<30	430	30	<10	550	<10	120	50	0.1			
SIKA-2017-156.1	Palojärvi	380573	6883472	49.38	1.07	15.63	10.45	0.17	5.12	8.29	2.88	1.52	0.42	94.93	<10	550	<30	30	500	150	60	<30	<30	<10	<20	60	<30	<10	200	<50	20	<30	790	<30	<10	240	20	110	130	0.12			
SIKA-2017-158.1	Palojärvi	378636	6883752	45.49	0.92	17.14	13.22	0.25	6.25	8.65	2.01	0.56	0.30	94.79	<10	240	<30	<30	200	<20	30	<30	<30	<10	<20	40	<30	<10	400	<50	30	<30	620	<30	<10	190	10	130	60	0.12			
SIKA-2017-159.1	Palojärvi	379742	6884165	49.15	0.74	17.62	10.53	0.17	4.93	9.16	1.69	0.97	0.04	95.00	<10	170	<30	50	200	60	30	<30	<30	<10	<20	40	<30	<10	100	<50	30	<30	470	30	<10	280	20	100	50	0.06			
SIKA-2017-159.2	Palojärvi	379756	6884160	45.79	1.35	9.80	18.95	0.28	9.29	6.17	0.79	1.37	0.03	93.83	<10	660	<30	<30	300	50	60	<30	<30	<10	<20	70	<30	<10	700	<50	20	<30	210	40	<10	490	20	160	60	<0.05			
SIKA-2017-161.1	Palojärvi	380024	6884060	40.15	0.71	22.43	11.25	0.13	5.73	10.90	1.49	0.64	0.05	93.48	<10	170	<30	<30	200	50	30	<30	<30	<10	<20	40	<30	<10	600	<50	<20	<30	640	30	<10	280	<10	80	60	0.06			
SIKA-2017-183.1	Palojärvi	382447	6883772	74.73	0.10	13.27	1.59	0.03	0.26	1.21	3.37	4.97	0.04	99.58	<10	830	<30	30	100	<20	<20	<30	<30	<10	<20	<20	<30	<10	<100	<50	<20	<30	220	30	<10	20	10	30	90	<0.05			
SIKA-2017-185.1	Palojärvi	379396	6884278	48.83	0.87	16.92	11.37	0.16	6.08	7.35	2.12	1.48	0.21	95.38	<10	520	<30	<30	400	40	20	<30	<30	<10	<20	60	<30	<10	200	<50	<20	<30	550	30	<10	110	20	110	60	0.08			
SIKA-2017-185.2	Palojärvi	379398	6884273	46.84	1.34	19.14	12.46	0.16	4.67	9.80	2.25	0.94	0.15	97.76	<10	220	<30	40	400	30	50	<30	<30	<10	<20	40	<30	<10	200	<50	30	<30	610	30	<10	380	20	110	70	<0.05			
SIKA-2017-185.3	Palojärvi	379410	6884280	43.59	1.16	18.72	16.07	0.19	7.82	8.55	1.76	0.62	0.14	98.61	<10	180	<30	40	300	40	70	<30	<30	<10	<20	50	<30	<10	200	<50	<20	<30	560	<30	<10	420	<10	120	70	0.11			
SIKA-2017-9.1	Hongonniittu	384982	6884775	40.14	0.44	17.59	12.50	0.17	10.20	10.28	0.65	0.38	0.04	92.39	<10	50	<30	40	200	150	60	<30	<30	<10	<20	50	<30	<10	200	<50	<20	<30	590	<30	<10	180	<10	80	50	0.07			
SIKA-2017-154.1	Hongonniittu	384758	6884788	44.46	0.62	25.02	6.95	0.08	2.92	13.62	1.66	0.36	0.14	95.83	<10	100	<30	<30	300	60	20	<30	<30	<10	<20	30	<30	<10	200	<50	<20	<30	830	30	<10	250	10	60	70	0.12	<5	<5	<5
SIKA-2017-154.2	Hongonniittu	384738	6884764	41.80	1.19	19.61	12.10	0.15	5.14	12.20	1.60	0.51	0.08	94.38	<10	120	<30	<30	300	90	50	<30	<30	<10	<20	40	<30	<10	900	<50	30	<30	640	<30	<10	480	10	100	60	0.1	6	<5	<5
SIKA-2017-154.3	Hongonniittu	384741	6884761	41.65	1.26	19.82	11.97	0.14	5.16	12.33	1.64	0.53	0.14	94.64	<10	140	<30	<30	300	90	50	<30	<30	<10	<20	40	<30	<10	700	<50	30	<30	660	30	<10	500	<10	90	60	0.08	<5	<5	<5

Appendix 2. CIPW norms for mafic-ultramafic rocks. $Fe^{2+}=0.85 \cdot Fe_{tot}$ was used in the calculation.

Sample	Group	Q	C	Or	Ab	An	Ne	Di	MgDi	FeDi	Wo	Hy	En	Fs	Ol	Fo	Fa	Dcs	Mt	Il	Ap	Fo*	En*	Di*	An*
SIKA-2017-6.1	Matokulma	0.00	0.00	2.36	8.63	26.17	0.00	28.86	20.25	8.61	0.00	24.82	16.69	8.14	5.85	3.81	2.05	0.00	2.39	0.89	0.05	65	67	70	75
SIKA-2017-6.2	Matokulma	0.00	0.00	3.90	13.88	32.57	0.00	22.28	15.26	7.03	0.00	17.19	11.25	5.94	7.20	4.55	2.65	0.00	2.05	0.82	0.12	63	65	68	70
SIKA-2017-6.3	Matokulma	0.00	0.00	2.42	9.82	29.98	0.00	26.86	18.58	8.28	0.00	22.00	14.56	7.44	5.89	3.77	2.12	0.00	2.26	0.76	0.02	64	66	69	75
SIKA-2017-6.4	Matokulma	0.00	0.00	2.13	9.82	22.84	0.00	30.29	20.32	9.98	0.00	30.85	19.74	11.12	0.27	0.17	0.11	0.00	2.60	1.16	0.07	62	64	67	70
SIKA-2017-7.1	Matokulma	0.00	0.00	3.49	8.29	19.59	0.00	35.15	24.92	10.24	0.00	20.77	14.12	6.65	9.12	6.00	3.12	0.00	2.51	0.91	0.19	66	68	71	70
SIKA-2017-20.1	Matokulma	0.00	0.00	2.84	11.68	36.24	0.00	26.88	18.47	8.42	0.00	11.78	7.74	4.05	7.59	4.82	2.77	0.00	1.92	0.93	0.17	63	66	69	76
SIKA-2017-21.1	Matokulma	0.00	0.00	2.66	12.27	41.36	0.00	20.85	13.90	6.95	0.00	13.89	8.82	5.06	6.24	3.83	2.42	0.00	1.86	0.72	0.17	61	64	67	77
SIKA-2017-42.1	Matokulma	0.00	0.00	4.49	7.79	17.67	0.00	35.77	25.52	10.24	0.00	23.60	16.16	7.44	6.98	4.63	2.35	0.00	2.49	1.05	0.19	66	68	71	69
SIKA-2017-44.1	Matokulma	0.00	0.00	8.45	10.15	34.92	0.00	23.49	16.41	7.08	0.00	7.19	4.81	2.38	13.00	8.41	4.59	0.00	1.89	0.76	0.17	65	67	70	77
SIKA-2017-104.1	Matokulma	0.00	0.00	3.90	8.97	22.08	0.00	27.41	19.12	8.29	0.00	31.82	21.25	10.57	2.06	1.33	0.73	0.00	2.50	1.10	0.19	65	67	70	71
SIKA-2017-105.1	Matokulma	0.00	0.00	4.85	9.99	17.66	0.00	34.18	24.14	10.04	0.00	21.18	14.34	6.84	8.27	5.42	2.85	0.00	2.50	1.18	0.24	66	68	71	64
SIKA-2017-108.1	Matokulma	0.00	0.00	5.67	11.25	17.66	0.00	28.88	20.13	8.75	0.00	24.92	16.63	8.29	7.44	4.80	2.64	0.00	2.60	1.37	0.21	65	67	70	61
SIKA-2017-111.1	Matokulma	0.00	0.00	3.96	13.37	37.34	0.00	23.85	16.62	7.23	0.00	12.22	8.15	4.07	6.53	4.22	2.32	0.00	1.72	0.82	0.19	65	67	70	74
SIKA-2017-112.1	Matokulma	0.00	0.00	2.84	6.35	15.08	0.00	41.20	29.72	11.48	0.00	19.11	13.24	5.87	11.55	7.76	3.79	0.00	2.64	1.05	0.21	67	69	72	70
SIKA-2017-115.2	Matokulma	0.00	0.00	2.96	7.87	11.35	0.00	46.81	33.84	12.96	0.00	19.33	13.43	5.90	7.80	5.26	2.55	0.00	2.53	1.16	0.21	67	69	72	59
SIKA-2017-167.1	Matokulma	0.00	0.00	4.85	12.02	21.66	0.00	32.65	22.60	10.05	0.00	22.02	14.58	7.44	3.35	2.15	1.21	0.00	2.26	1.05	0.17	64	66	69	64
SIKA-2017-173.1	Matokulma	0.00	0.00	3.13	9.90	15.83	0.00	40.77	28.86	11.91	0.00	16.68	11.32	5.36	9.82	6.45	3.37	0.00	2.52	1.10	0.26	66	68	71	62
SIKA-2017-174.1	Matokulma	0.00	0.00	3.37	10.24	24.84	0.00	18.76	12.61	6.15	0.00	27.22	17.45	9.77	11.15	6.90	4.26	0.00	2.92	1.37	0.14	62	64	67	71
SIKA-2017-174.2	Matokulma	0.00	0.00	4.08	13.29	39.29	0.00	13.94	9.15	4.79	0.00	21.90	13.68	8.22	4.58	2.76	1.83	0.00	2.04	0.70	0.21	60	62	66	75
SIKA-2017-27.3	Matokulma dikes	0.45	0.00	10.82	16.92	32.25	0.00	10.69	5.35	5.34	0.00	23.76	11.07	12.69	0.00	0.00	0.00	0.00	2.54	1.86	0.73			47	50	66
SIKA-2017-28.1	Matokulma dikes	0.00	0.00	24.53	15.99	24.36	0.00	5.78	2.85	2.93	0.00	9.04	4.15	4.89	14.82	6.45	8.37	0.00	2.81	1.96	0.73	44	46	49	60
SIKA-2017-28.2	Matokulma dikes	0.00	0.00	11.70	24.12	27.72	0.00	9.36	4.42	4.94	0.00	18.62	8.16	10.47	3.38	1.40	1.98	0.00	2.55	1.81	0.76	41	44	47	53
SIKA-2017-55.1	Matokulma dikes	0.42	0.00	7.80	22.59	28.37	0.00	15.31	8.13	7.18	0.00	20.80	10.33	10.47	0.00	0.00	0.00	0.00	2.34	1.71	0.69			50	53	56
SIKA-2017-58.1	Matokulma dikes	2.40	0.00	3.84	23.95	37.14	0.00	8.65	3.99	4.66	0.00	19.41	8.29	11.12	0.00	0.00	0.00	0.00	2.25	1.73	0.66			43	46	61
SIKA-2017-61.1	Matokulma dikes	0.00	0.00	10.28	9.82	28.92	0.00	16.78	10.75	6.03	0.00	28.13	17.11	11.02	1.38	0.81	0.57	0.00	2.41	1.60	0.71	59	61	64	75
SIKA-2017-119.1	Matokulma dikes	0.00	0.00	7.51	16.75	19.80	0.00	13.91	10.11	3.80	0.00	22.18	15.50	6.68	15.10	10.24	4.86	0.00	2.44	1.58	0.76	68	70	73	54
SIKA-2017-121.1	Matokulma dikes	3.05	0.00	16.49	22.42	20.52	0.00	9.27	5.91	3.37	0.00	22.99	13.90	9.09	0.00	0.00	0.00	0.00	1.87	1.98	1.45			60	64	48
SIKA-2017-169.2	Matokulma dikes	0.00	0.00	4.61	27.84	28.20	0.00	12.81	6.90	5.91	0.00	9.91	5.00	4.91	10.29	4.94	5.35	0.00	2.55	2.60	1.23	48	50	54	50
SIKA-2017-1.1	Palojärvi	0.00	0.00	3.01	14.55	36.94	0.00	1.18	0.48	0.70	0.00	29.03	10.81	18.21	7.48	2.62	4.86	0.00	4.09	3.06	0.69	35	37	41	72
SIKA-2017-1.2	Palojärvi	0.00	0.00	2.01	21.15	44.09	0.00	0.35	0.13	0.21	0.00	17.22	6.01	11.21	7.48	2.45	5.03	0.00	3.07	3.27	1.42	33	35	38	68
SIKA-2017-3.1	Palojärvi	0.00	0.00	2.25	9.65	49.42	0.00	10.11	6.02	4.09	0.00	12.69	7.13	5.56	11.95	6.42	5.52	0.00	2.39	1.31	0.26	54	56	60	84
SIKA-2017-4.1	Palojärvi	0.00	0.00	5.14	16.42	34.04	0.00	9.19	4.13	5.07	0.00	12.58	5.22	7.35	15.58	6.10	9.47	0.00	3.73	3.08	0.26	39	42	45	67
SIKA-2017-5.1	Palojärvi	0.00	0.00	1.54	9.90	37.26	0.00	19.52	9.13	10.39	0.00	3.58	1.56	2.03	20.45	8.39	12.06	0.00	3.93	3.65	0.21	41	43	47	79
SIKA-2017-8.1	Palojärvi	0.00	0.00	4.14	23.44	40.32	0.00	6.42	3.25	3.17	0.00	8.41	3.98	4.44	10.12	4.54	5.58	0.00	2.52	4.10	0.57	45	47	51	63
SIKA-2017-11.1	Palojärvi	0.00	0.00	4.08	16.67	34.14	0.00	1.09	0.44	0.65	0.00	27.16	10.12	17.04	9.36	3.28	6.08	0.00	4.08	2.58	0.88	35	37	41	67
SIKA-2017-11.2	Palojärvi	0.00	0.00	10.22	15.82	38.67	0.00	3.84	1.53	2.31	0.00	0.66	0.24	0.42	22.60	7.77	14.84	0.00	3.52	3.36	1.33	34	37	40	71
SIKA-2017-13.1	Palojärvi	0.00	0.00	3.55	11.42	41.53	0.00	1.91	1.12	0.79	0.00	20.26	11.22	9.04	17.14	9.08	8.06	0.00	3.06	0.84	0.31	53	55	59	78
SIKA-2017-14.1	Palojärvi	0.00	0.00	1.42	9.05	31.95	0.00	7.08	4.19	2.89	0.00	4.11	2.30	1.82	40.68	21.73	18.95	0.00	4.31	1.25	0.17	53	56	59	78
SIKA-2017-17.1	Palojärvi	0.00	0.00	2.96	35.12	40.95	0.46	1.87	0.58	1.30	0.00	0.00	0.00	0.00	13.53	3.51	10.01	0.00	2.23	1.62	1.30	26		31	54
SIKA-2017-49.1	Palojärvi	0.00	0.00	3.13	9.82	40.96	1.74	12.06	5.40	6.65	0.00	0.00	0.00	0.00	24.52	9.59	14.93	0.00	3.80	3.12	0.90	39		45	81
SIKA-2017-49.2	Palojärvi	0.00	0.00	2.96	10.17	36.48	1.37	18.75	9.35	9.40	0.00	0.00	0.00	0.00	21.06	9.27	11.79	0.00	3.70	5.23	0.31	44		50	78
SIKA-2017-51.1	Palojärvi	0.00	0.00	1.77	8.46	35.20	0.00	2.80	1.42	1.38	0.00	1.39	0.65	0.73	41.73	18.69	23.05	0.00	5.10	3.36	0.19	45	47	51	81
SIKA-2017-53.1	Palojärvi	0.00	0.00	2.72	9.99	46.23	0.00	11.31	5.79	5.52	0.00	16.13	7.70	8.43	8.83	4.00	4.83	0.00	2.86	1.77	0.19	45	48	51	82
SIKA-2017-54.1	Palojärvi	0.00	0.00	3.31	12.20	38.36	3.89	13.88	5.46	8.42	0.00	0.00	0.00	0.00	19.01	6.45	12.56	0.00	3.67	4.52	1.21	34		39	76
SIKA-2017-62.1	Palojärvi	0.00	0.00	1.95	10.15	35.33	0.00	8.35	4.96	3.39	0.00	2.65	1.49	1.16	36.57	19.64	16.93	0.00	3.81	0.93	0.28	54	56	59	78
SIKA-2017-67.1	Palojärvi	0.00	0.00	2.31	10.20	67.65	0.75	4.45	2.12	2.33	0.00	0.00	0.00	0.00	11.70	4.90	6.80	0.00	1.65	1.16	0.14	42		48	87
SIKA-2017-69.1	Palojärvi	3.94	0.00	7.86	13.79	30.39	0.00	6.99	3.04	3.95	0.00	30.29	12.17	18.12	0.00	0.00	0.00	0.00	3.32	2.43	1.00		40	44	69
SIKA-2017-75.1	Palojärvi	0.00	0.00	4.08	18.02	35.52	0.00	14.05	6.20	7.86	0.00	0.64	0.26	0.38	20.28	7.79	12.49	0.00	3.52	3.38	0.52	38	41	44	66
SIKA-2017-80.1	Palojärvi	0.00	0.06	5.56	12.78	43.64	0.00	0.00	0.00	0.00	0.00	9.45	4.45	5.00	23.12	10.32	12.80	0.00	3.41	1.54	0.47	45	47		77
SIKA-2017-81.1	Palojärvi	0.00	0.00	4.73	21.82	32.86	1.61	11.55	4.64	6.90	0.00	0.00	0.00	0.00	19.89	6.91	12.98	0.00	3.45	3.19	0.92	35		40	60
SIKA-2017-82.1	Palojärvi	0.00	0.00	3.01	16.67	41.38	2.57	9.07	3.37	5.70	0.00	0.00	0.00	0.00	18.36	5.85	12.51	0.00	3.38	4.05	1.56	32		37	71
SIKA-2017-88.1	Palojärvi	0.00	0.00	1.18	15.12	44.99	1.30	7.81	3.01	4.80	0.00	0.00	0.00	0.00	21.03	6.97	14.06	0.00	3.57	3.72	1.33	33		39	75
SIKA-2017-88.2	Palojärvi	0.00	0.00	2.13	15.58	43.79	0.45	8.21	3.26	4.95	0.00	0.00	0.00	0.00	21.24	7.28	13.96	0.00	3.57	3.72	1.35	34		40	74
SIKA-2017-88.3	Palojärvi	0.00	0.00	2.42	11.27	45.25	0.82	8.75	3.66	5.09	0.00	0.00	0.00	0.00	22.77	8.26	14.51	0.00	3.70	3.80	1.28	36		42	80
SIKA-2017-140.1	Palojärvi	0.00	0.00	7.74	16.75	41.13	0.00	7.40	3.43	3.97	0.00	5.74	2.47	3.28	14.51	5.89	8.62	0.00	2.81	2.66	1.30	41	43	46	71
SIKA-2017-142.1	Palojärvi	0.00	0.00	3.72	8.88	45.98	0.42	1.01	0.53	0.49	0.00	0.00	0.00	0.00	33.60	15.51	18.09	0.00	3.84	2.36	0.19	46		52	84
SIKA-2017-156.1	Palojärvi	0.00	0.00	9.46	25.64	26.61	0.00	11.46	5.94	5.52	0.00	19.16	9.28	9.89	2.13	0.98	1.15	0.00	2.39	2.13	1.04	46	48	52	51
SIKA-2017-158.1	Palojärvi	0.00	0.00	3.49	17.94	38.07	0.00	4.27	2.13	2.14	0.00	23.29	10.82	12.47	7.33	3.23	4.10	0.00	3.03	1.84	0.76	44	46	50	68
SIKA-2017-159.1	Palojärvi	4.11	0.00	6.03	15.06	39.61	0.00	6.61	3.29	3.32	0.00	24.59	11.40	13.19	0.00	0.00	0.00	0.00	2.41	1.48	0.10		46	50	72
SIKA-2017-159.2	Palojärvi	0.00	0.00	8.63	7.11	20.40	0.00	9.95	5.07	4.88	0.00	46.09	21.91	24.17	0.62	0.28	0.34	0.00	4.39	2.74	0.10	45	48	51	74
SIKA-2017-161.1	Palojärvi	0.00	0.00	4.02	9.32	56.34	2.24	0.98	0.51	0.47	0.00	0.00	0.00	0.00	22.93	10.54	12.39	0.00	2.63	1.44	0.12	46		52	86
SIKA-2017-185.1	Palojärvi	0.32	0.00	9.16	18.79	33.86	0.00	2.50	1.33	1.17	0.00	30.57	15.25	15.32	0.00	0.00	0.00	0.00	2.60	1.73	0.50		50	53	64
SIKA-2017-185.2	Palojärvi	0.00	0.00	5.67	19.46	40.27	0.00	7.08	3.22	3.86	0.00	13.35	5.63	7.72	8.43	3.35	5.08	0.00	2.77	2.60	0.36	40	42	46	67
SIKA-2017-185.3	Palojärvi	0.00	0.00	3.66	15.06	41.97	0.00	0.06	0.03	0.03	0.00	9.34	4.44	4.91	23.79	10.73	13.07	0.00	3.54	2.22	0.36	45	47	51	74
SIKA-2017-9.1	Hongonniittu	0.00	0.00	2.42	5.92	47.60	0.00	6.01	3.76	2.26	0.00	8.58	5.08	3.51	25.52	14.50	11.03	0.00	2.94	0.91	0.10	57	59	62	89
SIKA-2017-154.1	Hongonniittu	0.00	0.00	2.19	14.64	62.39	0.00	5.95	2.84	3.11	0.00	4.73	2.10	2.63	6.98	2.93	4.05	0.00	1.58	1.22	0.36	42	44	48	81
SIKA-2017-154.2	Hongonniittu	0.00	0.00	3.19	11.65	47.47	1.48	13.46	6.50	6.95	0.00	0.00	0.00	0.00	17.40	7.40	10.00	0.00	2.78	2.39	0.19	43		48	80
SIKA-2017-154.3	Hongonniittu	0.00	0.00	3.31	10.86	47.72	2.05	13.28	6.50	6.78	0.00	0.00	0.00	0.00	17.17	7.40	9.77	0.00	2.76	2.53	0.36	43		49	81

Appendix 3. Trace element analysis for selected samples. Method 308M uses ICP-MS, 308P uses ICP-OES. Highlighted samples have been analyzed twice because of quality issues. Both analyzes are shown.

Analysis method		308M (ICP-MS)																			308P (ICP-OES)				
Element		Ce	Dy	Er	Eu	Gd	Hf	Ho	La	Lu	Nb	Nd	Pr	Rb	Sm	Ta	Tb	Th	Tm	U	Yb	Co	Sc	V	Y	Zr
Detection limit		0.5	0.06	0.04	0.03	0.09	0.5	0.04	0.5	0.03	3	0.2	0.04	0.8	0.06	1	0.04	2	0.03	0.06	0.03	5	2	5	2	5.00
Sample	**Group**																									
SIKA-2017-6.4	Matokulma	6.37	2.17	1.19	0.66	2.12	<0.5	0.42	2.12	0.15	<3	6.35	1.15	14.5	1.97	<1	0.35	<2	0.16	<0.2	0.97	50	53.5	373	9.2	13
SIKA-2017-7.1	Matokulma	13.4	2.34	1.33	0.67	2.39	0.65	0.47	5.29	0.16	<3	9.25	1.93	18.7	2.34	<1	0.39	<2	0.18	0.3	1.11	56.6	51.8	311	10.6	31
SIKA-2017-42.1	Matokulma	14.2	2.66	1.48	0.75	2.7	0.68	0.52	5.77	0.18	<3	9.94	2.1	31	2.63	<1	0.44	<2	0.2	0.39	1.24	52.8	57.6	356	11.2	31
SIKA-2017-112.1	Matokulma	14.5	2.74	1.5	0.72	2.75	0.73	0.54	5.34	0.18	<3	10.2	2.1	14.6	2.63	<1	0.44	<2	0.2	0.39	1.26	65	59.4	362	11	31
SIKA-2017-115.2	Matokulma	16	3.07	1.72	0.74	3.13	0.74	0.6	6.47	0.21	<3	11.4	2.34	15.6	2.95	<1	0.5	<2	0.23	0.48	1.4	54.8	67.6	426	12.8	37
SIKA-2017-173.1	Matokulma	18.7	2.99	1.66	0.81	3.1	0.82	0.59	7.87	0.21	<3	12.1	2.64	17.9	3	<1	0.48	<2	0.23	0.49	1.4	57.1	59	367	12.2	40
SIKA-2017-27.3	Matokulma dikes	31.6	3.9	2.23	1.39	4.21	2.25	0.78	13.6	0.3	5.44	19.2	4.25	77.8	4.33	<1	0.65	2.12	0.3	0.58	1.99	31.3	34.8	250	17.4	59
SIKA-2017-55.1	Matokulma dikes	31.8	4.01	2.2	1.41	4.53	1.67	0.79	14.6	0.28	3.12	19.9	4.34	45.1	4.52	<1	0.69	2.09	0.3	0.51	1.86	29.8	35.7	242	16.8	45
SIKA-2017-58.1	Matokulma dikes	21.8	2.97	1.61	1.06	3.08	1.61	0.58	9.81	0.2	3.27	13	2.89	23.1	3.1	<1	0.49	2.25	0.22	0.45	1.36	34	34	293	12.1	45
SIKA-2017-61.1	Matokulma dikes	27.4	3.66	2.09	1.55	3.98	2.13	0.72	11.5	0.28	5.02	17.1	3.77	73.9	4.01	<1	0.62	2.47	0.29	0.75	1.85	38.6	36	228	16.3	61
SIKA-2017-119.1	***Matokulma dikes***	***33.7***	***2.99***	***1.65***	***1.18***	***3.5***	***2.45***	***0.58***	***14.9***	***0.22***	***4.22***	***18.9***	***4.35***	***36.1***	***3.79***	***<1***	***0.51***	***2.59***	***0.23***	***0.76***	***1.47***	***50.5***	***27.9***	***214***	***12.8***	***53***
		33.4	***2.97***	***1.66***	***1.16***	***3.48***	***1.12***	***0.58***	***14.8***	***0.22***	***3.68***	***18.6***	***4.33***	***36.7***	***3.8***	***<1***	***0.51***	***2.18***	***0.23***	***0.77***	***1.48***	***51***	***27.7***	***210***	***12.3***	***51***
SIKA-2017-169.2	Matokulma dikes	53.7	5.61	3.06	2.22	6.7	5	1.08	22.1	0.39	11.3	34.2	7.59	23.1	7.35	<1	0.98	2.3	0.4	1.66	2.6	28.9	30.6	255	23.3	103
SIKA-2017-3.1	***Palojärvi***	***15.4***	***2.55***	***1.44***	***0.92***	***2.68***	***6.57***	***0.5***	***6.32***	***0.18***	***<3***	***10***	***2.14***	***11.7***	***2.55***	***<1***	***0.41***	***2.57***	***0.19***	***0.41***	***1.23***	***45.9***	***35.8***	***339***	***11.3***	***47***
		15.6	***2.55***	***1.44***	***0.89***	***2.6***	***3.29***	***0.5***	***6.54***	***0.18***	***<3***	***10.2***	***2.17***	***11.6***	***2.58***	***<1***	***0.42***	***2.14***	***0.2***	***0.41***	***1.21***	***44.1***	***35.6***	***335***	***10.7***	***40***
SIKA-2017-4.1	Palojärvi	26.4	3.59	2.1	1.08	3.69	1.99	0.72	10.9	0.28	4.78	16.2	3.66	25.3	3.7	<1	0.58	2.01	0.3	0.53	1.9	49.7	30.3	500	16.1	37
SIKA-2017-14.1	Palojärvi	9.2	1.2	0.72	0.49	1.25	1.14	0.23	4.16	<0.1	<3	5.5	1.25	3.63	1.26	<1	0.2	<2	0.1	0.27	0.63	90	18.9	346	4.6	24
SIKA-2017-17.1	Palojärvi	27.9	1.78	0.96	2.1	2.41	1.41	0.34	13.3	0.12	<3	14.3	3.41	16	2.6	<1	0.33	<2	0.13	0.52	0.79	16.2	3.5	90	8	23
SIKA-2017-22.1	Palojärvi	31.6	2.25	1.44	0.96	2.41	3.16	0.46	15.9	0.21	4.66	13.3	3.51	16.8	2.63	1.28	0.37	10.8	0.2	2.06	1.39	34	8.8	144	11.1	82
SIKA-2017-51.1	Palojärvi	9.34	1.05	0.61	0.58	1.15	1.34	0.21	4.31	<0.1	<3	5.3	1.21	12.1	1.18	<1	0.18	<2	<0.1	0.28	0.55	75.1	14.8	459	3.8	27
SIKA-2017-54.1	Palojärvi	64.4	9.54	5.58	2.66	9.88	3.5	1.91	22.5	0.74	14	43.1	9.49	5.25	10	<1	1.55	<2	0.77	0.25	4.84	27.9	58.4	408	43.3	77
SIKA-2017-62.1	Palojärvi	8.49	1.97	1.06	0.84	2.1	0.74	0.38	3.31	0.12	<3	6.99	1.32	7.38	1.92	<1	0.32	<2	0.14	<0.2	0.82	68.2	20.1	89.1	7.4	16
SIKA-2017-80.1	Palojärvi	18.6	2.02	1.19	0.91	2.24	1.53	0.4	8.7	0.17	3.3	10.4	2.4	29.4	2.29	<1	0.34	<2	0.16	0.57	1.1	62.7	15.4	230	8.5	40
SIKA-2017-9.1	Hongonniittu	8.85	0.79	0.45	0.41	0.79	2.04	0.15	3.3	<0.1	<3	3.54	0.84	13.5	0.76	<1	0.13	<2	<0.1	0.22	0.42	66.4	15.8	206	2.7	17